SERI/TR-252-3116
UC Category: 62

DRAFT

Evaluation of Thermally Activated Heat Pump/Desiccant Air Conditioning Systems and Components

Brian K. Parsons
Ahmad A. Pesaran
Desikan Bharathan
Benjamin Shelpuk

April 1987

Prepared under Task No. 7563.200
FTP No. 669

Solar Energy Research Institute
A Division of Midwest Research Institute

1617 Cole Boulevard
Golden, Colorado 80401-3393

Prepared for the
Oak Ridge National Laboratory
Award Number 10X-67892V

SERI/TR-252-3116
UC Category: 62

DRAFT

Evaluation of Thermally Activated Heat Pump/Desiccant Air Conditioning Systems and Components

Brian K. Parsons
Ahmad A. Pesaran
Desikan Bharathan
Benjamin Shelpuk

April 1987

Prepared under Task No. 7563.200
FTP No. 669

Solar Energy Research Institute
A Division of Midwest Research Institute

1617 Cole Boulevard
Golden, Colorado 80401-3393

Prepared for the
Oak Ridge National Laboratory
Award Number 10X-67892V

PREFACE

Air conditioning of commercial and residential buildings utilizes a significant amount of energy. In an effort to decrease cooling costs and reduce energy consumption, the U.S. Department of Energy has sponsored research to improve cooling system efficiencies. Research performed by Oak Ridge National Laboratories (ORNL) on a vapor compression heat pump driven by a gas-fired internal combustion engine is one of the technologies being examined. Use of gas as the primary energy source may lead to reduced operating cost compared to conventional electric vapor compression machines in areas of the United States with relatively high electric costs.

The efficiency of a thermally activated heat pump system could be increased if the gas engine waste heat was somehow utilized. Preliminary analysis by ORNL has indicated that using the waste heat to drive a desiccant cooling subsystem could considerably improve the overall cooling performance. A desiccant cooling system utilizes a dehumidifier to remove moisture from the process air, reducing or eliminating the latent portion of a given building cooling load. Heat is required to regenerate the desiccant, allowing the process to operate continuously. In a vapor compression/desiccant hybrid system, the vapor compression evaporator needs only to handle the sensible load and does not have to operate at the low temperatures needed for dehumidification.

The potential applications for such a hybrid system which efficiently handles both latent and sensible cooling loads is great. Applications include buildings with high internal moisture generation (such as supermarkets, health clubs, etc.) and buildings in humid climates with significant ventilation requirements. The recent high growth rates in the humid southeastern portion of the United States points toward every increasing potential for such systems.

In order to thoroughly evaluate the potential of a thermally activated heat pump coupled to a desiccant cooling subsystem, possible desiccant materials and system configurations must be examined. In this report we identify materials which efficiently utilize the gas engine waste heat and quantify the performance of two alternative systems configurations. The hybrid systems increase the amount of cooling delivered for a given amount of energy input by 70-90% over a TAHP alone at standard American Refrigeration Institute (ARI) design conditions. An estimate of the additional capital cost of the most promising desiccant subsystem is included. By using this cost and performance data, design engineers can perform an analysis examining the trade-off between higher initial capital cost and reduced operating expenses due to lower fuel consumption.

This work was performed during FY 1987 by the Thermal Science Research Branch of SERI under Task 7563.200, with funding provided

by ORNL. The authors especially thank Terry Penney of SERI and Noberto Domingo of ORNL for their constructive review of the work.

Approved for

SOLAR ENERGY RESEARCH INSTITUTE

_____
David H. Johnson, Manager
Thermal Sciences Research Branch

_____
Donald L. Feucht, Acting Director
Solar Heat Research Division

SUMMARY

Objective

The objective of the work documented in this report is to analytically study desiccant dehumidification materials and system configurations for use in conjunction with a thermally activated heat pump (TAHP) and to determine performance under design conditions.

Discussion

We identified three promising desiccants from the materials studied: molecular sieve, lithium chloride and silica gel. A rotating parallel plate dehumidifier geometry was selected because of high heat-and-mass transfer rates and low pressure drop. Material property relations were integrated with a detailed dehumidifier model. Dehumidifier performance was predicted and compared using the three materials. The silica gel dehumidifier was found to have the highest moisture removal efficiency with the lithium chloride wheel having only 5% less moisture removal at the evaluated conditions. Integrated system models for two hybrid TAHP/desiccant configurations were developed and performance was evaluated at design conditions.

For a total system cooling load of around 13 tons, the TAHP subsystem met 8½ tons of the load while the desiccant subsystem met around 4½ tons. The desiccant subsystem required very little additional fuel for regeneration of the dehumidifier and the gas based COP increased by 70%. A cost estimate for one of the desiccant subsystems was developed. Estimated manufacturer cost for the add-on desiccant subsystem was $490/ton.

Conclusion

This study strongly supports the addition of a desiccant cooling subsystem to a thermally activated heat pump as first costs per unit of cooling do not increase and energy consumption is significantly reduced.

TABLE OF CONTENTS

Page

1.0 Introduction.....

1.1 Objectives.....
1.2 Organization.....

2.0 Background.....

2.1 Vapor Compression Systems.....
2.2 Desiccant Cooling Systems.....
2.3 Hybrid Cooling Systems.....

3.0 Desiccant Materials Study.....

3.1 Purpose of the Study.....
3.2 Background.....
3.3 Materials Selection.....
3.4 Properties of Selected Desiccant Materials.....
3.4.1 Silica-Gel.....
3.4.2 Molecular Sieves.....
3.4.3 Lithium Chloride.....
3.4.4 Desiccant Materials Limitations.....
3.5 Summary.....

4.0 Rotary Dehumidifier Modeling.....

4.1 Modeling Approach.....
4.2 Model Validation.....
4.3 General F_1, F_2 Method.....
4.4 Dehumidifier Design Parameters.....

5.0 Dehumidifier Parametric Studies.....

5.1 Comparison of Three Desiccant Wheels.....
5.2 Effect of Varying the Air Mass Flow Rate on Wheel Performance..
5.3 Unbalanced Flow Performance.....

6.0 System Modeling.....

6.1 Component Performance Models.....
6.2 System Configurations.....
6.3 Component Performance and Design Point.....
6.4 Influence of Design Conditions on Operating Mode.....

7.0 System Studies Results.....

7.1 System 1 Performance Results.....
7.2 System 2 Performance Results.....
7.3 System Selection.....
7.4 Other Possible Performance Improvements.....

TABLE OF CONTENTS (Concluded)

Page

8.0 Physical Description of a Waste Heat Driven Desiccant Cooling Subsystem.....

8.1 System Layout and Cost.....
8.2 Component Description.....

9.0 Conclusions and Recommendations.....

9.1 Conclusions.....
9.2 Recommendations.....

10.0 References .....

Appendix A.....

Distribution List.....

LIST OF FIGURES

Page

3-1 Brunauer and Linear Adsorption Isotherm Types.....

3-2 Adsorption Isotherms of Commercial Desiccant Materials.....

3-3 Microbead Silica-Gel Isotherms at Several Temperatures.....

3-4 Ratio of Heat Adsorption of Microbead Silica Gel to Latent Heat of Condensation of Water .....

3-5 Comparison of Curve-Fits of Manufacturer's Isotherm Data for Type 4A Molecular Sieves .....

3-6 Type 4A Molecular Sieves Isotherms at Several Temperatures.....

3-7 Ratio of Heat of Adsorption of Type 4A Molecular Sieves to Latent Heat of Condensation of Water .....

3-8 Isotherms of Lithium Chloride Solutions at Various Temperatures....

3-9 Vapor Pressure Composition Diagram for Lithium Chloride.....

3-10 Equilibrium Isotherm of Lithium Chloride/Water System at Low Relative Humidities at 50°C.....

3-11 Ratio of Heat of Sorption of Lithium Chloride to the Latent Heat of Condensation of Water.....

3-12 Comparison of Isotherms of Lithium Chloride, Silica Gel, and Molecular Sieves at 50°C.....

3-13 Comparison of Heat of Sorption of Lithium Chloride, Silica Gel, and Molecular Sieves.....

4-1 Heat and Mass Transfer Process in Dehumidifier.....

4-2 Lines of Constant Combined Potentials F_i for a Simplified Silica Gel-Water-Air System.....

4-3 Specific Capacity Ratios for a Simplified Silica Gel-Water-Air-System.....

LIST OF FIGURES (Concluded)

Page

4-4 Comparison of Infinite and Finite Transfer Coefficient Solutions for Counterflow Regenerator, Plotted as Transfer Effectiveness η_1 vs. Rotational Speed C_1 .....

4-5 Measured F_1 Transfer Effectiveness vs. Theory.....

4-6 Measured F_2 Transfer Effectiveness vs. Theory.....

4-7 Graphical Representation of F_1, F_2 Solution Method.....

5-1 Micro-Bead Silica Gel Wheel Performance with Air-Flow Rates of 0.6 kg/s as a Function of Regeneration Temperature.....

5-2 Lithium Chloride Wheel Performance with Air Flow Rates of 0.6 kg/s as a Function of Regeneration Temperature.....

5-3 Molecular Sieve Wheel Performance with Air Flow Rates of 0.6 kg/s as a Function of Regeneration Temperature.....

5-4 Comparison of Wheel Performance with Air Flow Rates of 0.6 kg/s and an Inlet Regeneration Temperature of 85°C.....

5-5 Effect of Air-Mass Flow Rate on the Silica Gel Wheel Performance...

5-6 Effect of Air-Mass Flow Rate on the Dehumidifier Pressure Drop.....

5-7 Silica-Gel Wheel Performance with Unbalanced Flow and Constant Regeneration Temperature.....

5-8 Silica Gel Wheel Performance with Unbalanced Flow and Constant Regeneration Heat Input.....

6-1 Schematic and Psycometric Chart Representation of System 1.....

6-2 Schematic and Psycometric Chart Representation of System 2.....

8-1 Integrated System Schematic.....

8-2 Desiccant Subsystem Layout.....

LIST OF TABLES

Page

3-2 Physical Properties of Type 4A Molecular Sieves.....

3-3 Properties of Lithium Chloride.....

3-4 Comparison of Properties of the Selected Desiccant Materials.....

4-1 Design Dimensions and Masses of the Dehumidifier.....

4-2 Solid Particle Wheel Parameters Dependent on Desiccant Material.....

5-1 Parameters for Unbalanced Flow Studies.....

6-1 Engine Characteristics.....

6-2 Component Pressure Drop.....

7-2 System 1 Performance Results for Low Component Efficiencies.....

7-3 Affect of Commercial vs. Developmental Component Performance.....

7-4 System 2 Performance Results.....

NOMENCLATURE

Å	angstrom (10^{-10} meter)
C	capacitance rates (J/S °C)
C_{ij}	combined potential i for period j
°C	degrees Celsius
Cd	specific heat capacity of desiccant (J/kg °C)
Ci	specific heat capacity of inert material (J/kg °C)
C_i	dimensionless rotational speed
c	concentration by weight (kg/kg)
COP	coefficient of performance, cooling/energy input
Cp	fluid specific heat (J/kg °C)
dp	diameter of desiccant particle (m)
D_W	diffusivity of moisture in the desiccant (m/s)
E	efficiency parameters used in Equations A-26 to A-29
e_s	solid-side resistance geometry factor
F	combined potentials used for dehumidifier performance
FLR	Fractional load ratio (load/capacity)
Gr	Graetz number
h	specific enthalpy of air/water vapor mixture (J/kg)
H	specific enthalpy of desiccant/water matrix (J/kg)
ha	ratio of heat transfer coefficient - area product for process and regeneration periods
hlv	latent heat of condensation of water (J/kg)
hs	heat of adsorption/absorption
J	joules
K	degrees kelvin
kg	kilogram
Le	effective Lewis number
$\dot{m}$	mass flow (kg/s)
m	meter
mm	millimeter
mdsg	moisture diffusivity of desiccant (m/s)
mdd	mass of dry desiccant (kg)
NTU	number of transfer units
Nu	Nusselt number
Pv	vapor pressure of water (Pa)

NOMENCLATURE (Continued)

Ps	saturation vapor pressure of water
P_{va}	vapor pressure of a salt solution at a reference temperature (Pa)
P	pressure (Pa)
Pa	Pascals
Pr	Prandtl number
p	partial pressure (Pa)
pf	packing factor of particles
Q	heat rate (J/s)
r	relative humidity (P_v/P_{sat})
rhod	density of desiccant (kg/m^3)
rhos	true density of material, no porosity (kg/m^3)
R	universal gas constant
S	derivative of natural log of saturation pressure with respect to temperature
Sc	Schmidt number
Sh	Sherwood number
s	second
sgf	desiccant fraction of matrix
t,T	temperature
Tvpi	temperature of isotherm data (°K)
v	specific volume (m^3/kg)
v_p	pore volume of solid desiccant
W	watt
W	desiccant water content by weight (kg/kg)
W	work (J/s)
w	absolute humidity of air (kg/kg)
x	distance (m)
X_{eff}	effective desiccant fraction (kg/kg)

<u>Greek</u>

α	partial derivative of temperature with respect to absolute humidity
β	sorbability of the porous medium for the sorbate
θ	time (s)
Ω	one minus the partial pressure
∂	partial derivative

NOMENCLATURE (Continued)

γ	specific combined capacity ratios
η	transfer effectiveness, or component efficiency
ε	component effectiveness
Δ	change in a property
ρ	density (kg/m^3)
μ	ratio of mass of desiccant/mass of air in wheel
τ	residence time per period (s)
ν	partial derivative of temperature with respect to matrix water content
λ	ratio of heat of sorbtion and enthalpy of sorbate in fluid mixture
ζ	partial derivative of desiccant water content with respect to relative humidity times the relative humidity at constant temperature
Λ	dimensionless transfer coefficient
σ	ratio of specific heats of desiccant matrix to air/water mixture
Ψ	partial derivative of air/water enthalpy with respect to absolute humidity divided by the saturation enthalpy

Superscripts

*	saturation conditions
-	average value

Subscripts

air	refers to air/water mixture
cold	refers to lower temperature fluid entering a heat exchange
cond	refers to vapor compression condenser
d	desiccant property
dd	dry desiccant
DEC	refers to direct evaporative cooler
evap	refers to vapor compression evaporator
fan	refers to air fan
h	constant specific enthalpy
hot	refers to higher temperature fluid entering a heat exchange
i, in	inlet to a component or initial value
i	index with a numerical value (i.e., i = 1,2)
IEC	indirect evaporative cooler
int	refers to intersection point of F_1 and F_2 lines
j	index with a numerical value (i.e., j = 1,2)

NOMENCLATURE (Concluded)

lat	latent load
m	mean
max	maximum
min	minimum
O, out	outlet of a component
p	process air stream, desiccant pore
r	regeneration air stream
room	building return air conditions
sup	supply air stream, or saturation conditions
sen	sensible load
th	theoretical
w	constant relative humidity
wb	wet bulb conditions
1,2,3,4	indicies

1.0 INTRODUCTION

Over the past several years the U.S. Department of Energy (DOE) has sponsored research to develop energy-efficient methods for cooling buildings. Part of this research program has been to examine technology in Thermally Activated Heat Pumps (TAHP). Adding a desiccant dehumidification subsystem can increase performance of TAHP air conditioners. The high efficiency is a result of the fact that the two subsystems operate most efficiently on different portions of the cooling load. The vapor compression machine efficiently lowers the temperature of the air (sensible cooling load) while the desiccant subsystem efficiently removes moisture (latent cooling load). Since the desiccant subsystem utilizes waste heat from the TAHP to regenerate the dryer, very little additional energy is required to run the desiccant subsystem. As a result, adding desiccant subsystem hardware increases the total cooling capacity for a given energy input. Conversely, for a given building design load, the TAHP hardware size and initial cost is reduced by adding the desiccant subsystem and operating costs (fuel consumption) are also reduced.

The Solar Energy Research Institute (SERI) has been involved in research funded by the Solar Buildings Active Heating and Cooling Program of DOE; the work has focused on understanding and improving the desiccant materials and the heat-and-mass-transfer characteristics of the dehumidifier component of solar desiccant-cooling systems. In conjunction with their TAHP work, Oak Ridge National Laboratory contracted with SERI to examine hybrid desiccant/TAHP issues.

1.1 Objectives

The objective of this work is to analytically evaluate desiccant dehumidification materials and system configurations for use in conjunction with a thermally activated heat pump and to determine the performance of those alternatives under design conditions. The additional initial capital cost is estimated and performance is quantified allowing the reduction operating costs per unit of cooling to be determined.

The work presented in this report includes assessing and determining what desiccant materials can take advantage of waste heat supplied by the ORNL internal combustion engine, using a baseline cooling load and design conditions to assess desiccant system configurations, defining component sizes and performance under design conditions, and preparing a system schematic and cost estimate for the chosen configuration.

1.2 Organization

This report contains seven sections discussing the research areas plus conclusions and recommendations. The Background (Section 2) presents the differences between vapor-compression and desiccant cooling and outlines the advantages of hybrid systems. Section 3 covers materials studies that include an overview of desiccant materials and criteria for selection. This section also reviews properties of the three materials chosen for detailed dehumidifier modeling. Section 4 contains a discussion of the modeling of the rotary regenerative dehumidifier. Results of dehumidifier studies and a comparison of the performance of the dehumidifier using the three desiccant materials are found in Section 5. The component performance models, system models and system configurations appear in Section 6. Section 7 contains results of the systems studies that include baseline performance and component capacities. Section 8 contains a system layout and cost estimate for the selected system configuration. Finally, conclusions which can be drawn from the research and recommendations for further concept development are discussed in Section 9. Listings of the dehumidifier and systems computer codes used for this study are available through ORNL.

2.0 BACKGROUND

In order to maintain comfort in buildings during the cooling season, two types of energy building load must be met, sensible load and latent load. The sensible load is characterized by changes in temperature. Heat added to the building from internal sources such as occupants and equipment, and external sources such as solar gain through windows, infiltration, and conduction through outside walls, must be removed. The latent load is characterized by differences in humidity from similar sources. Meeting these loads involves adding cool, dry air to the building while removing warm, moist air.

2.1 Vapor Compression Systems

The majority of building cooling equipment utilize electric-driven vapor-compression machines. Vapor-compression systems are very good at meeting sensible loads. Air passed over the coils of the vapor-compression evaporator gives up heat to the refrigerant; this process chills the air. High heat transfer rates and high efficiency components make this a very attractive way to sensibly cool air.

It is less efficient to use vapor-compression equipment to meet latent loads. In order to remove moisture from the air, the air must be cooled past its dew point; at that temperature the water condenses on the coils. In some systems, the air is now colder than the required delivery temperature dictated by comfort and the sensible load. Depending on the cycle and system configuration, additional energy may be needed to reheat the air to the delivery temperature. In most vapor-compression systems, the evaporator coil must operate 5°C to 15°C cooler than the delivery temperature in order to chill the air to its dew point. The coefficient of performance (COP), defined as cooling output divided by energy input, of the vapor-compression machine is lowered by around 10 to 20 percent as a result. (See section 6.1 on vapor-compression modeling).

2.2 Desiccant Cooling Systems

Desiccant systems are designed to reduce latent loads. The process air is brought in contact with a material with a high affinity for water. Moisture

is adsorbed or absorbed by the desiccant material. During this process the heat of absorbtion or absorbtion is released to the air. In order to meet sensible loads, desiccant systems must over-dry the air then evaporatively cool the air to the desired supply temperature. Since the dehumidification process results in dryer and warmer supply air, the process may be considered a way to convert latent loads into sensible loads.

The desiccant requires regenerating (drying) after removing moisture from the process air. A hot, regeneration air stream is passed over the moisture laden desiccant. The regeneration air can be heated by solar collectors, electric heaters, gas burners, or waste heat sources. Since contamination of the desiccant can be a problem, the regeneration air stream is generally not heated by direct firing or other methods which may introduce pollutants.

2.3 Hybrid Cooling Systems

Combining components of a vapor-compression system with a desiccant system results in a hybrid which can efficiently meet both the sensible and latent cooling loads. The vapor compression machine operates with higher evaporator temperatures (resulting in a higher thermal COP), and no reheat is required. The dehumidifier must only remove the moisture to meet the latent load; no excessive drying is required. This process reduces the amount of energy required to regenerate the desiccant. In addition, reducing the amount of moisture which must be removed results in a smaller dehumidification subsystem.

Another advantage of the hybrid system is the reduction of required energy input (increased overall COP). Heat rejected by some components may be utilized to regenerate the desiccant which eliminates or reduces the need for external regenerative heat from solar collectors or other heat sources. Hybrid systems have the option of utilizing the heat rejected by the vapor-compression condenser for regeneration. In addition, depending on the type of driver which provides the work for the vapor compressor, significant amounts of engine waste heat may be available.

Several different hybrid systems have been installed in specialized applications with unique cooling requirements. A summary of several of these projects is provided in Schlepp & Shultz (1984). The success of these commercial systems show hybrid cooling strategies and components are currently economical and reliable for many applications. Hybrid systems for general applications have been examined by several researchers (Schlepp & Schultz 1984; Bowlen 1986; Howe 1983; Maclaine-Cross 1986). This study examines promising materials and system configurations for hybrid systems which incorporate a gas-fired internal-combustion engine to drive the refrigerant compressor (Thermally Activated Heat Pump).

3.0 DESICCANT MATERIALS STUDY

3.1 Purpose of the Study

The choice of the desiccant material has a major impact on the performance and to a lesser extent, the cost of desiccant dehumidifiers. The purpose of this study is to determine and to assess what desiccant materials are required for dehumidifiers in a hybrid desiccant cooling system to take advantage of the regenerative temperatures supplied by waste heat from the ORNL internal combustion engine.

This section presents: a brief background about desiccants for use in cooling and dehumidification applications; rationale for first-cut selection of desiccant materials desirable for use in a hybrid desiccant cooling system; and the pertinent properties of these selected desiccants to cooling applications. The final selection of the desiccant material will be discussed in Section 5.1.

3.2 Background

The performance of a desiccant dehumidifier depends mainly on the type of desiccant material that is used, the internal geometry of the dehumidifier (i.e., how the desiccant is deployed within the dehumidifier matrix), and the steady-state operating parameters.

The type of material affects size, range of operation (temperature, humidity), efficiency, cost, and service life of a dehumidifier and the thermal COP and cooling capacity of a system. The geometry of a dehumidifier affects its pressure drop, size, and cost and, thus, the thermal and electrical COPs and cost of a cooling system. Control strategies can also affect the overall performance. The optimum combination of desiccants and geometries can provide high-efficiency and low-cost dehumidifiers for commercial applications. The important desiccant material properties that influence the performance of dehumidifiers are equilibrium capacity, isotherm shape, heat of sorption, rate of sorption of moisture (diffusivity), thermal capacity, cyclic repeatability (hysteresis) of sorption capacity, and resistance to degradation (Jurinak

1982; Collier et al. 1986). The desiccant should also be nontoxic, odorless, and noncorrosive. The important parameters that are geometrically dependent are heat and mass transfer rates, pressure drop and porosity of the dehumidifier, desiccant containment in the dehumidifier, and manufacturing method (Pesaran et al. 1986). The cost of a dehumidifier depends on the cost of material and ease of construction.

The use of desiccants for dehumidification of air for cooling applications is relatively new. Desiccants have been used for many years for a variety of applications for removing moisture from gases, liquids, and solids. The desiccants may be solids or liquids. The moisture removal mechanism of desiccants may be classified as follows (Encyclopedia of Chemical Technology 1979):

- o Type 1 - Chemical reaction (a) formation of a new compound; (b) formation of a hydrate,
- o Type 2 - Physical absorption with constant relative humidity (solid + water → saturated solution),
- o Type 3 - Physical absorption with variable relative humidity (solid or liquid + water → diluted solution),
- o Type 4 - Physical adsorption (no phase change or solution of adsorbent).

Solid desiccants such as silica-gel, molecular sieves, and natural zeolites are examples of Type 4 desiccants. Liquid desiccants such as triethylene glycol and lithium chloride solutions are examples of Type 3 desiccants. Calcium chloride is a Type 1 desiccant when it is dry. It reacts with water to form a hydrate. Then, the more highly complex hydrates of calcium chloride absorb more water and exhibit the characteristics of a Type 2 desiccant. The saturated calcium chloride solution then absorbs more water and exhibits the characteristics of a Type 3 desiccant. Other hygroscopic salts, such as lithium chloride, may be similar to calcium chloride. Theoretically, any of these types of desiccant can be used in a dehumidifier for cooling applications. For simplicity, we have categorized commercial desiccants into three distinct groups: solid desiccants, liquid desiccants, and, hygroscopic salts.

The common solid desiccants previously considered for desiccant cooling and dehumidification are microporous silica-gel (Nienberg 1977; Rousseau 1981; Work and Lavan 1981; Jurinak 1982; Schlepp and Barlow 1984) for low temperature regeneration applications (60°C to 90°C), and molecular sieves (or zeolites) (Wurm et al. 1979) for high regeneration temperature applications (120°C to 220°C). The common salts and liquid desiccants previously considered for desiccant cooling and dehumidification are lithium chloride (McCormick et al. 1983), calcium chloride (Robison et al. 1982; Griffiths), and ethylene glycol (Peng et al. 1981). The most common hygroscopic salt is lithium chloride (Lof et al. 1987; Cargocaire 1982; Maclaine-cross 1974), although lithium bromide and calcium chloride have been studied theoretically (Maclaine-cross 1974). Salt/water mixtures for relative humidities common to air conditioning applications result in a solution and may behave as liquid desiccants do.

Usually, the solid desiccants, depending on their equilibrium isotherm shape, can be categorized into five Brunauer types and a linear type (See Figure 3-1). The mathematical formulations of isotherm shape were adapted from Jurinak (1982) and Collier et al. (1986). Molecular sieves are Type 1 Brunauer desiccants; activated aluminum approximates a Type 4 Brunauer isotherm, and activated carbon has a Type 5 Brunauer isotherm. Microporous silica-gel has been characterized as linear type or Type 2 Brunauer at low relative humidities and Type 1 at high relative humidities. Recently Collier et al. (1986) defined a desired desiccant with a preferred isotherm shape for indirect gas-fired desiccant cooling applications (regeneration temperature of 160°C). The shape of this isotherm is similar to Type 1 Brunauer isotherm (e.g., molecular sieves); however, it is not as steep as molecular sieves. To make a distinction between the two, Collier (1985) identified the isotherm of the molecular sieves as "Type 1 Extreme" and referred to the isotherm of his desired hypothetical material as "Type 1 Moderate" (Type 1M). The applicability of this Type 1M material to this project is discussed later.

3.3 Materials Selection

In selecting a desiccant material that can offer the greatest performance/cost potential for a hybrid/desiccant cooling system using the waste heat from an

internal combustion engine for desiccant regeneration, we should consider both the properties of the desiccants and how these desiccants are contained in the dehumidifier, i.e., the internal geometry of the dehumidifier. For example, liquid desiccants cannot be deployed in the dehumidifier the same way the solid desiccants or hygroscopic salts are deployed. Liquid desiccants are usually sprayed into droplets or jets or distributed over packing in a column for the purpose of dehumidification or regeneration. Solid desiccants usually are used in packed columns on beds of small particles or in laminar-flow channel geometries with the walls coated with fine particles of desiccant (Nienberg 1977; Kim et al. 1982; Schlepp and Barlow 1984). Hydroscopic salts are contained in a matrix by impregnating a porous carrier with the salt solution. Solid, liquid and hygroscopic salt systems are all commercially available (Meckler 1986; Meckler 1987).

Detailed analyses of all of these configurations (material and geometry combinations) are beyond the scope and the resources of this project. Based on the available information in the literature, experience, and engineering judgement, we narrowed the number of desiccant materials and geometries to be examined in detail.

This project did not pursue detailed modeling and evaluation of liquid desiccants. With limited resources, we decided to concentrate mainly on areas of existing expertise at SERI, namely rotating parallel plate dehumidifiers. Additional factors which influenced this decision are:

- Existing commercial liquid desiccant systems are designed mainly for large commercial and industrial application (Meckler 1982). The current capacity is >20 tons, with thermal latent COP's around 0.5. Oak Ridge TAHP projects are concentrating on small to medium capacity commercial and residential applications.
- The corrosive nature of liquid desiccants has resulted in somewhat expensive materials being used in existing large commercial liquid desiccant systems. It is anticipated that use of plastics may reduce material costs in future smaller capacity systems, but this has yet to be demonstrated.

- Liquid desiccant components and systems have not received as much DOE research attention as advanced solid desiccant components and systems. Much of the data on performance of liquid systems is proprietary, resulting in a limited data base.
- Development of a detailed phenomenological model for spray or packed column liquid desiccant dehumidifiers comparable to the existing model for rotating parallel plate dehumidifiers is beyond the scope of this work. Several models for liquid desiccant components are available in the open literature (Kettleborough 1986; Sick 198 ; and Baschulte 198) but most contain empirical relations from proprietary sources and a degree of uncertainty is associated with applying these models to a wide range of TAHP/desiccant hybrid system operating conditions.

While we have not examined liquid spray or packed column dehumidifiers further in this report, we feel that they may be applicable for larger capacity hybrid systems and that anticipated developments extending the range of economical application of liquid systems to smaller capacities could warrant examination in future efforts.

Among the hygroscopic salts (lithium chloride, calcium chloride, lithium bromide and possible mixtures), we selected lithium chloride for further system analysis for the following reasons:

- Lithium chloride dehumidifier wheels are commercially available and are considered the state-of-the-art with over 10,000 commercial dehumidifiers in operation. Using lithium chloride would provide a baseline for comparison with other desiccants.
- To obtain the same performance for a dehumidifier, a much greater mass of lithium bromide than that of lithium chloride is required (Maclaine-cross, 1974). This is due to lower absorption capacity of lithium bromide. The cost of lithium bromide ($31/kg*) is higher than that of lithium chloride ($21.5/kg*). Therefore, a dehumidifier with lithium chloride is cheaper and smaller.

---

*Small volume sale of approximately 2 kg, 1987 dollars (Aldrich 1987).

- Calcium chloride ($15/kg*) is more corrosive and has lower absorption capacity than lithium chloride and, thus, is not suitable.
- Data on thermodynamic properties of mixtures of salts are not sufficiently available for modeling and analysis.

Among the commercially available solid desiccants (see Figure 3-2), we selected microporous silica-gel and molecular sieves for further system analysis. Silica-gel was selected because:

- Nienberg (1977) and Pla-Barby et al. (1978), recommend microporous silica-gel rather than other industrial solid desiccants because of the gel's high moisture recycling capacity in the temperature range of 60°C to 90°C, which reduces the amount of desiccant needed for a given dehumidifier performance; this can be seen in Figure 3-2 for the relative humidity range of one to 70 percent which can be encountered in the operation of desiccant cooling systems;
- Jurinak (1982), investigated the properties of desiccants (maximum water capacity, isotherm shape, heat of adsorption, hysteresis upon thermal cycling, thermal capacity, and moisture diffusivity in the desiccant particles) that can influence the performance of a dehumidifier. He concluded that the microporous silica-gel, out of all the available commercial solid desiccants, is the most attractive material for use in dehumidifiers for cooling applications;

Molecular sieves were chosen for the following reasons:

- Molecular sieves were recommended by Wurm et al. (1979) for use in gas-fired desiccant cooling systems because of their physical stability, resistance to fouling, and high moisture recycling capacity at the high temperature ranges available from gas-fired heaters (120°C to 220°C). It is expected that at high regeneration temperatures (above 120°C) silica-gel gradually sinters (collapse of internal fine pores) and loses its adsorption capacity. Also, if gas exhaust is directly used to regenerate the desiccant, the combustion products will not reduce the adsorption capacity of molecular sieves as much as they will reduce the capacity of silica-gel.

---

*Small volume sale of approximately 2 kg, 1987 dollars (Aldrich 1987).

At the beginning of this project, we anticipated that a wide range of temperatures (70°C to 300°C) would be available from the waste heat from the internal combustion engine. We investigated desiccant materials desirable for high regeneration and low regeneration temperatures and, thus, silica-gel (suitable for low regeneration temperature) and molecular sieves (suitable for high regeneration temperatures) were selected. Attention focused on commercially available desiccants rather than on hypothetical desiccants like Collier's hypothetical Type 1M (Collier 1985) since the project includes defining performance and cost of a physical system.

A parallel passage, rotary dehumidifier wheel was selected for further analysis in this study for the following reasons:

- Packed beds (for solid desiccants) and packed columns (for liquid/salt solution desiccants) exhibit excessive pressure drop for the large air volumes handled by air-conditioning systems.
- Parallel passage geometries have high rates of heat and mass transfer and low pressure drop.
- Switched bed dehumidifiers add another level of complexity to system control. Performance, costs, and sizes for switched beds are similar to continuously rotating dehumidifiers.
- A verified model for silica-gel rotating parallel passage dehumidifiers was available and could be extended to molecular sieve and impregnated lithium chloride dehumidifiers.

To summarize, among all the commercially available desiccants, we selected three desiccant materials (microporous silica-gel, molecular sieves, and lithium chloride) and the parallel passage rotary wheel geometry for further analysis and assessment to arrive at an optimum desiccant material for the best system performance. Final assessment will be done in Section 5.1. The thermophysical properties of these selected desiccants are needed for dehumidifier analysis.

3.4 Properties of Selected Desiccant Materials

The thermophysical properties of desiccants that are needed to be used in the detailed dehumidifier model, outlined in Section 4, are:

- o Equilibrium adsorption isotherms (i.e., desiccant water content W as a function of air relative humidity r and temperature T);
- o Heat of adsorption or absorption of the desiccant, hs, as a function of desiccant water content, W;
- o Density of the desiccant, rhod;
- o Specific heat capacity of desiccant, Cd;
- o Moisture diffusivity in the desiccant, mdsg;.

If the desiccant material is supported in a dehumidifier matrix using an inert material, the following matrix properties are also needed:

- o Specific heat capacity of the inert material, Ci;
- o Desiccant fraction of the matrix, sgf;
- o Fraction of desiccant mass that is effective for sorption process, Xeff.

Note that the equilibrium isotherm, hs, rhod, Cd, mdsg and Ci are material properties and are not dependent on the dehumidifier geometry. However, sgf and Xeff can change depending on the dehumidifier design.

3.4.1 Silica-Gel

Microporous silica-gel, one of the leading adsorbents in the field of dehydration, is an amorphous, extremely porous form of silica (SiO_2) and is completely inert (W. R. Grace 1966). Because of its high internal surface area and its enormous number of angstrom-sized pores, this desiccant has the ability to adsorb nearly 40 percent of its weight of an adsorbate such as water. Table 3-1 shows some of the physical properties of the microporous silica-gel. The microporous silica-gel comes in various shapes (crushed irregular or spherical bead) and sizes (mm to micron). The thermophysical properties of microporous gel are independent of its shape and size.

Fine, crushed, irregular silica-gel particles have been used or investigated for desiccant dehumidifiers (Kim et al. 1984; Schlepp and Barlow 1984; Schultz 1985) Recently, Bharathan et al. (1986a) used the finer spherical bead (microbead) silica-gel in a spirally wound parallel plate dehumidifier wheel. This method resulted in more uniform air passage gaps than previously obtained with crushed, irregular gel in a similar wheel (Schultz 1985).

Bharathan et al. (1986b) have also shown that more compact and slightly more efficient dehumidifiers are possible with microbead silica-gel compared with crushed gel. For these reasons, we selected the superior performing microbead silica-gel (Grade 3A, Fuji Davison Chemical Ltd.).

3.4.1.1 Equilibrium Adsorption Isotherm

The manufacturer's data on microbead Grade 3A silica gel (Fuji Davison Chemical, Ltd.) at 298.15K (77°F) were fit with a fourth order polynominal (Bharathan et al. 1986a).

$$W = 0.475\ r + 0.787\ r^2 - 1.428\ r^3 + 0.596\ r^4 \qquad (3\text{-}1)$$

The manufacturer's data are in good agreement with the experimental data obtained by Pesaran et al. (1986). We have used Dubinin-Polanyi theory (Ruthven 1984) to obtain equilibrium isotherm at other temperatures. Jury and Edwards (1979) have shown that this theory is highly accurate for microporous silica-gel. The Dubinin-Polayni theory predicts that

$$W = f\ (T \ln r)\ . \qquad (3\text{-}2)$$

Combining equations 3-1 and 3-2, one can obtain

$$W = 0.475\ rr + 0.787\ (rr)^2 - 1.428\ (rr)^3 + 0.596\ (rr)^4 \qquad (3\text{-}3)$$

where $rr = \exp\ (T \ln r/Tvpi)$.

W is the desiccant water content in equilibrium with air at relative humidity of r and temperature of T. Tvpi is the temperature at which the isotherm is originally obtained, i.e., Tvpi = 298.15 K. Figure 3-3 shows the equilibrium isotherms of microbead silica-gel at various temperatures.

3.4.1.2 Heat of Adsorption

The heat of adsorption is heat released when the water molecules transform from the vapor phase to the adsorbed phase (adsorption process), a process similar to condensation. During desorption, heat is required (analogous to evaporation). The integral heat of adsorption is the sum of the latent heat of condensation of water and heat of wetting (Bullock and Threlkeld 1966). The heat of adsorption of silica-gel is about 1 to 1.4 times that of the heat of condensation of water (Bullock and Threlkeld 1966). Heat of adsorption, hs, decreases to latent heat of condensation, hlv, at high desiccant water contents. The heat of adsorption can be obtained from vapor pressure equilibrium relations by using the Clausius-Clapeyron equation which is a consequence of the Second Law of Thermodynamics. The Clausius-Clapeyron relation ties the temperature dependence of the isotherms and the heat of adsorption (Ruthven 1984).

$$hs = -RT^2 \left(\partial \ln P_v / \partial \ln P_s\right)_W \qquad (3\text{-}4)$$

P_v is the partial pressure of water vapor in equilibrium with the gel at desiccant water content W and temperature T. Writing the same relation for pure water vapor and combining the two, one can obtain

$$hs/hlv = \left(\partial \ln P_v / \partial \ln P_s\right)_W . \qquad (3\text{-}5)$$

According to the Dubinin-Polayni theory,

$$W = f\ (T \ln r) = f\ (g(W)) \qquad (3\text{-}6)$$

where

$$g\ (W) = T \ln r .$$

Since

$$r = P_v/P_s \ ,$$

one can write

$$g\ (W) = T \ln\ (P_v/P_s)$$

or

$$\ln P_v = \ln P_s + g\ (W)/T \ . \qquad (3\text{-}7)$$

Combining equations 3-5 and 3-7, one can obtain

$$hs(W)/hlv = 1 + (T \ln r\ (W))\ \partial\ (1/T)/\partial\ (\ln P_s) \qquad (3\text{-}8)$$

Note that since r is a function of W, hs is also a function of W. According to Clausius-Clapeyron relation, hs/hlv is not a function of temperature. Water vapor saturation pressure is only a function of temperature and can be obtained from the following correlation (Maclaine-cross 1974):

$$P_s(T) = \exp\left(23.28199 - 3780.82/T - 225805/T^2\right) \ . \qquad (3\text{-}9)$$

P_s is in Pascals and T is in Kelvin. This relation is accurate within 0.5 percent for temperatures from 0°C to 95°C and care should be used for temperatures far from this range. Figure 3-4 shows the variation of heat of adsorption of the microbead silica-gel with desiccant water content.

3.4.1.3 Density of Individual Desiccant Particles

Density of particles depends on the true density of nonporous solid desiccant, rhos, and pore volume of particles, v_p, through the relation

$$rhod = rhos/\left(1 + v_p\ rhos\right) \ . \qquad (3\text{-}10)$$

Using the data given in Table 3-1, we obtained

$$rhod = 1131 \ kg/m^3 \ .$$

The particle density affects:

- o The calculation rate of diffusion of moisture in the particle or the effective Lewis number; and
- o The amount of mass per unit volume in the dehumidifier.

3.4.1.4 Thermal Heat Capacity

The specific heat capacity of microbead silica-gel is given in Table 3-1 and is

$$Cd = 921 \ J/kg \ K \ .$$

The presence of heat capacity within the desiccant matrix affects the behavior of heat and mass transfer processes and, thus, the performance of a dehumidifier.

3.4.1.5 Moisture Diffusivity

The mechanism of diffusion of water molecules into the microporous silica-gel is surface diffusion (Pesaran 1983). For surface diffusivity of water molecules on the adsorbent surface, Sladek et al. (1974) provides a general correlation. Pesaran (1983) has shown that with a correction factor, this correlation can be used for microporous silica-gel.

$$mdsg = 1.6 \times 10^{-6} \exp(-0.974 \times 10^{-3} \ hs/T) \ m^2/s \ . \qquad (3\text{-}11)$$

For microporous microbead silica-gel, the value of mdsg varies from 5×10^{-11} to 3.5×10^{-9} m^2/s for the temperature range of 25 to 90°C. According to this correlation, the moisture diffusivity increases with increase of desiccant water content. mdsg is used in the calculation of the effective Lewis number.

3.4.1.6 Heat Capacity of Inert Support

At present, to contain the silica-gel particles in a laminar flow channel geometry, a support matrix is needed. A polyester tape, consisting of a Mylar film and pressure sensitive adhesive layers on both sides, has been researched (Bharathan et al. 1986a) and used in the fabrication of a bench scale microbead silica-gel test dehumidifier. The heat capacity of the tape can be taken to be that of Mylar (Smith et al. 1956).

$$Ci = 1039 + 4.14\ t\ (J/kg\ K) \qquad (3\text{-}12)$$

t is temperature in °C.

3.4.2 Molecular Sieves

Molecular sieves (W. R. Grace Co., Davison Molecular Sieves) are crystalline alkali metal aluminosilicates with a three-dimensional interconnecting network of silica (SiO_2) and alumina tetrahedra (Al_2O_3). Molecular sieves are a synthetic form of zeolites and have stronger sorption characteristics than natural zeolites such as chabazite, gmelinite and heulandiate. Molecular sieves are usually used in dehydration of gases where low effluent dew points are required and for removal of H_2S, CO_2, and mercaptans. Various types of commercial molecular sieves are available: A, X and Y molecular sieves. Type A is usually used for dehydration purposes. Type 4A was selected for further analysis because this type is considered the universal product for dehydration of most fluids (W. R. Grace, Davison Molecular Sieves). Type 4A is the sodium form of molecular sieves and has an effective pore opening of about 4 Å. They will adsorb molecules with effective pore sizes of less than 4 Å, such as water which has critical molecular diameter of 3.2 Å, and exclude the large molecules. This makes Type 4A molecular sieves resistant to adsorption of most hydrocarbons and pollutants. Because of its high internal surface area and its enormous number of pores, this desiccant, in bead form, has the ability to adsorb nearly 23 percent of its weight of an adsorbate such as water. Table 3-2 shows some of the physical properties of the Type 4A molecular sieves.

3.4.2.1 Equilibrium Adsorption Isotherm

The manufacturer's data on Type 4A molecular sieves (W. R. Grace, Davison Molecular Sieve) at 25°C and 60°C were fitted to several mathematical relations by using the least squares method. The best fits were obtained using the relation

$$W = a \exp \left[b (\ln r)^2\right] \tag{3-13}$$

rather than the relation

$$W = a * r/(1 + b * r) , \tag{3-14}$$

which is usually used for Brunauer Type 1 isotherms.

Figure 3-5 shows the least square fits according to Equation (3-13) to the manufacturer's data. Note that above 25 percent relative humidity, the molecular sieve is almost saturated at 25°C and 60°C. The fitted values are within eight percent of the data. For further analysis, we used the curve fit at 25°C, which is a better fit, and corrected it for other temperatures by using the Dubinin-Polayni theory explained in Section 3.4.1. We obtained the following correlation to define the isotherms of Type 4A molecular sieves.

$$W = 0.228 \exp \left[-0.01404 (T \ln r)^2/(Tvpi)^2\right] \tag{3-15}$$

Tvpi is the reference temperature of 298.15 K.

Figure 3-6 shows the equilibrium isotherms of the Type 4A molecular sieves at various temperatures according to Equation (3-15). Note that the molecular sieve has a high adsorption capacity at low relative humidities.

3.4.2.2 Heat of Adsorption

The heat of adsorption of Type 4A molecular sieves can be as much as 80 percent greater than the latent heat of condensation (W. R. Grace, Davison 4A Molecular Sieves). The heat of adsorption of molecular sieves is higher than

that of silica-gel because of different orientation of water molecules in the smaller molecular sieves' pores. Similar to silica-gel, the heat of adsorption of molecular sieves can be obtained using the Clausius-Clapeyron relation. Using Equations 3-8 and 3-15, the heat of adsorption of the molecular sieves can be obtained. Figure 3-7 shows the variation of heat of adsorption of Type 4A molecular sieves with desiccant water content. Note that the trend of variation of the heat of adsorption of the molecular sieve with desiccant water content is different than the silica-gel as shown in Figure 3-4. Similar trends were obtained by Barrer and Fender (1961) for natural zeolites and it is due to the size of the pores of the molecular sieves.

3.4.2.3 Density of Individual Desiccant Particles

The density of the molecular sieves' beads depends on the amount of the clay binder used in the pelletizing of the particles and varies from 978 to 1138 kg/m^3, as shown in Table 3-2. We have used the data from Carter and Barret (1973) on Davison Type 4A in this project.

$$rhod = 1121.8\ kg/m^3$$

3.4.2.4 Thermal Heat Capacity

As a conservative estimate, we used the lower value of heat capacity given in Table 3-2 for further analysis,

$$Cd = 963\ J/kg\ K\ .$$

3.4.2.5 Moisture Diffusivity

Very small molecular sieve crystals (1-10 μm) are pelletized in usable sizes by means of a clay binder. By this production process, molecular sieves obtain a very characteristic bimodal pore structure: macropores and micropores (Carter and Barret 1973). The mechanism of diffusion in the macropores is pore diffusion (most probably Knudsen diffusion), and in the micropores it is surface diffusion. Carter and Barret (1973) obtained overall

moisture diffusivity in the W. R. Grace 4A molecular sieves at 26.7°C at two water content levels:

W (kg/kg)	mdsg (m/s)
0.1660	1.52×10^{-10}
0.1864	4.28×10^{-10}

The average value of the two points has been used for all the temperatures and water contents for further analysis, i.e.,

$$mdsg = 2.90 \times 10^{-10} \ m^2/s$$

The diffusivity increases with temperature in an Arrhenius-type behavior (Sladek et al. 1974). Therefore, we expect this to be a conservatively low estimate of the diffusivity of moisture in molecular sieve particles.

3.4.2.6 Heat Capacity of Inert Support

We have assumed that the same polyester tape coated with pressure sensitive adhesive that was used for the silica-gel wheel is used to contain the molecular sieves particles.

Therefore $$Ci = 1039 + 4.14\ t \ (J/kg\ k)$$

where t is temperature in °C.

3.4.3 Lithium Chloride

Of the metal halides and glycols, lithium chloride (LiCl) is the most effective for water removal (Hougen and Dodge, 1947). It is available in the form of deliquescent crystals. Anhydrous lithium chloride is very hygroscopic and, in the presence of water vapor, turns into hydrates ($LiCl.nH_2O$ where n = 1, 2, or 3). The hydrates go into saturated solutions at constant relative humidity and then into diluted solutions. The lithium chloride solutions have

been used for dehumidification in air conditioning applications for many years (Gifford 1957) because of its characteristics: high moisture capacity; noncorrosive; odorless; stable; low vapor pressure; nontoxic; and nonflammable. Table 3-3 summarizes some of the properties of lithium chloride.

3.4.3.1 Equilibrium Adsorption Isotherm

Because of the formation of hydrates, saturated solutions and diluted solution, the isotherms of a lithium chloride/water system are quite complicated. Depending on the temperature and humidity, lithium chloride/water may go through all these phases. For the temperatures and humidities encountered in the operation of desiccant cooling systems, one can expect that the lithium chloride/water system goes through these phases. Therefore, we need to know the isotherm of lithium chloride/water at these phases.

A large body of data is available for the isotherms of lithium chloride solutions (e.g., Umera 1967; Schlunder 1963; and Johnson and Molstad 1951). Some of the available data were discussed and analyzed by Maclaine-cross (1974). He found that Johnson and Molstad's data were the most reliable. Johnson and Molstad obtained vapor pressure data of lithium chloride solutions at 30°C, 50°C, and 70°C at concentrations of 0.05 to 1 kg LiCl/kg water. Maclaine-cross (1974) fitted a quartic polynomial by least squares method to experimental data of Johnson and Molstad at temperature of 50°C. The resulting polynomial was

$$P_{va} = 12339 - 6738\ c - 50608\ c^2 + 82955\ c^3 - 36944\ c^4\ \text{Pa}\ . \qquad (3\text{-}16)$$

P_{va} is the water vapor pressure of the LiCl solution at 50°C and c is the concentration of LiCl in the water in kg LiCl/kg water. The relation between desiccant water content W and c is

$$W = 1/c\ (\text{kg } H_2O/\text{kg LiCl})\ . \qquad (3\text{-}17)$$

The relative humidity can be simply obtained by $r = P_{va}/P_s$ (Tvpi = 323.15). Then the isotherm at 50°C can be built by plotting W as a function of r, as shown in Figure 3-8.

To evaluate the water vapor pressure (P_v) of the solution at other temperatures (T), Maclaine-cross (1974) gives

$$P_v = P_{va} \exp \left[G_o (c) (1 - tvpi/T) - G_1 (c) \ln (Tvpi/T)\right] \qquad (3\text{-}18)$$

where

$$G_1 (c) = -5.013918 + 3.726854 c^2 + 14.101374 c^3 - 23.440175 c^4 \qquad (3\text{-}19)$$

and

$$G_o (c) = 15.977747 (hs/hlv)_{Tvpi} - G_1 (c) , \qquad (3\text{-}20)$$

and

$$(hs/hlv)_{Tvpi} = 1 - 0.3755 c^2 + 3.1321 c^3 - 4.5742 c^4 + 1.9829 c^5 . \qquad (3\text{-}21)$$

$(hs/hlv)_{Tvpi}$ is obtained by fitting a quintic polynomial to the values of hs/hlv calculated from Johnson and Molstad's heat of dilution data at 50°C. Figure 3-8 shows the isotherms of LiCl solutions at several other temperatures. It can be seen that the equilibrium capacity of LiCl solution is not a strong function of temperature.

At lower relative humidities, diluted LiCl solutions do not exist as shown by Thakker et al. (1968) (See Figure 3-9). When the water vapor pressure in equilibrium with the diluted solution decreases, a point will be reached that the solution becomes saturated (Point A on Figure 3-9). The concentration of LiCl in water at the saturation point depends on the temperature of the solution. At this water vapor pressure and lower water content, a hydrate will form and coexist with the saturated solution (line A-B on Figure 3-9). Depending on the temperature, three lithium chloride hydrates can exist: monohydrate, dihydrate and trihydrate. At temperatures between 20°C and 60°C, only a monohydrate exists. As the water content of the monohydrate/ saturated solution decreases at the constant relative humidity, a point will be reached that only the monohydrate salt is present (Point C on Figure 3-9).

Monohydrate salt exists over a range of relative humidities at a constant water content (Line C-D on Figure 3-9) until anhydrous LiCl salt starts appearing (Point C on Figure 3-9). After this point, if the water content is decreased, more of the LiCl becomes anhydrous (Line C-D on Figure 3-9), until LiCl completely becomes anhydrous (Point D on Figure 3-9). As it can be seen, at low relative humidities (e.g., below 10.7 percent for 50°C), the isotherm of LiCl will consist of two vertical and two horizontal lines. Although simple for modeling purposes, they will act as discontinuities and will result in instabilities in most numerical models and procedures such as the ones that are discussed in Section 4 for modeling of the performance of dehumidifiers. Using lines with slightly different slopes is also expected to result in numerical instabilities. In order to avoid these instabilities, we have used a polynomial at these low relative humidities to replace the horizontal and vertical lines. The polynomial was obtained for 50°C with the following conditions:

- The polynomial passes through relative humidity of 10.7 percent (Thakker et al. 1968) and water content of 1.0576 kg H_2O/kg LiCl data from Johnson and Molstad.
- The polynomial passes through the middle of Line B-C of Figure 3-9 i.e., relative humidity of 0.078 (= (0.107 + 0.05)/2) and water content of 0.4245 kg H_2O/kg LiCl.
- The polynomial passes through the origin, i.e., relative humidity of zero and water content of zero.
- The derivative of the polynomial with respect to relative humidity passes through the origin.

By using the above conditions, the following third order polynomial was obtained for 50°C:

$$W = 8.98266\ r^2 + 779.3669\ r^3 \text{ for values of } r < 0.107 \qquad (3\text{-}22)$$

To correct for other temperatures, we assumed that the Dubinin-Polayni theory holds for LiCl salts. We have made this assumption with some reservation.

Figure 3-10 shows the isotherm of LiCl at 50°C over the whole range of relative humidities. Data from Thakker et al. (1968) are shown on this figure also.

3.4.3.2 Heat of Sorption

Since lithium chloride goes through different phases as it picks up moisture, the correlation to define the heat of sorption is different for each phase. For dilute solutions of lithium chloride, Maclaine-cross (1974) fitted a polynomial to the values of hs/hlv calculated from differential heat of dilution data by Johnson and Molstad (1951) to obtain Equation 3-21. This equation is expected to be valid below c of 0.9455 kg LiCl/kg H_2O or W above 1.0576 kg H_2O/kg LiCl. Using this equation, heat of sorption of LiCl solutions is up to 15 percent higher than that of latent heat of condensation.

The value of heat of sorption of LiCl monohydrate in equilibrium with the anhydrous LiCl is 3466 kJ/kg water at 25°C (Thakker et al. 1968), or about 42.05 percent higher than latent heat of condensation at 25°C. In order to approximate the heat of sorption of LiCl below W of 1.0576, a straight line was passed through the following points:

W	hs/hlv	Source
0	1.4205	Thakker et al. (1968)
1.0576	1.1544	Equation (3-21)

The resultant correlation is

$$hs/hlv = 1.4205 - 0.2518\ W,\ W < 1.0576\ . \qquad (3\text{-}23)$$

Figure 3-11 shows the variation of heat of sorption of lithium chloride as a function of desiccant water content.

3.4.3.3 Density of Lithium Chloride

The density of lithium chloride below W of 1.0576 is taken to be that of the anhydrous salt from Table 3-3, i.e.,

$$\text{rhod} = 2068 \text{ kg/m}^3, \; W \leq 1.0576 \; .$$

For W > 1.0576, the density of the solution is taken to be that of water; i.e.,

$$\text{rhod} = 1000 \text{ kg/m}^3, \; W > 1.0576 \; .$$

As can be seen later, because of high diffusivity of moisture in lithium chloride, the effective Lewis number is at the lowest value in using either of these two limits.

3.4.3.4 Specific Heat Capacity

The heat capacity of the lithium chloride below W of 1.0576 is taken to be that of anhydrous salt from Table 3-3.

$$Cd = 1140 \text{ (J/kg K)}, \text{ for } W \leq 1.0576 \; .$$

For W > 1.0576, Maclaine-cross (1974) has fitted a correlation by the method of least squares to the heat capacity data by Lange and Durr (1926) at 26.5°C

$$Cd = 4182 - 5140/W + 6860/W^2 - 3606/W^3 \text{ (J/kg K) for } W > 1.0576 \; . \quad (3\text{-}24)$$

3.4.3.5 Moisture Diffusivity

The sorption rates of water vapor pickup by anhydrous and hydrated salts of lithium chloride are frequently assumed to be so fast that diffusion in the gas controls the process (Anzelius and Angew 1926; Hougen et al. 1953; Lightfoot et al. 1962). However, Onischak and Gidaspow (1969) do not agree with this assumption and suggest that the sorption rate is controlled by

diffusion of a solution into the dry salt matrix. The value of diffusivity for this sorption mechanism is not presented. No other information on the diffusivity of moisture into the anhydrous and hydrated salt of LiCl could be found in the open literature. Hawlicka (1984) provides data on diffusivity of moisture in dilute solutions of H_2O - LiCl at 25°C. His lowest value of diffusivity is

$$msdg = 2.0 \times 10^{-9}\ m^2/s\ .$$

At higher temperatures, one can expect higher diffusivities because of Arrhenius type behavior. This value was selected for all water content and temperature ranges. Using this value, conservative estimates of effective Lewis numbers will be made. However, because mdsg is high, a lower bound of an effective Lewis number is expected.

3.4.3.6 Heat Capacity of Inert Support

Lithium chloride cannot be contained in laminar flow parallel passage geometries the same way that solid desiccants are contained. Instead of bonding fine particles to a tape, lithium chloride is usually impregnated within a porous material such as fiberglass (Maclaine-cross 1974). The heat capacity of fiberglass is Edwards et al. (1979).

$$Ci = 800\ J/kg\ K\ .$$

3.4.4 Desiccant Materials Limitations

Each of the above discussed desiccant materials have limitations for practical use. These limitations are processability, regeneration temperature, and resistance to pollutants.

The processability is the ease with which the desiccant can be used for fabrication of a dehumidifier. As discussed before, the preferred dehumidifier geometries are laminar flow channel geometries. At present, none of these desiccants (silica-gel, molecular sieves, and lithium chloride) can be directly employed in a dehumidifier, they all need a support structure.

The silica-gel and molecular sieves particles can be bonded by adhesive to both sides of a very thin polyester film. Then the coated film can be wound into a laminar flow channel dehumidifier. This process is somewhat costly and limits fabrication of large diameter dehumidifiers with uniform passage sizes. The lithium chloride salt can be supported by a thin porous film. At high relative humidities (above 15%) the lithium chloride/water solution is kept in the porous film by capillary forces. Depending on the amount of the lithium chloride in the porous film and operating relative humidities, the lithium chloride solution may supersaturate the porous material. Super saturated conditions may result in dripping as the capillary forces cannot hold the lithium chloride in the porous material (Maclaine-cross 1974). As the solution drips off of the dehumidifier, the mass of desiccant in the dehumidifier is reduced which adversely affects the performance of the dehumidifier. In these circumstances the dehumidifier needs to be re-impregnated with lithium chloride. Some consider this a drawback of lithium chloride dehumidifiers.

The temperature limit for regeneration depends on properties of the desiccant and support structure. Silica gel is susceptible to sintering at high temperatures. According to W. R. Grace (1986) silica-gel can be regenerated with temperatures up to 315°C. High temperature results in collapse of the internal fine pores forming larger pores and reducing the internal surface area and the adsorption capacity of the desiccant. A recommended maximum temperature for regeneration of silica gel is 176°C (W. R. Grace). One source suggests that this may be too high; Mikhail and Shebl (1970) present a case with sintering starting gradually at 120°C. No practical temperature limitation exists for clay binder molecular sieves. Solid particle wheel limitations may be influenced by the temperature tolerance of the winding tape and adhesive. The upper temperature bound for the Mylar used in the SERI test article is 150°C. The only temperature limitation of lithium chloride is its melting temperature of 614°C--well above practical regeneration temperatures. Similarly, the temperature at which the fiberglass matrix begins to deform is much greater than temperatures expected in the system.

All desiccants can adsorb or absorb materials (pollutants) other than water vapor. This can reduce (degrade) the water vapor sorption capacity of the

desiccant at a rate which depends on the level and type of the pollutants. This degradation or desiccant contamination results in reduced performance of the dehumidifier. In the industrial applications, desiccants can lose up to 50% of their capacity after five to ten years of use. However, industrial drying operating conditions are much more severe than those of air conditioning applications. Little data are available in the open literature on the degradation of desiccants in dehumidifiers for air conditioning applications. Because molecular sieves have smaller pores than silica-gel, molecular sieves are more resistance to adsorption of large pollutant molecules. Smaller pores are desirable when exhaust gases from a combustion engine are directly used for regeneration of desiccants. It should be pointed out that adsorption of process-side pollutants by a desiccant dehumidifier can have the advantage of improving the indoor air quality and may be considered a desirable feature of desiccant cooling systems.

3.5 Summary

The performance of a desiccant dehumidifier depends on the properties of the desiccant material. Based on information in the literature, previous experience and engineering judgment, we selected three desiccant materials among the commercially available solid, liquid and hygroscopic salt desiccants. These desiccants were: microporous silica-gel, Type 4A molecular sieves, and lithium chloride. The thermophysical properties of these desiccants, required for modeling efforts, were presented. Table 3-4 compares some of the properties of the three desiccants. Figure 3-12 compares the equilibrium isotherms of these desiccants at 50°C, and Figure 3-13 compares the heat of sorption upon moisture pickup. Note that these isotherms are for the desiccant materials only. The moisture adsorption capacity of a desiccant matrix (desiccant plus support matrix) is generally lower than the capacity for the desiccant alone. These data will be used in the modeling effort for final assessment of optimum dehumidifier and system performance in Section 5.

Table 3-1. Physical Properties of Microporous Silica-gel (W. R. Grace, 1984)

Pore Volume (v_p)	0.43×10^{-3} m^3/kg
Average Pore Diameter	22 Angstroms (22×10^{-10}m)
Internal Surface Area	$(720 - 800) \times 10^3$ m^2/kg
True Density, no porosity (rhos)	2200 kg/m^3
Thermal Conductivity	0.144 W/m °K
Thermal Heat Capacity (Cd)	921 J/kg °K

Table 3-2. Physical Properties of Type 4A Molecular Sieves (W. R. Grace, Davison Molecular Sieves; W. R. Grace, 1966)

Pore Volume (v_p)	0.78×10^{-3}/kg
Average Pore Diameter	4 Angstroms (4×10^{-10} m)
Internal Surface Area	$(600 - 800) \times 10^3$ m^2/kg
Particle Density (rhod)	978 - 1138 kg/m^3
Thermal Heat Capacity (Cd)	963 - 1046.75 J/kg K

Table 3-3. Properties of Lithium Chloride (Foote Miteral Company, 1957)

Melting Point	614°C
Density of Anhydrous Salt at 25°C	2068 kg/m^3
Thermal Heat Capacity (Cd)	1140+ J/kg K
Solubility in Water	0.637 kg/1 kg water at 0°C 1.300 kg/1 kg water at 95°C

+ value at 47°C (Touloukian and Buyco 1970)

Table 3-4. Comparison of Properties of the Selected Desiccant Materials

Property	Desiccant Material		
	Silica Gel	Molecular Sieves	Lithium Chloride
Manufacturer	Fuji Davison	W. R. Grace	Lithium Corporation of America
Type	Grade 3A Microbead	4A Pellets	Anhydrous
Dry Density (rhod) kg/m^3	1131	1121.8	2068
Heat Capacity of Dry Desiccant (Cd) J/kgK	921	963	1140
Heat Capacity of Support per Unit Mass of Support (Ci) J/kgK	1039 + 4.14tc (Mylar)	1039 + 4.14tc (Mylar)	800 (fiberblass)
Moisture Diffusivity in Desiccant (mdsg) m^2/s	5.0e-11 to 3.5e-9	2.9e-10 (average value)	2.0e-9

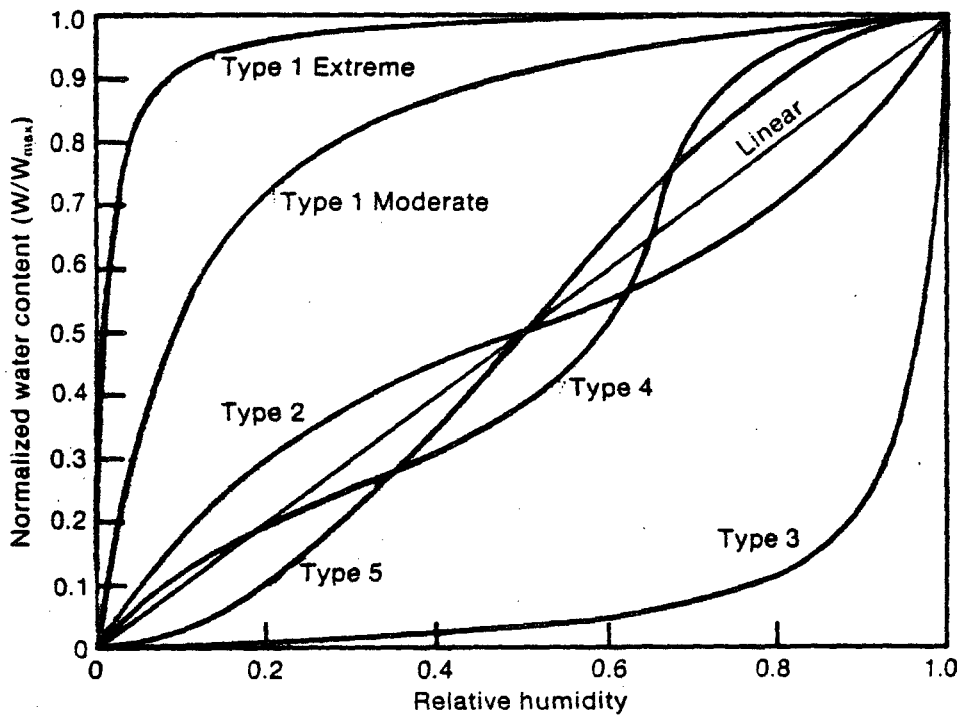

Figure 3-1. Brunauer and Linear Adsorption Isotherm Types

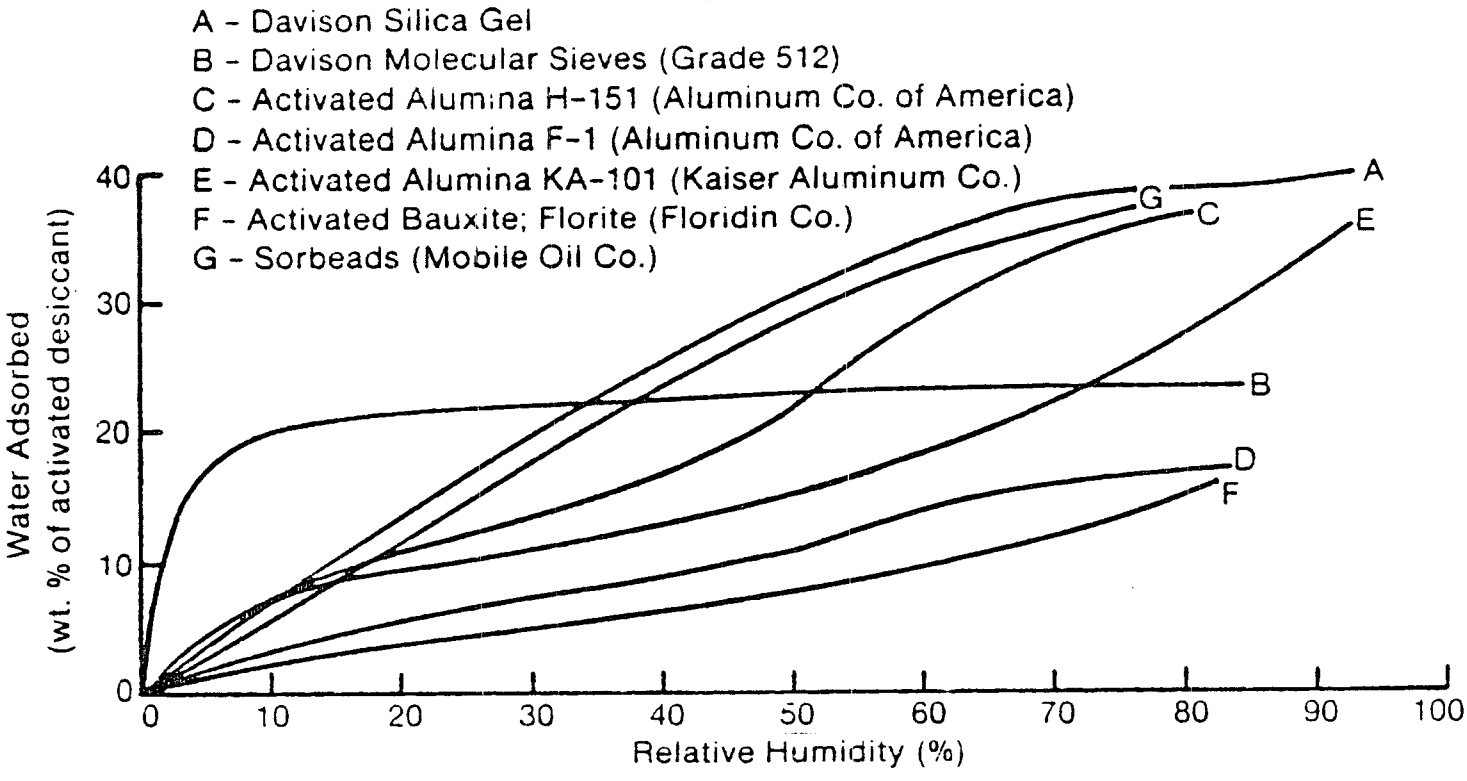

Figure 3-2. Adsorption Isotherms of Commercial Desiccant Materials (Source: W. R. Grace, 1966)

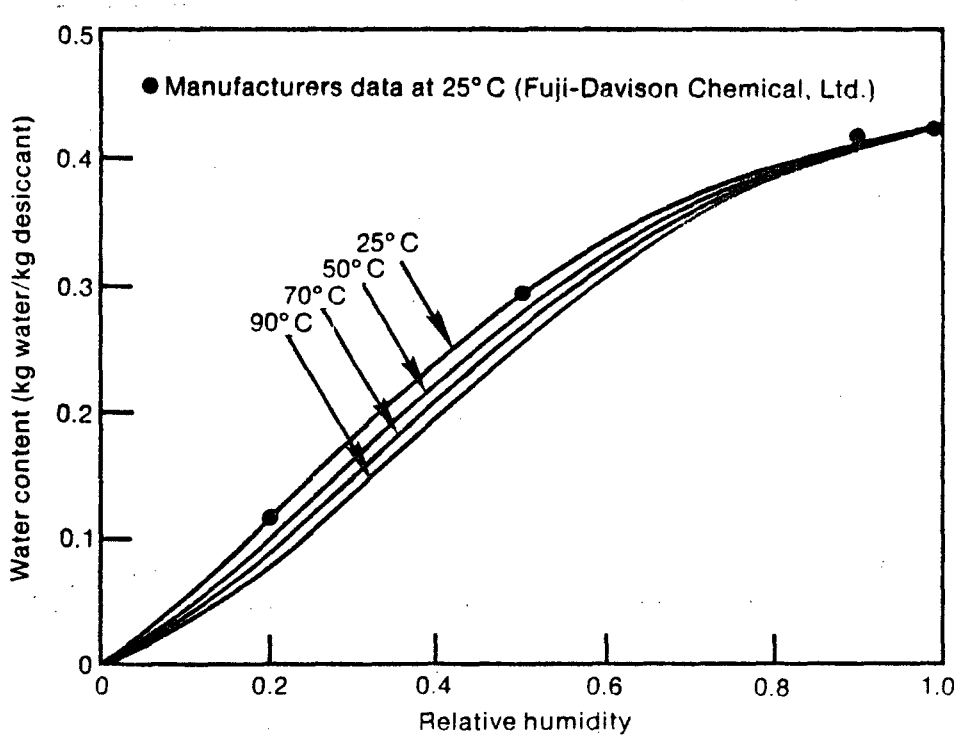

Figure 3-3. Microbead Silica-Gel Isotherms at Several Temperatures

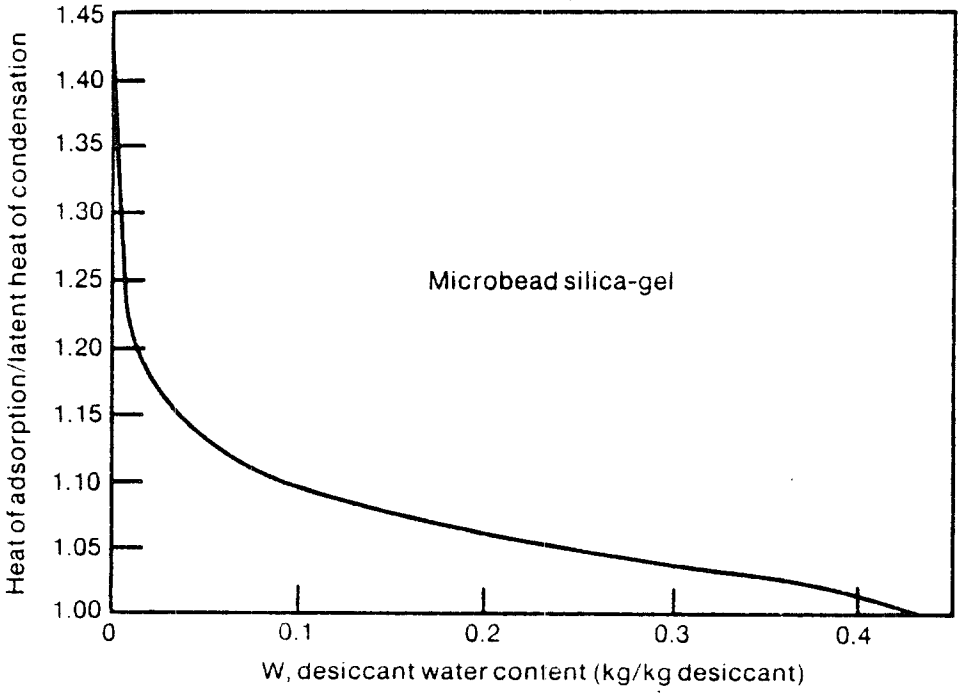

Figure 3-4. Ratio of Heat Adsorption of Microbead Silica Gel to Latent Heat of Condensation of Water (Latent Heat of Condensation of Water is 2.437×10^6 J/kg at 300K and 2.77×10^6 J/kg at 365K)

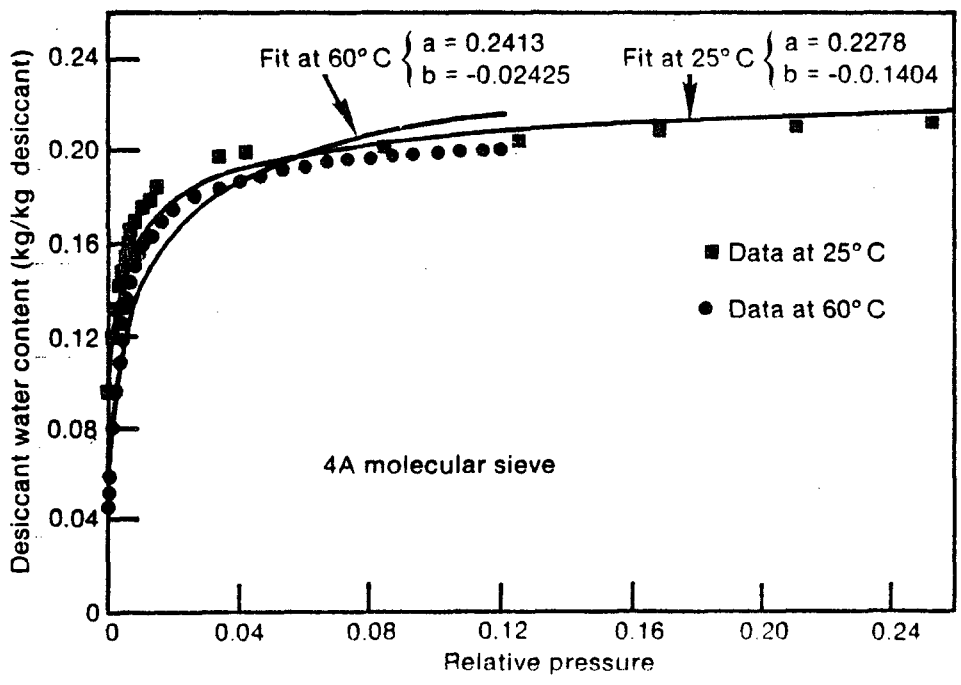

Figure 3-5. Comparison of Curve-Fits of Manufacturer's Isotherm Data for Type 4A Molecular Sieves (fit correlation $W = a \times \exp(b \times (\ln r)^2)$)

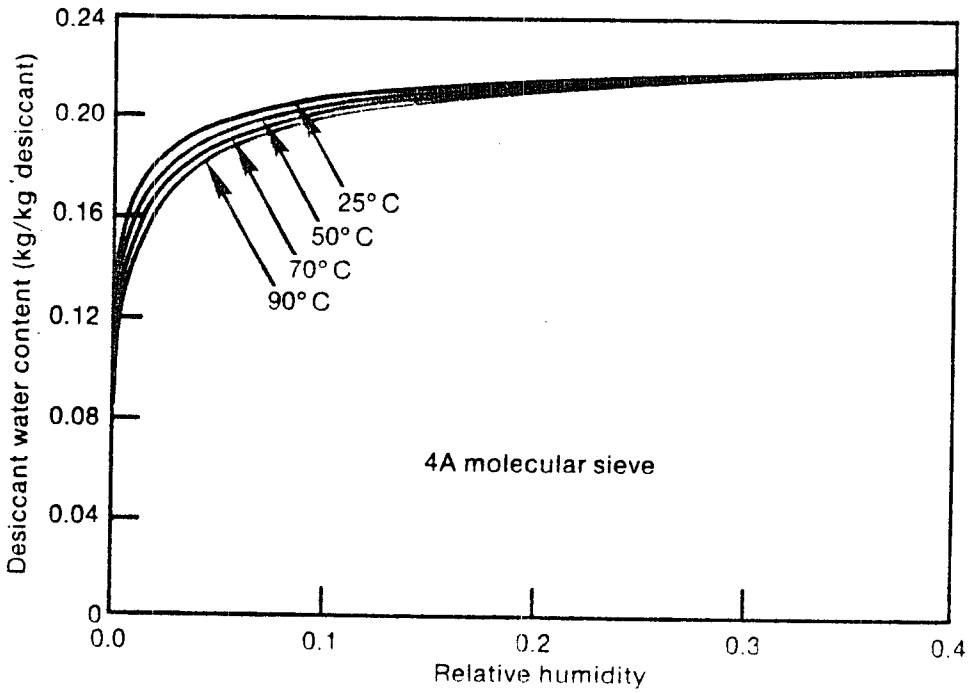

Figure 3-6. Type 4A Molecular Sieves Isotherms at Several Temperatures

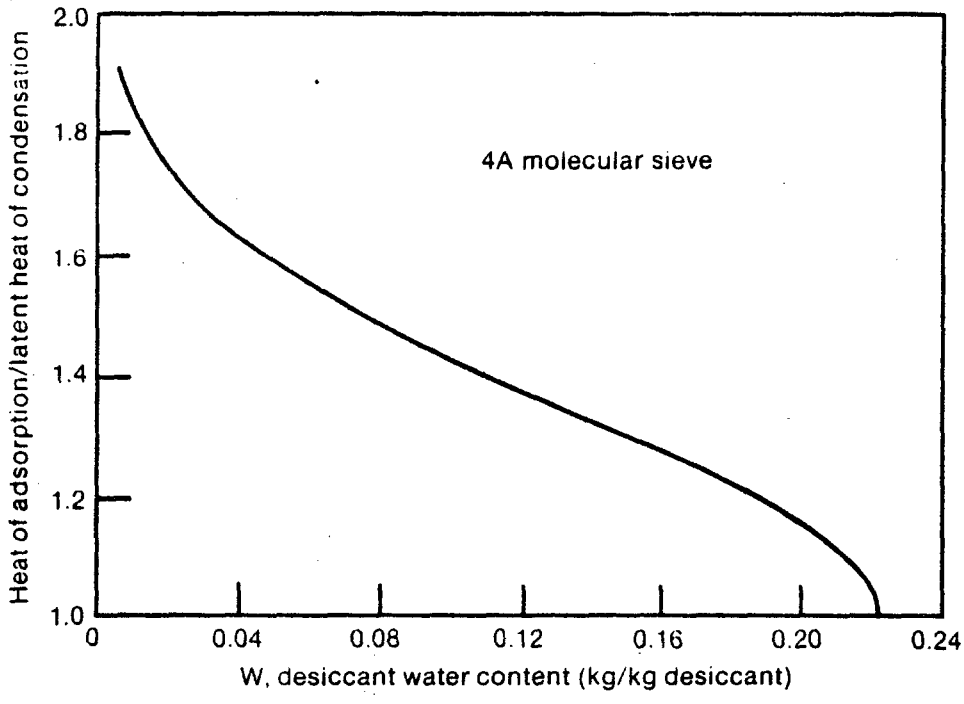

Figure 3-7. Ratio of Heat of Adsorption of Type 4A Molecular Sieves to Latent Heat of Condensation of Water (Latent Heat of Condensation of Water is 2.437×10^6 J/kg at 300K and 2.277×10^6 J/kg at 365K)

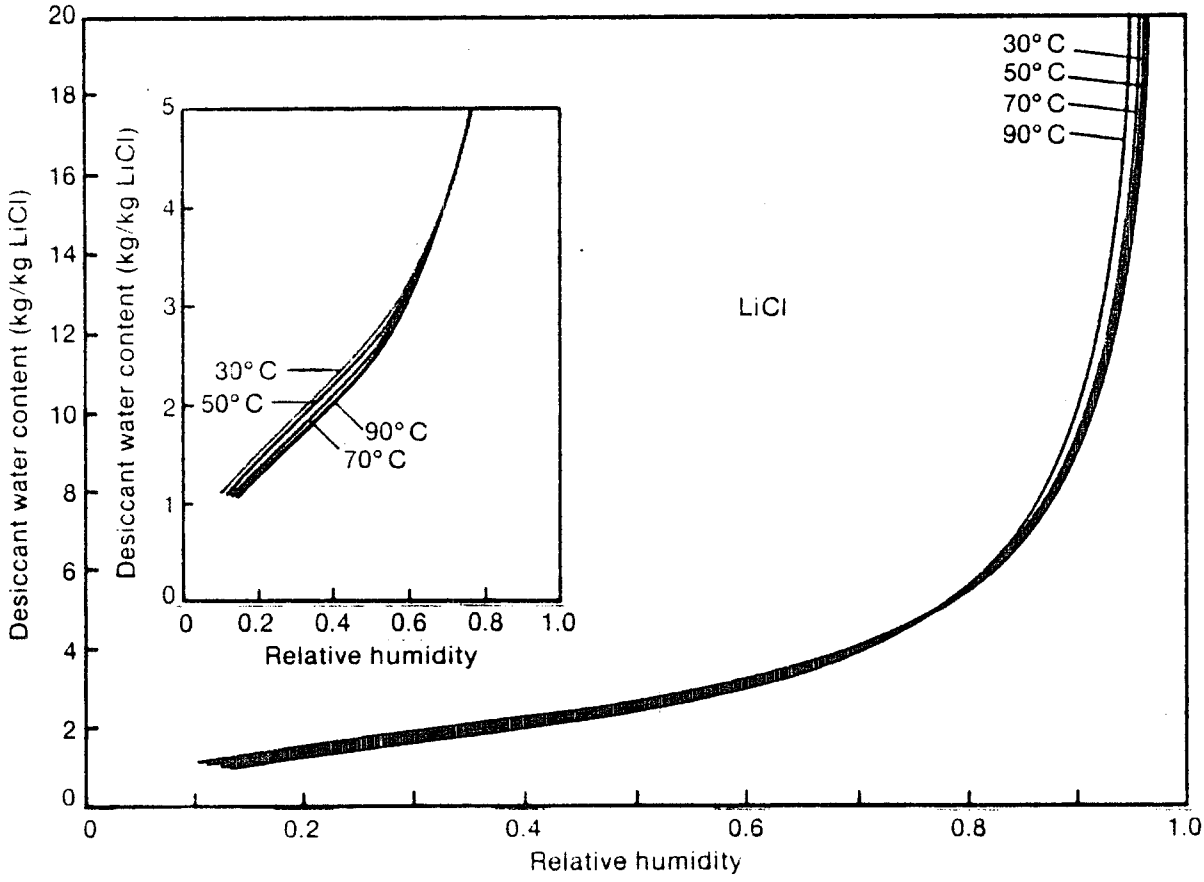

Figure 3-8. Isotherms of Lithium Chloride Solutions at Various Temperatures (From equations 3-16 to 3-21)

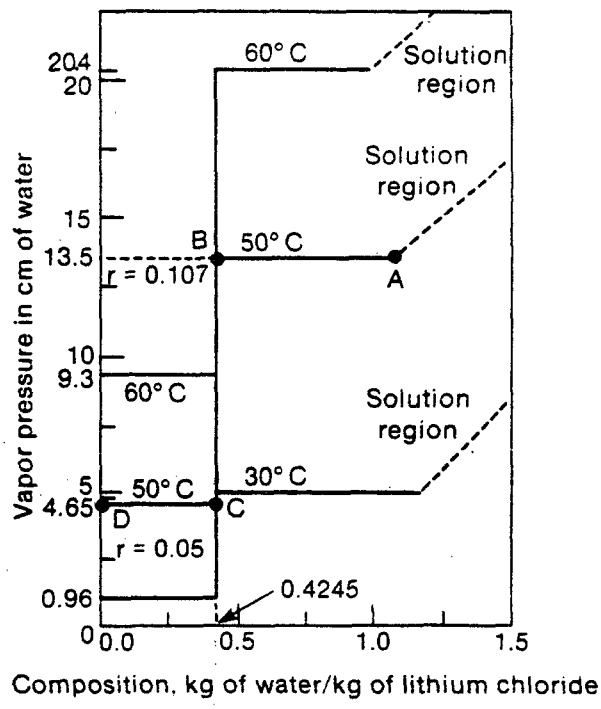

Figure 3-9. Vapor Pressure Composition Diagram for Lithium Chloride (Source: Thakker, et al., 1968)

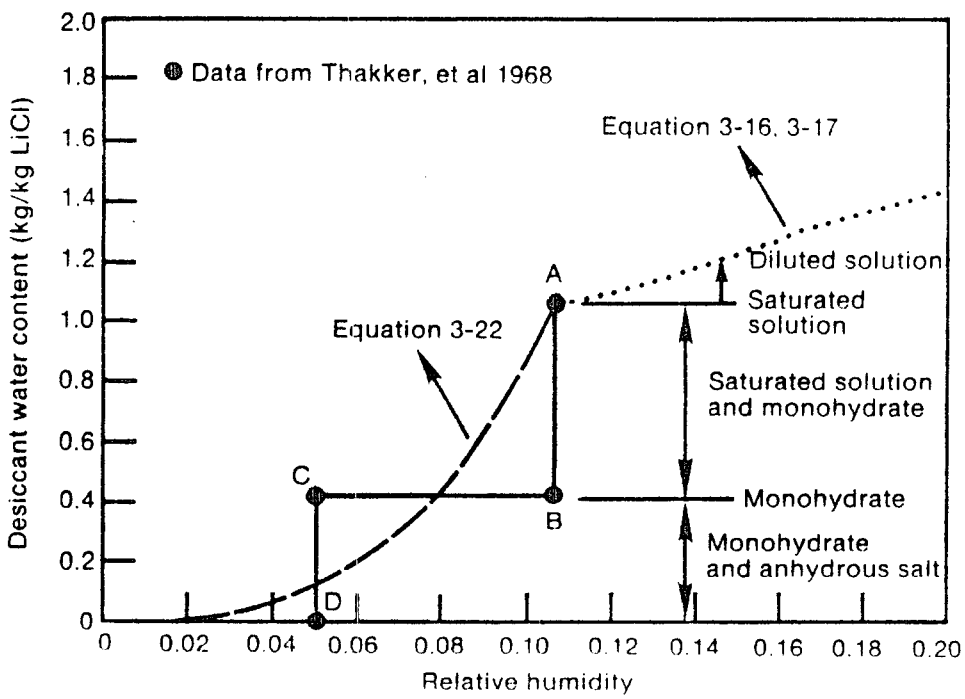

Figure 3-10. Equilibrium Isotherm of Lithium Chloride/Water System at Low Relative Humidities at 50°C. (Point A to D corresponds to the ones on Figure 3-9)

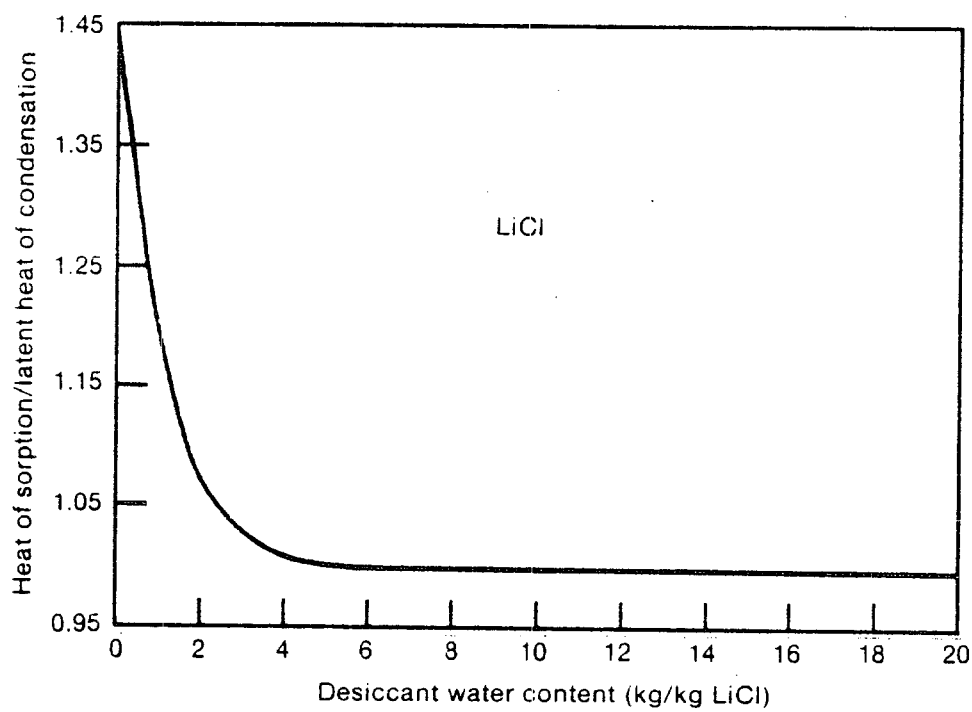

Figure 3-11. Ratio of Heat of Sorption of Lithium Chloride to the Latent Heat of Condensation of Water (Latent Heat of Condensation of Water lt 50°C is about 2.38×10^6 J/kg)

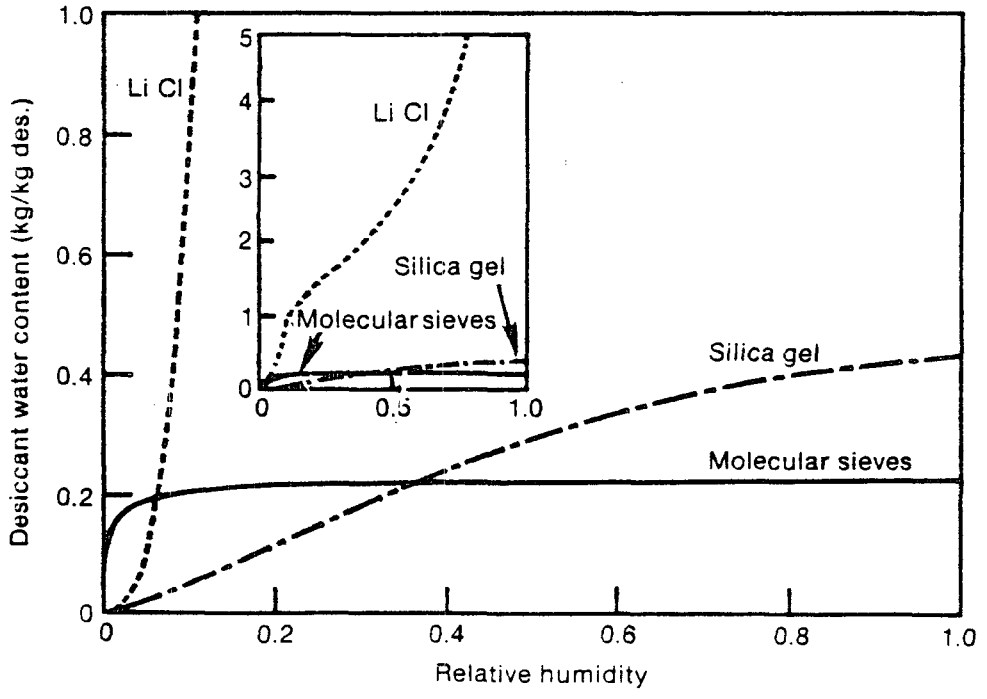

Figure 3-12. Comparison of Isotherms of Lithium Chloride Silica Gel, and Molecular Sieves at 50°C

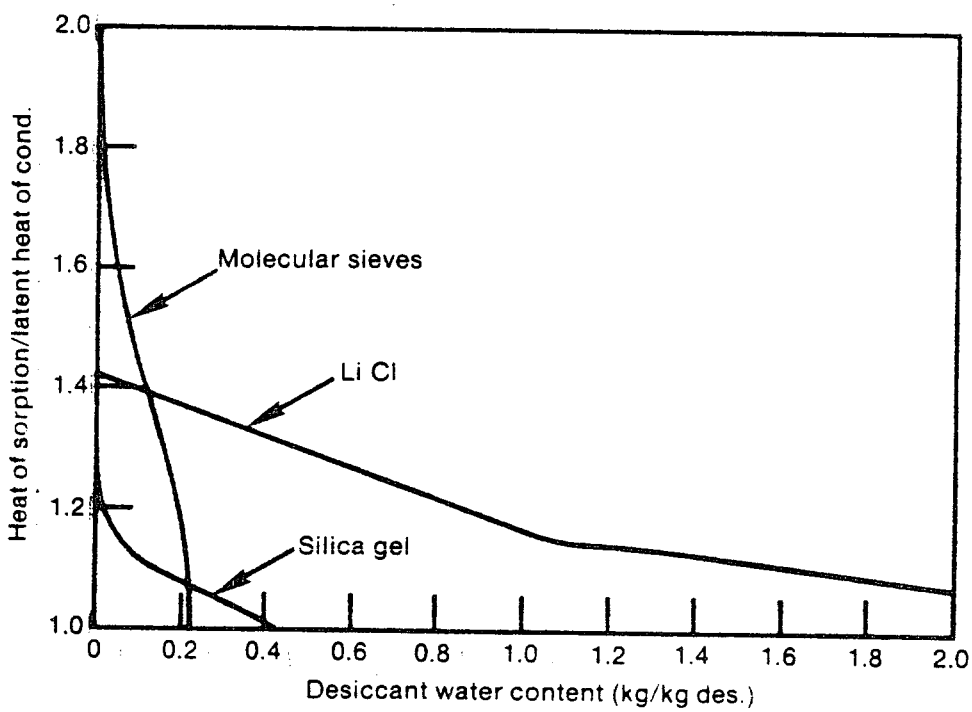

Figure 3-13. Comparison of Heat of Sorption of Li, Silica Gel, and Molecular Sieves

4.0 ROTARY DEHUMIDIFIER MODELING

This section discusses the rotary regenerative dehumidifier computer model. In addition to the general model approach and equations, we included the design parameters for the silica-gel, lithium chloride and molecular sieve wheels studied in this project.

4.1 Modeling Approach

In rotary dehumidifiers, the process airstream transfers moisture to a rotating desiccant matrix and absorbs sensible heat from the matrix. Subsequently, the matrix transfers the moisture to a counterflow regeneration airstream and absorbs sensible heat from the regeneration air. The matrix may be homogeneous or a composite of a carrier with the necessary mechanical properties to support the desiccant, possibly an adhesive film to bind desiccant to carrier, and the desiccant material itself. Combined heat-and-mass transfer occurs in the air, the desiccant, and the contaminants (if present). Heat transfer occurs in the carrier and any adhesive. Figure 4-1 shows these components, transfers, and unknowns schematically.

The combined heat and mass transfer processes in the air are well understood and are similar to those for the wet-bulb psychrometer. Wylie (1968, 1981) found for the wet bulb psychrometer that of the ten known combined heat and mass transfer effects, six almost canceled one another within a fraction of a percentage point. The remaining important four are diffusion, conduction, convection, and accommodation coefficient at the surface. These effects have been measured within a few percentage points (Hilsenrath et al. 1968; Mason and Monchick 1965). Combined heat and mass transfer in air can be represented by heat-transfer and mass transfer coefficients free of interaction effects, and for simple geometries they can be predicted accurately.

In the desiccant dehumidifier, combined heat-and-mass transfer can be more difficult to predict, especially if the dimensions of the desiccant particles in the transfer direction are comparable with those of the air passage. For high performance and low cost, the desiccant dimensions are usually made as small as practical compared with the air passage. This makes the desiccant

almost isothermal, and only the mass transfer resistance in the desiccant must be considered. The diffusivity of liquid or crystalline desiccants is reproducible, but for amorphous polymers, such as silica-gel, it can be highly dependent on manufacturing conditions. Contaminants commonly found in buildings can be adsorbed by the desiccant. Their likely chemical composition and effect on desiccant cooling systems is not known at present.

The Solar Energy Research Institute has extensive experience in modeling and experimentation with parallel passage silica gel dehumidifiers (Bharathan et al. 1986a). The model developed and used in this several year effort is outlined below.

For high-performance dehumidifier designs, temperature and concentration differences between the desiccant and matrix are small. The transfer rates between desiccant and air can be modeled adequately by independent sensible heat-and-mass transfer coefficients. Their values depend on geometry and physical properties of air and matrix. Geometry may be difficult to describe and to analyze mathematically, and matrix properties may be unknown. The dimensionless ratio of mass transfer to heat transfer resistance or effective Lewis number is a useful index of matrix performance because reducing mass transfer resistance improves dehumidifier performance.

Simultaneous, partial differential equations can be written for transfer rates, conservation, and equilibrium to describe combined heat and mass transfer in dehumidifiers. The transfer coefficients and matrix mass may be corrected for a variety of effects, such as conduction in the flow direction; so additional terms do not need to be added to the equations and the boundary conditions do not need to be modified (Maclaine-cross 1973, 1980). The same set of partial differential equations (Maclaine-cross 1973) can be used to describe all dehumidifiers of interest. Coupling in the rate equations and coupling and nonlinearity in the equilibrium relations complicate the solution of the equations. There are many empirical, approximate, (Biswas et al. 1984) and semianalytical methods that have been used in predicting dehumidifier performance, but most useful methods are: analogy to heat transfer alone (Banks et al. 1970) and finite difference (Maclaine-cross 1973) solution.

D'Alembert's classical mathematical method for solving simultaneous differential equations consists of finding multipliers for the equations that convert them to a number of independent sets of equations in canonical variables. These appear in only one equation, which then can be solved independently from the others. This approach was first applied to a combined heat and mass transfer system by Henry (1939). Banks (1972) improved the usefulness of this method by introducing the concept of combined potentials F_i and combined specific capacity ratios γ_{ij}.

When this method is applied to dehumidifiers (Maclaine-cross and Banks 1972), the enthalpy and moisture contents of the air and matrix are replaced in the equations by the combined potentials of the air and matrix. The equations are then reduced to two sets of equations, each individually describing the behavior of one combined potential. Each set of equations is analogous to those for heat transfer (alone) in rotary heat exchangers, and there exist literature tables, charts, and simplified equations for their solution (Kays and London 1964). In the analogy to heat transfer, the combined potentials are analogous to temperature or the driving potential and the combined specific capacity ratios are analogous to the ratio of matrix to fluid specific heat. The specific equations for combined potentials, specific capacity ratios and efficiencies are contained in Appendix A.

Figure 4-2 shows the combined potentials, and Figure 4-3 shows the combined specific capacity ratios for a simplified silica-gel (Banks et al. 1970). The combined potentials and specific capacity ratios used here were calculated by using the algorithms and equations described in Appendix A. It can be seen from Figures 4-2 and 4-3 that the equations are still coupled because the combined specific capacity ratios are functions of both the combined potentials. Maclaine-cross and Banks (1972) suggested that errors due to this coupling could be reduced if appropriate average values of the combined specific capacity ratios were used in the dimensionless parameters of the analogous heat transfer alone solutions. The accuracy of this suggestion and other details of the analogy method have been examined in subsequent studies and refinements (Maclaine-cross 1973, 1974; Jurinak and Banks 1982; Banks 1985).

The effect of rotational speed and mass flow ratio on the heat transfer alone regenerator effectiveness is shown in dimensionless form in Figure 4-4 (Maclaine-cross 1973). The matrix fluid capacity rate ratio for period 1, C_1 (Eq. A-23), is proportional to the rotational speed and the matrix desiccant mass and inversely proportional to the fluid stream capacity rate ratio. The overall number of transfer units, E_1, is proportional to the heat transfer coefficients. For $C_1<1$, the effectiveness is proportional to rotational speed and almost independent of the transfer coefficients. For $C_1>>1$, the effectiveness is independent of rotational speed and is asymptotic to the effectiveness of a counterflow heat exchanger.

A dehumidifier with $C_{ij}>>1$ for both combined potentials i and periods j is operating at high rotational speed. The analogy theory and Figure 4-4 predict that at high speed rotational speed effects are small and that the temperature and moisture effectiveness depend mainly on the heat- and mass-transfer coefficients and the dehumidifier outlet state is relatively uniform.

A dehumidifier with $C_{ij}<<1$ for both combined potentials i and periods j is operating at low rotational speed. The analogy theory and Figure 4-4 predict that the effectiveness are almost proportional to rotational speed and almost independent of the transfer coefficients. The temperature and moisture gradients in the desiccant matrix are strong.

If the analogy theory is used to reduce results with $C_{ij}>0.5$, the analogous heat-transfer-alone solutions should include the effect of variable specific heat (Maclaine-cross 1978; Banks 1985). Combined potential two effectiveness (η_2) is almost proportional to the active mass of desiccant on the matrix, which is an important dehumidifier performance parameter. Combined potential one effectiveness (η_1) is almost proportional to combined specific capacity ratio one (γ_1), which is strongly dependent on the effective heat capacity of the matrix.

When C_{ij} is about one, the dehumidifier is operating at a medium rotational speed. The best rotational speed for dehumidifier operation is at the low end of this speed range (Jurinak 1982; Van den Bulck et al. 1985).

4.2 Model Validation

Bharathan et al. (1986), reported on extensive experimental investigations for balanced flow silica-gel rotary-dehumidifiers. Predicted effectiveness of exchange using the above analogy method were confirmed to lie within ±10% of the measured values. Figures 4-5 and 4-6 illustrate the comparison between F_1 and F_2 effectivenesses from experiment and theory for medium wheel rotational speed. The proposed dehumidifier design for the present application is similar to the tested configurations, and thus the predicted performance is expected to be well within acceptable engineering uncertainty limits for a silica gel parallel passage dehumidifier. The method has been extended to molecular sieve and lithium chloride wheels but verification of predictions has not been performed.

4.3 General F_1, F_2 Method

The detailed description of the method used to model the dehumidifier performance was presented in Section 4.1 and equations are outlined in Appendix A. This section graphically illustrates the method and explains the influence of NTU on performance.

The F_1, F_2 method can be illustrated on a temperature-humidity diagram as in Figure 4-7. The process and regeneration inlet states are represented by A and B, respectively. The values of the pseudo-properties, F_1 and F_2, for both airstreams are then found. Note that F_1 and F_2 are only dependent on materials properties of the desiccant/water vapor/air system. F_1 is close to a constant enthalpy line while F_2 is close to a constant relative humidity line. The intersection points, C and D, can then be found. The intersection points correspond to the ideal process and regeneration outlet conditions. The efficiencies which account for non-ideality for F_1 and F_2 transfer for the process and regeneration are calculated from the physical parameters of the wheel, the rotational speed, etc. as in Appendix A. The actual process and regeneration outlet states, E and F, are calculated using the following definitions:

$$CH/CB = \eta_{F1,p}$$
$$DI/DA = \eta_{F1,r}$$
$$BJ/BD = \eta_{F2,r}$$
$$AG/AC = \eta_{F2}$$

Changing the wheel speed affects the outlet conditions of the airstreams by changing the efficiencies. Increasing the wheel speed moves the outlet conditions along the lines in the directions of the arrow. For the lowest humidity process outlet conditions, high F_2 efficiencies and low F_1 efficiencies are desired. However, increasing the rotational speed has the effect of increasing both F_1 and F_2 efficiencies as shown in Figure 4-4. The graph has the same shape for both the F_1 and F_2 exchange efficiencies. For a typical silica-gel wheel, the rotational speed ratio of C_2/C_1 is typically around 30. Adding more inert material to the wheel has the effect of decreasing this ratio. Therefore, for a given wheel, minimum process humidity is obtained at a wheel speed which balances the F_1 and F_2 efficiencies.

The effect of increasing NTU (parameter E_1) on efficiencies is also shown on Figure 4-4. Higher NTU results in higher efficiencies for a given wheel speed with the largest differences in F_1 and F_2 effectiveness occurring at lower wheel speeds. The increased NTU has the effect of shifting the process outlet condition line down and closer to the intersection point.

4.4 Dehumidifier Design Parameters

The procedure and equations presented earlier in this section and in Appendix A were used with specific wheel and material design parameters to evaluate dehumidifier performance. Variations in performance of the designed wheels are discussed in Section 5.

A design flow rate of 0.6 kg/s was used for both the process and regeneration steams. Based on the experience from the experiments discussed in Bharathan et al. (1986a) and a desired pressure loss of around 130-150 Pa, we arrived at a wheel outside diameter of 1.0 m and a wheel depth of 0.1 m. The hub diameter (inside diameter of the active portion of the dehumidifier) was set to 0.2 m. A parallel passage geometry was chosen for its high transfer rates

and low pressure drops with respect to various other flow passage geometries. Maximum number of transfer units is achieved with the minimum practicable passage size. A matrix with a center-to-center spacing of 0.8 mm for the substrate sheets seems to be practicable with current wheel manufacturing techniques. Sixteen support spokes are assumed. These parameters result in 500 layers, a winding material length of 954 m, and an available transfer area of 191 m^2.

This basic geometry was used for designs of three dehumidifier wheels utilizing the three desiccant materials selected in Section 3: Silica-gel, Molecular Sieve and Lithium Chloride. Table 4-1 presents a summary of these parameters. The remaining design parameters depend on the type of wheel. The following discussions are divided into solid particle desiccant wheels (applicable to silica-gel and molecular sieve) and hygroscopic salt desiccant wheels (applicable to lithium chloride).

Solid Particle Wheel

Experimental results of silica-gel wheels indicate the superiority of spherical (microbead) particles over crushed particles. This higher performance seems to be a result of increased particle uniformity and ease of winding resulting in more uniform passages. For the design of the solid particle wheel (silica gel and molecular sieve) we used 150-200 Tyler mesh microbead particles with a size range of 75-105 microns. The winding substrate is 10 micron thick polyester tape coated on both sides with 10 microns of adhesive. The resulting nominal air passage gap is 0.580 mm, and the hydraulic diameter is 1.16 mm. Blockage of the nominal frontal area is 27.5%, and the actual flow area per period is 0.273 m^2. The packed volume is the space that would be occupied by the desiccant if there were no unfilled volume between spheres. Packed volume of the design is 191 X 105e-06 = 0.020 m^3. The packing factor, or ratio of actual desiccant volume to the packed volume, is 0.442 based on experiment and geometric considerations. The desiccant volume is then 0.088 m^3. The tape and adhesive weight used for this design is 0.030 kg/m^2, the value used in fabricating the SERI silica-gel test article. The remaining wheel design parameters required to specify the wheel, the weight of desiccant, the desiccant per unit area, and the desiccant

fraction (weight of desiccant/total weight of tape, adhesive and desiccant) depend on the desiccant density. Table 4-2 presents these quantities for the two 105 micron particle silica-gel and molecular sieve wheels.

Hygroscopic Salt Wheel

The hygroscopic salt desiccant wheel design is similar to that of the solid particle wheel except that instead of a thin tape with particles attached by adhesive, a porous fiberglass matrix impregnated with the salt is used. We set the thickness of the matrix equal to 0.22 mm so that the blockage and design pressure drop would be equal for both solid and hygroscopic salt desiccant wheels. In order to prevent dripping of the salt solution from the matrix, the matrix should be impregnated with salt/water solution in equilibrium with air at the worst possible operating condition. For this condition we selected a temperature of 35°C and 95% relative humidity. From the LiCl/water isotherm (Figure 3-8), this results in a water/desiccant ratio of 16.6 kg H_2O/kg LiCl. For the matrix we selected fiberglass with a porousity of 85% and a density of 2600 kg/m^3 similar to the material used in commercial hygroscopic salt desiccant wheels. These parameters result in a design with 8.19 kg of fiberglass, 1.07 kg of lithium chloride, and a desiccant fraction of 0.116.

Table 4-1. Design Dimensions and Masses of the Dehumidifier

Description	Quantity	Remarks
Dimensions		
Outer diameter (nominal)	1000.0 mm	
Winding outer diameter	1000.0 mm	
Hub outside diameter	200.0 mm	
Number of spokes	16	
Number of windings	500	
Winding material center-to-center spacing	0.800 mm	Average over the wheel
Wheel depth	100.0 mm	
Nominal air passage gap	0.580 mm	
Desiccant plus support thickness	0.22 mm	
Total wheel frontal area (nominal)	0.785 m^2	
Total wheel midsection flow area	0.754 m^2	
Total wheel winding area	191 m^2	
Flow cross-sectional area per period	0.273 m^2	
Transfer area per period	86 m^2	includes blockage due to spokes

Table 4-2. Solid Particle Wheel Parameters Dependent on Desiccant Material

Property	Units	Silica-gel	Molecular Sieve
density	kg/m^3	1131	1121
desiccant mass	kg	10.00	9.91
dessicant/area	kg/m^2	0.105	0.103
desiccant fraction	kg/kg	0.778	0.775

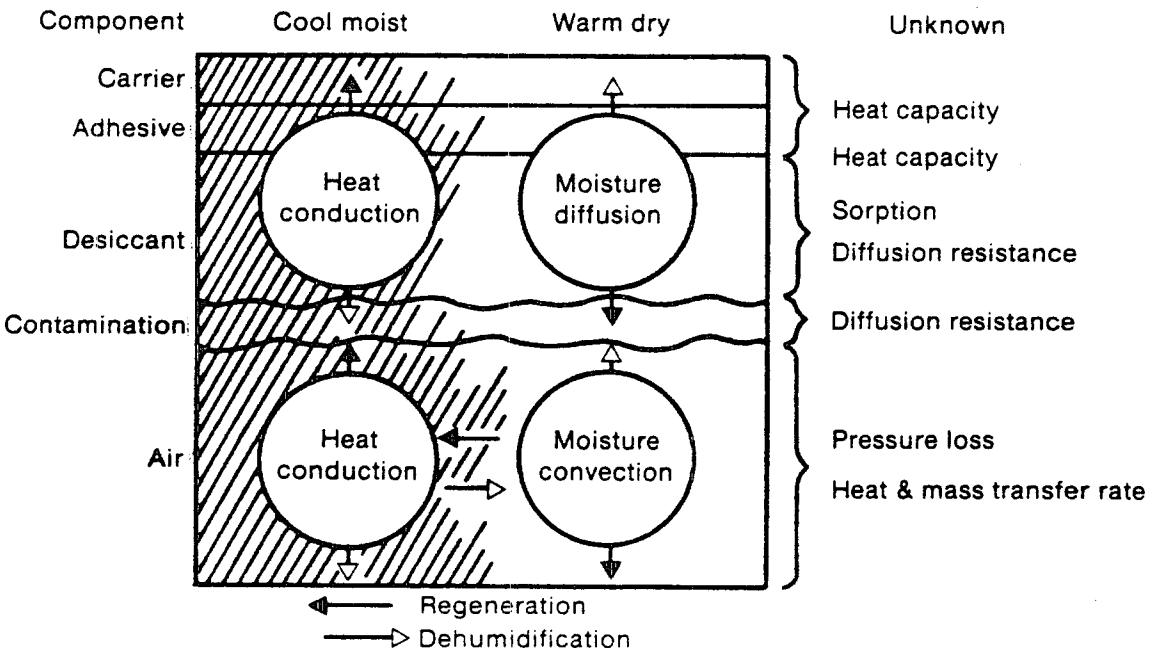

Figure 4-1. Heat and Mass Transfer Process in Dehumidifier

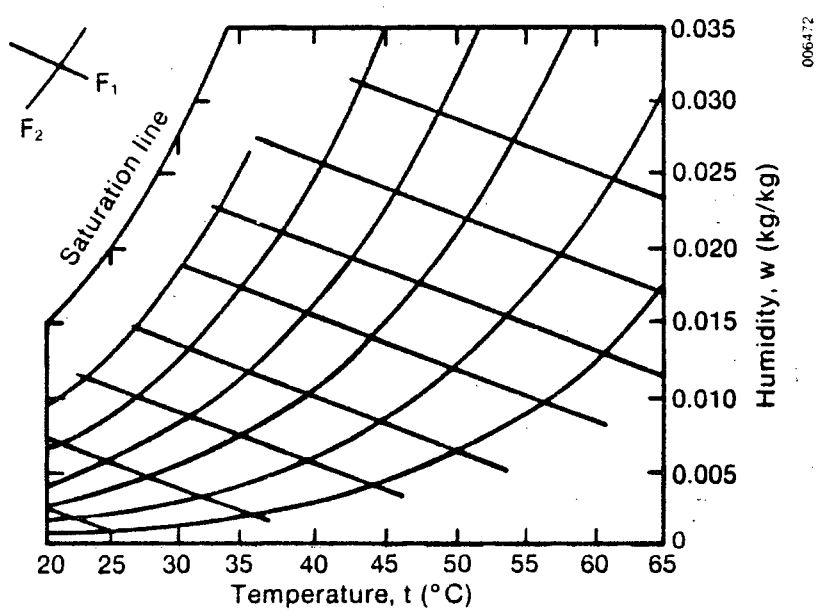

Source: Maclaine-cross 1974

Figure 4-2. Lines of Constant Combined Potentials F_i for a Simplified Silica-gel-Water-Air System

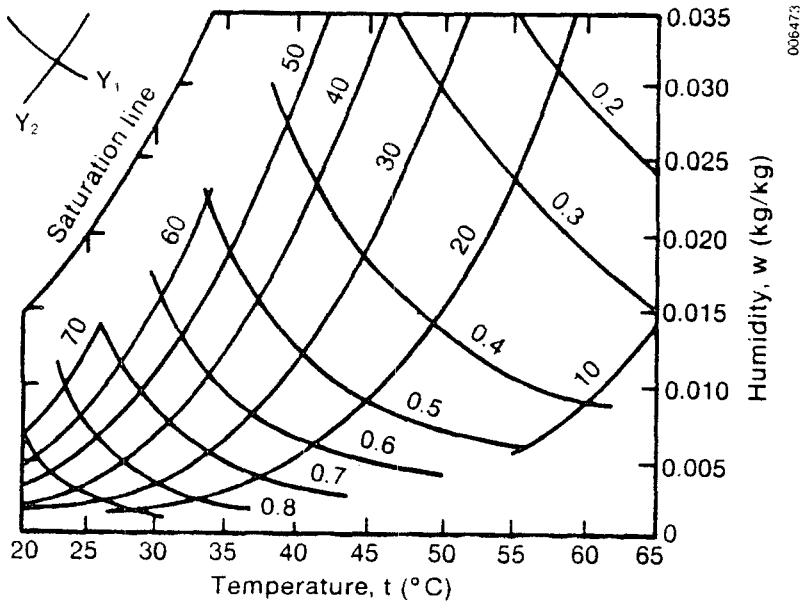

Source: Maclaine-cross 1974

Figure 4-3. Specific Capacity Ratios F_i for a Simplified Silica-Gel-Water-Air-System

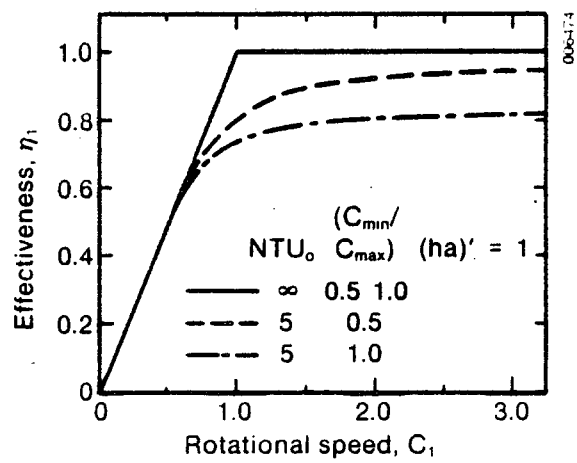

Source: Maclaine-Cross, 1974

Figure 4-4. Comparison of Infinite and Finite Transfer Coefficient Solutions for Counterflow Regenerator, Plotted as Transfer Effectiveness η_1 vs. Rotational Speed C_1

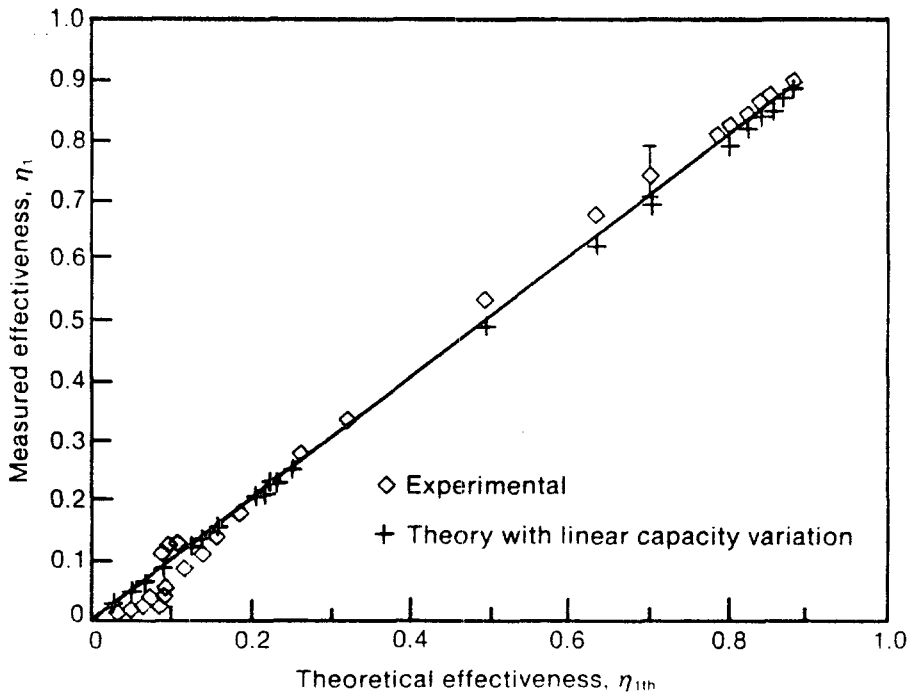

Figure 4-5. Measured F_1 Transfer Effectiveness vs. Theory

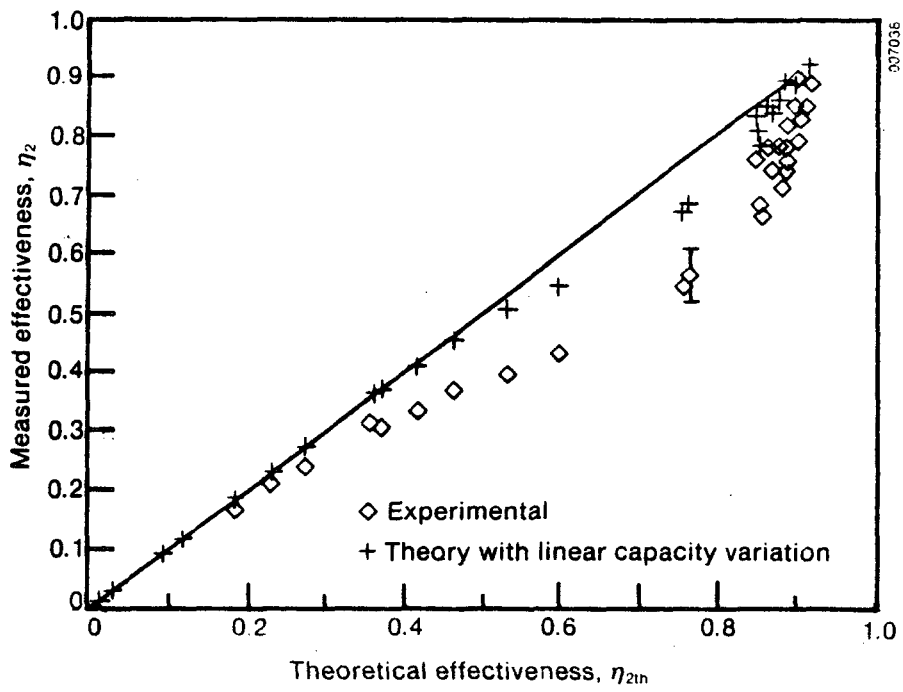

Figure 4-6. Measured F_2 Transfer Effectiveness vs. Theory

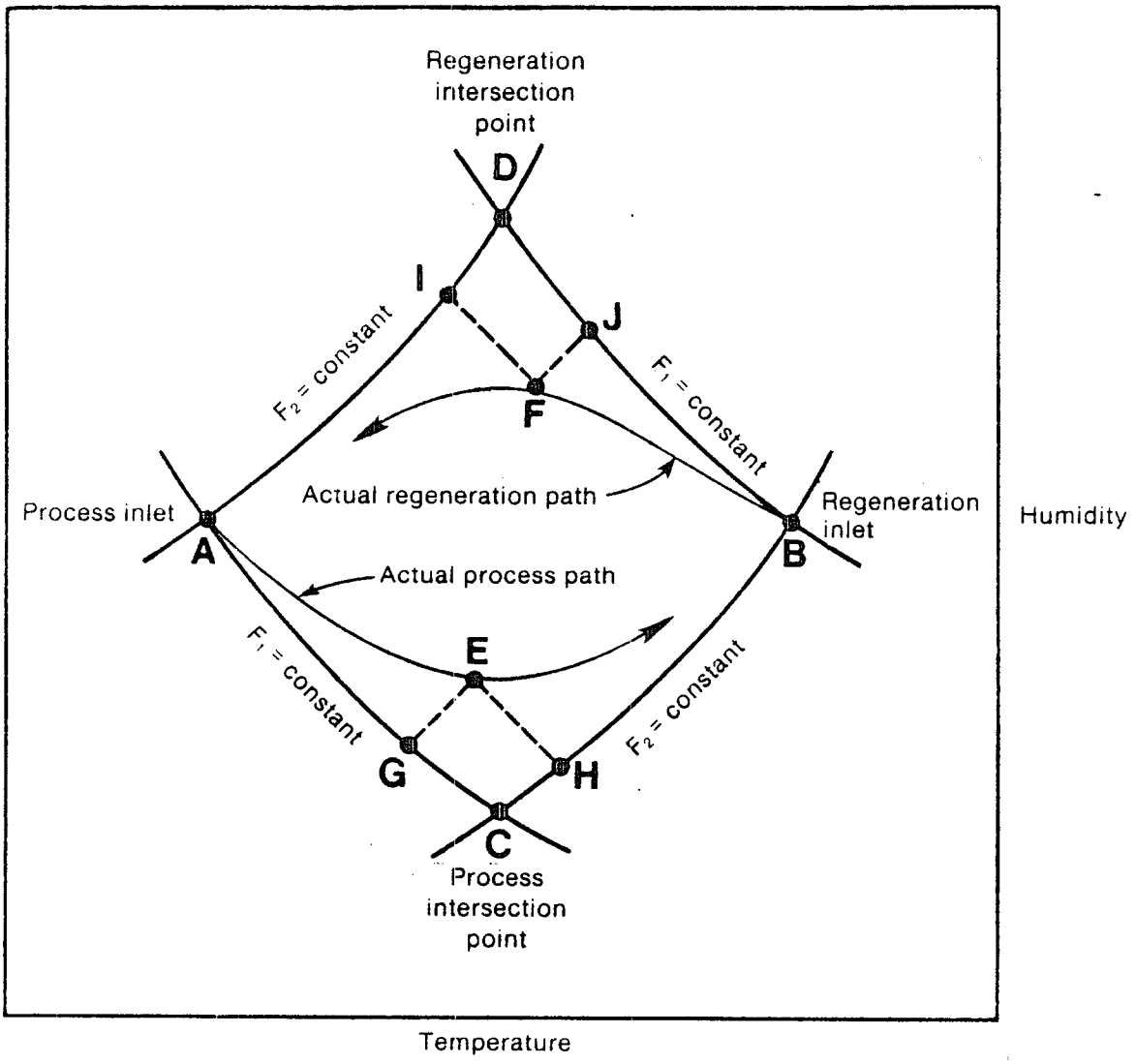

Figure 4-7. Graphical Representation of F_1, F_2, Solution Method

5.0 DEHUMIDIFIER PARAMETRIC STUDIES

This section presents the results of dehumidifier studies. The dehumidifier model is written in Turbo-Pascal for IBM-PC's and compatibles. We compared wheels with three desiccant materials, quantified the effects of varying the air mass flow rates and regeneration temperature, and examined the unbalanced flow between the regeneration and process streams.

The designs described in Section 4.4 are utilized in the discussions and analysis of this chapter. Air mass flow rate is a primary parameter. These results may be utilized for larger dehumidifier wheels (therefore, larger capacity machines), if the mass flow per unit area is held constant.

The operating conditions used to evaluate dehumidifier performances in this section generally coincide with the specified operating conditions of the systems presented in Section 6. The selection of those operating conditions is dependent on both system and component performance, particularly the dehumidifier performance and ambient and building conditions. Therefore, the selection of operating conditions is an iterative procedure. This section covers differences in performance and explanation of performance trends, while Section 6 presents the rational for selecting the operating conditions.

5.1 Comparison of Three Desiccant Wheels

Predictions of outlet process and regeneration air states for the three materials selected, microbead silica-gel, lithium chloride, and molecular sieve are compared. Both the process and regeneration airflow rates were set to the design value of 0.6 kg/s of dry air. In many TAHP/desiccant hybrid systems configurations, the amount of waste heat available results in regeneration temperatures in the same range as found in solar desiccant systems (75-90°C). Inlet airstream humidities of 0.015 kg water/kg dry air were used and the process air stream inlet temperature was set at a constant 35°C. Figures 5-1, 5-2 and 5-3 show the outlet air states for the three wheel materials for various inlet regeneration temperatures. The various outlet states for a given regeneration temperature are obtained by varying the dehumidifier wheel rotational speed as discussed in Section 4.3. There is a

minimum outlet process air humidity at a certain rotational speed which corresponds to the maximum outlet regeneration air humidity.

The process airstream outlet condition is the main desired result, since system performance depends on this condition. Increasing the regeneration temperature results in a lower process humidity and a higher process temperature. Therefore, a high regeneration temperature results in an outlet stream with lower latent but higher sensible load.

Figure 5-4 compares the three wheel materials at a regeneration inlet temperature of 85°C. Use of the microbead silica-gel wheel results in the lowest outlet humidity, but the difference between the silica-gel and lithium chloride wheel is not large. At the lowest humidity point, the silica-gel wheel produces an outlet condition of 68°C and 0.0057 kg/kg while the lithium chloride wheel produces an outlet of 64°C and 0.0061 kg/kg. The molecular sieve wheel does not remove as much water vapor from the process air as the other materials, therefore, it is less desirable. Molecular sieve materials are better suited for higher regeneration temperatures as discussed in Section 3.4.

For TAHP/desiccant hybrid systems where the vapor compression machine efficiently handles sensible cooling, it is desirable, when regeneration and supply flow rates are near equal, to use all available waste heat to obtain as high a regeneration temperature as possible. The highest regeneration temperature results in a lower flow rate through the dehumidifier to meet the latent load. A lower air flow rate in the dehumidifier minimizes the size (and cost) of the dryer component. Therefore, we have selected the microbead silica-gel wheel as the baseline wheel for the additional parametric studies and the systems analysis presented in Section 6.

5.2 Effect of Varying the Air Mass Flow Rate on Wheel Performance

A design mass flow rate of 0.6 kg/s was selected for the dehumidifier based mainly on pressure drop considerations (see Section 4.4). Figure 5-5 illustrates the effect of varying the air mass flow rate for the specified wheel design using microbead silica-gel as the desiccant. The presented

results are for equal process and regeneration flow rates, inlet humidities of 0.015 kg/kg, and inlet temperatures of 35°C and 85°C. Decreasing the mass flow rate increases the NTU resulting in higher transfer rates. Therefore, lower mass flow rate results in slightly lower outlet process humidity, but the differences in outlet air conditions are not great. This may indicate a slight over-design in the wheel and it may be desirable to redesign the wheel to reduce costs. Resolution of this question requires a full economic/performance trade-off system analysis which is beyond the scope of this study.

Increasing the mass flow rate also increases the pressure drop through the dehumidifier. Figure 5-6 illustrates the magnitude of the change. Note that the pressure drop varies linearly with mass flow since flow in the wheel passages is laminar. Since the pressure drops are calculated by using an air temperature midway between the inlet regeneration and supply conditions and not actual averages based on inlet and resulting outlet conditions, the graph is linear and applicable to any desiccant material wheel with the same air passage design as described in Section 4.4. This approximation is adequate within the tolerance of manufacturing the wheel air passages.

The small variation in process outlet conditions with changes in mass flow indicate that varying the volumetric flow to meet changing system loads is a practical control strategy as long as the air handling system is designed for the changing pressure drops.

5.3 Unbalanced Flow Performance

This section examines the performance of a silica-gel dehumidifier wheel with unbalanced flow. Unbalanced flow, as used in this report, means that is the process and regeneration air flow rates are not equal. Unbalanced flow may be particularly applicable to TAHP/desiccant hybrid cooling systems since waste heat from the engine used to drive the vapor compression machine is available at high temperatures (see Section 6). By reducing the air flow rate, the regeneration inlet temperature can be raised which results in a more effective use of the waste heat. Lower air-flow rates also allows the dehumidifier size and cost to be reduced.

To examine the performance of dehumidifiers with unbalanced flow, we identified two ideal situations which bound the operating conditions in an actual system. While engine waste exhaust heat is available at quite high temperatures (620°C), the engine cooling jacket water temperature is near the regeneration temperatures used in the parametric studies already presented (water temperature of around 100°C). Therefore, heat transfer to the regeneration air may be limited by the heat source temperature dictated by engine design. In addition the dehumidifier matrix temperature limits discussed in Section 3.4.4 must be considered. The second limit and the upper bound on regeneration air temperature is defined by constant heat transfer to the regeneration air stream, with no limit on the air stream temperature. Actual heat transfer to the regeneration air stream and temperatures of that stream lie between these two bounds.

Several conditions for these two dehumidifier studies are held constant and are similar to the conditions used in the previous parametric examinations: inlet regeneration and process humidities of 0.015 kg/kg, an inlet process temperature of 35°C, a process mass flow rate of 0.6 kg/s, and a process side cross sectional area of 0.274 m^2. Table 5-1 illustrates the regeneration air flow rates, temperatures, and the cross sectional flow area on the regeneration side which were used in the unbalanced flow studies. The regeneration cross sectional area was adjusted with the regeneration mass flow rate so that the flow per unit area and, therefore, the pressure drop would remain constant. The regeneration temperatures for the constant heat input study were calculated by using a baseline balanced flow condition of 0.6 kg/s regeneration air flow, dehumidifier inlet temperature of 85°C, and a regeneration supply initial temperature of 25°C. The diameter of the wheel is also shown in Table 5-1 assuming a constant hub diameter of 0.2 meters.

For a constant regeneration temperature, Figure 5-7 shows that balanced flow with 0.6 kg/s of air flow on the regeneration side results in maximum moisture removal. Reducing the regeneration air flow rate from the baseline balanced flow condition of 0.6 kg/s has little effect on the regeneration outlet condition. The regeneration air is picking up as much moisture as it can for the given regeneration temperature. Consequently, as the regeneration air

flow is increased from 0.2 to 0.6 kg/s, the process air outlet condition gets progressively drier and hotter.

Increasing the regeneration air flow to 0.7 kg/s, however, results in more heat being transferred to the desiccant bed, and the desiccant temperature increases. Increasing the desiccant bed temperature has two main effects which can be best illustrated by referring to Figure 3-3 which shows the desiccant water content as a function of relative humidity. Increasing the temperature slightly reduces the desiccant equilibrium water content, W, for a constant relative humidity. In addition, raising the bed temperature reduces the relative humidity for a given absolute humidity resulting in a further reduction in the bed water content. If the desiccant equilibrium water content is lowered, then less water is being removed from the air. Consequently, the process outlet conditions for 0.7 kg/s regeneration flow are not as dry as those using 0.6 kg/s regeneration flow. The increased bed temperature and the reduced moisture removal are also illustrated by the hotter and drier regeneration outlet conditions.

Figure 5-8 illustrates that for constant heat input of around 36 kW, the driest process outlet condition is obtained with nearly balanced flow of around 0.5 to 0.6 kg/s. The response is explained in a similar fashion to the constant temperature results. At lower regeneration air flow rates (and higher temperature), the bed temperature rises and less moisture is removed from the process air resulting in hotter outlet temperatures and humidities closer to the inlet states of 0.015 kg/s. Higher regeneration air flow rates and lower inlet regeneration temperatures result in inadequate moisture removal from the bed on the regeneration side. Therefore, there is less driving potential for moisture removal on the supply side.

Both the constant temperature and constant regeneration heat input studies indicate that for maximum moisture removal the regeneration air flow rate should be near or equal to the supply air flow rate. Consequently, for maximum dehumidifier performance, it is not desirable to reduce the size of the regeneration portion of the dehumidifier, even if higher temperature waste heat is available.

The conclusions and results presented in this section were used to establish the system designs and the operating conditions for the systems studies of Sections 6.0 and 7.0.

Energy Inputs	kW
Internal combustion engine (gas)	19.5
Auxiliary regeneration (gas)	6.9
Fans (electric)	5.8

Performance	COP
Complete System	
Gas	1.75
Electric	7.97
Vapor Compression Subsystem	
Gas	1.2
Desiccant Subsystem	
Gas	3.3

Flow Rates	kg/s
Supply	2.47
Regeneration	2.47
Vapor compression condenser	2.47
Engine cooling water	0.21
Engine exhaust	0.008

Cooling loads	kW	
Building		
sensible	27.7	Internal/environmental gains
latent	9.3	
total	37.0	
Ventilation		
sensible	4.6	Difference between ambient and
latent	4.6	room for dehumidification air
total	9.2	flow
Total loads		
sensible	32.3	
latent	13.9	
total	46.2	

Hardware Capacities	kW	
Vapor compression		
evaporator	23.4	All sensible cooling
condenser	39.6	Heat rejection
compressor	7.2	Work input
Dehumidification subsystem		
sensible	8.9	Due to DEC and IEC
latent	13.9	
total	22.8	
Total hardware		
sensible	32.3	
latent	13.9	
total	46.2	

Table 5-1. Parameters for Unbalanced Flow Studies

Regeneration Mass Flow (kg/s)	Regeneration Flow Frontal Area (m^2)	Wheel Diameter (m)	Regeneration Inlet Temperature	
			Constant Temperature Runs (°C)	Constant Heat Runs (°C)
0.2	0.091	0.824	85.0	—
0.3	0.137	0.871	85.0	145.0
0.4	0.182	0.916	85.0	115.0
0.5	0.227	0.958	85.0	97.0
0.6	0.273	1.000	85.0	85.0
0.7	0.318	1.040	85.0	76.0

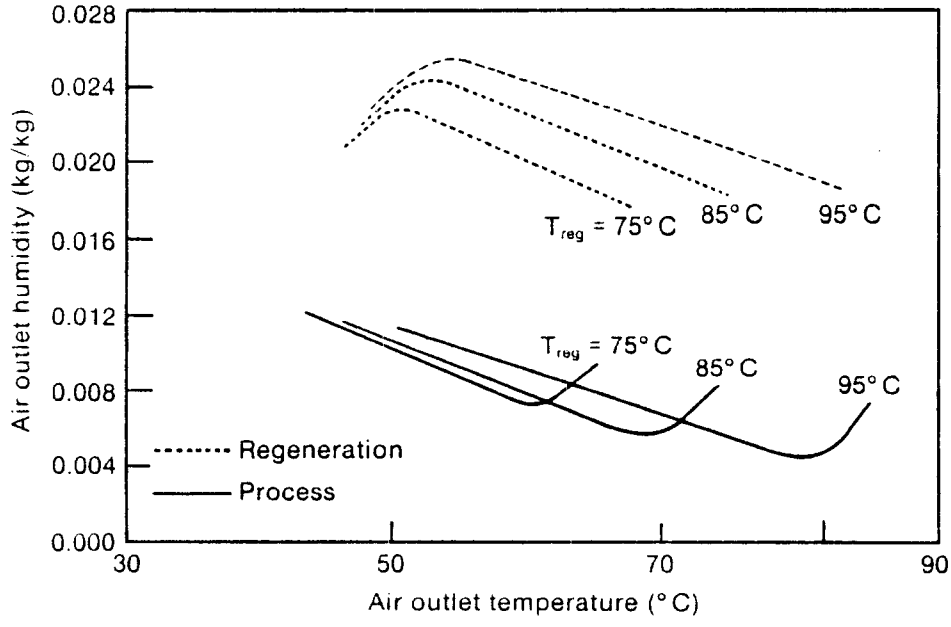

Figure 5-1. Micro bead Silica Gel Wheel Performance with Air-Flow Rates of 0.6 kg/s as a Function of Regeneration Temperature

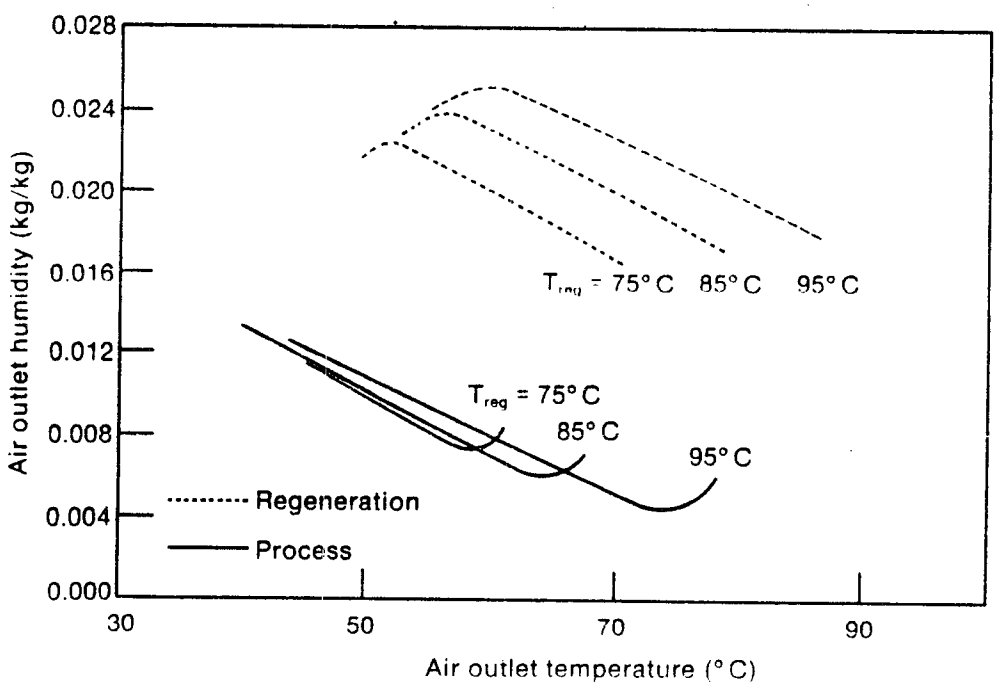

Figure 5-2. Lithium Chloride Wheel Performance with Air Flow Rates of 0.6 kg/s as a Function of Regeneration Temperature

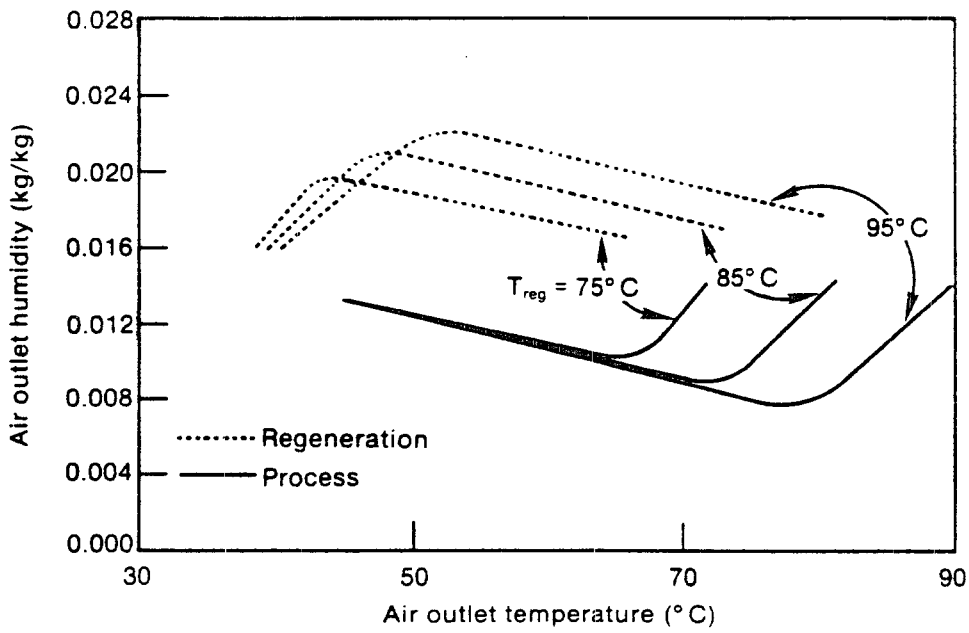

Figure 5-3. Molecular Sieve Wheel Performance with Air Flow Rates of 0.6 kg/s as a Function of Regeneration Temperature

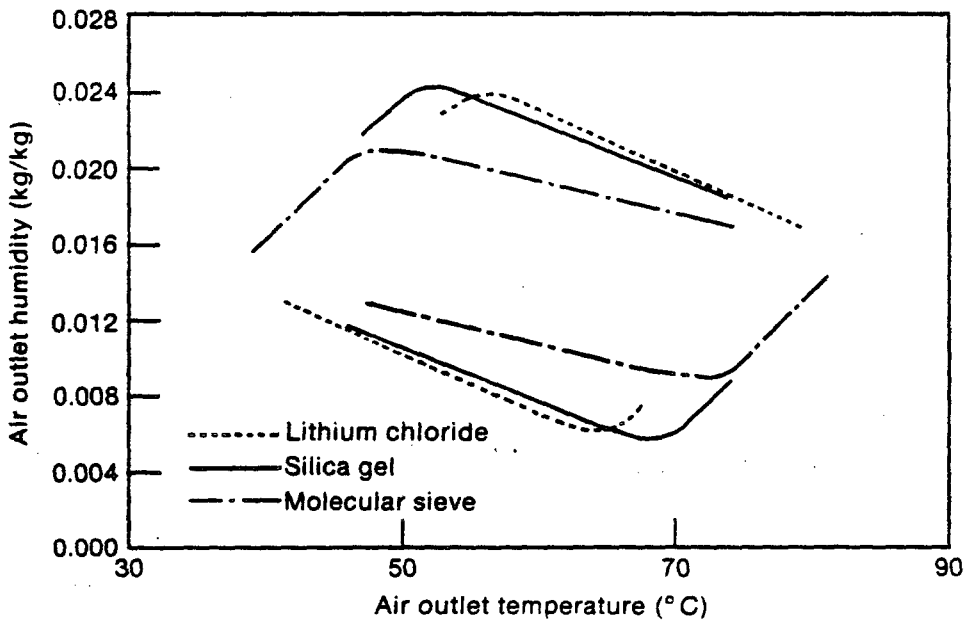

Figure 5-4. Comparison of Wheel Performance with Air Flow Rates of 0.6 kg/s and an Inlet Regeneration Temperature of 85°C

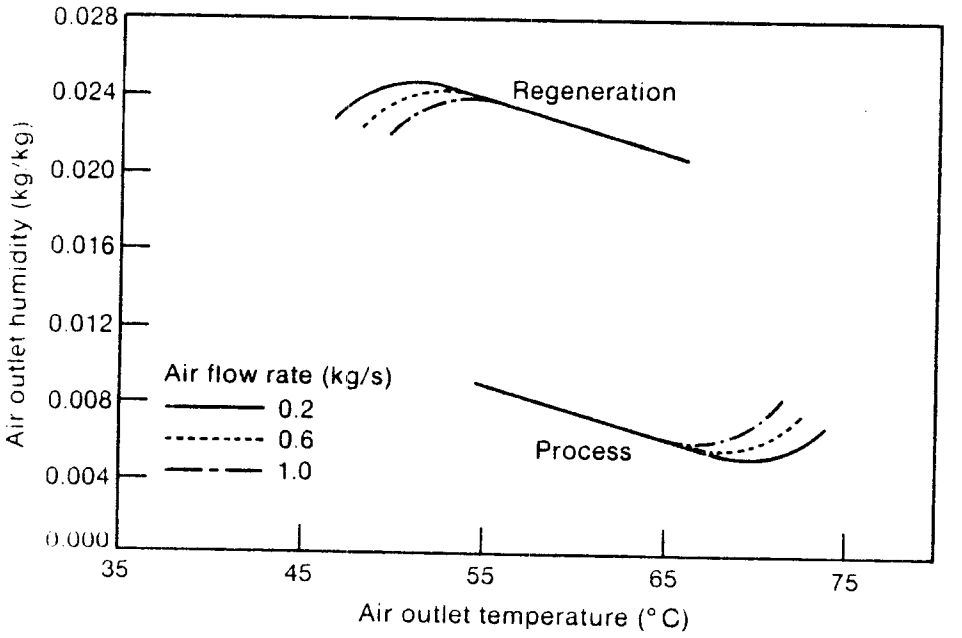

Figure 5-5. Effect of Air-Mass Flow Rate on the Silica Gel Wheel Performance

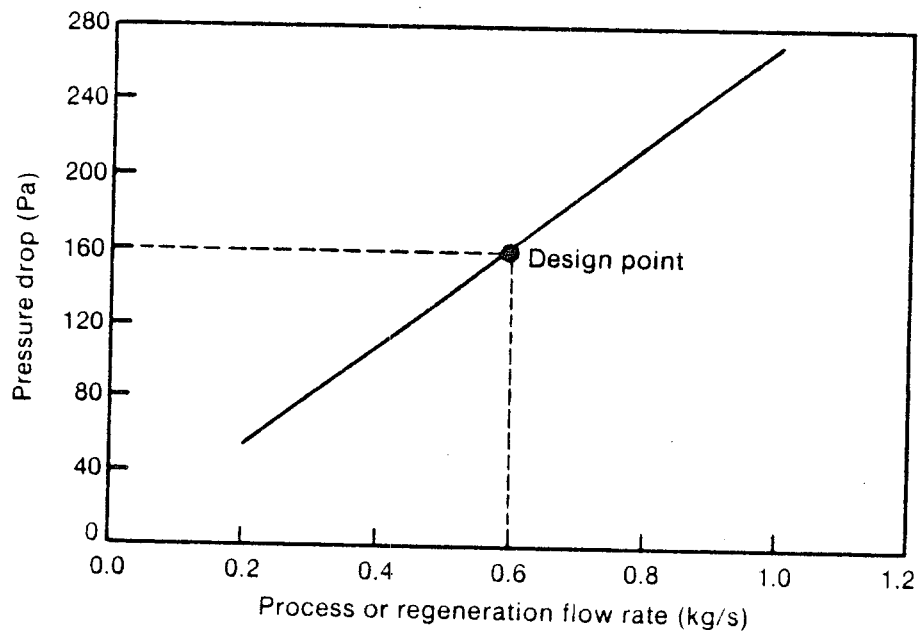

Figure 5-6. Effect of Air-Mass Flow Rate on the Dehumidifier Pressure Drop

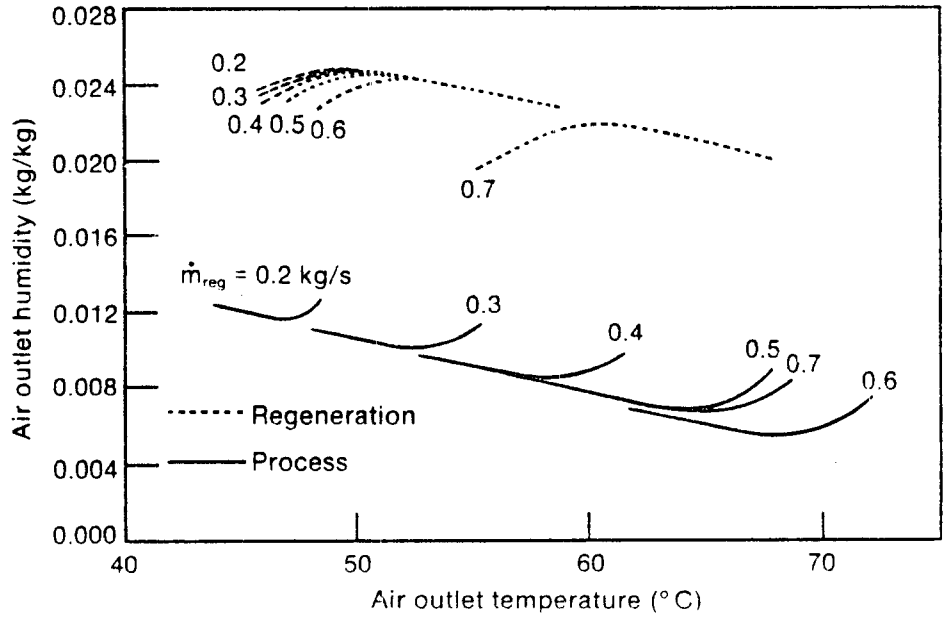

Figure 5-7. Silica-Gel Wheel Performance with Unbalanced Flow and Constant Regeneration Temperature

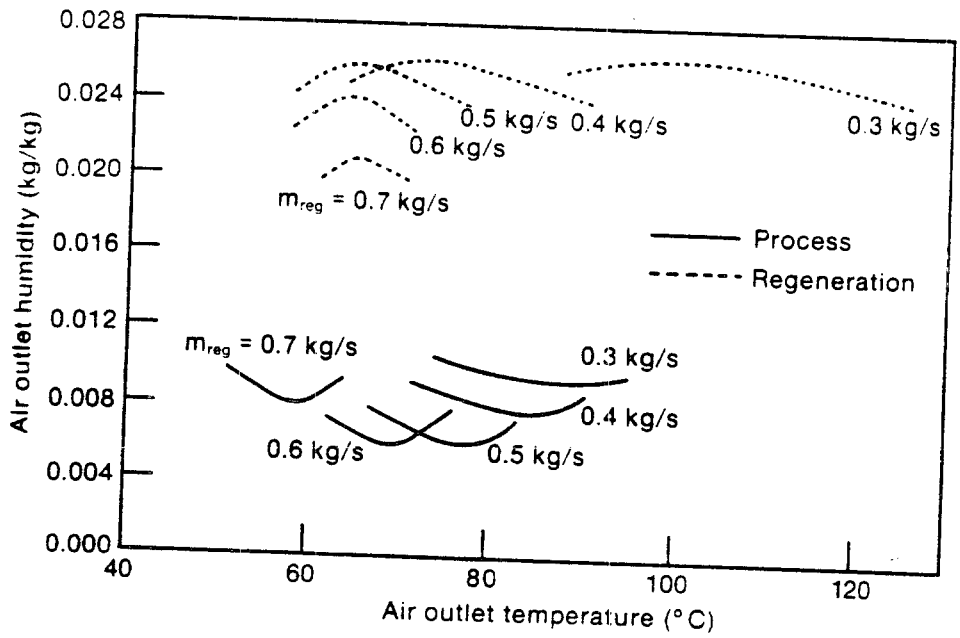

Figure 5-8. Silica Gel Wheel Performance with Unbalanced Flow and Constant Regeneration Heat Input

6.0 SYSTEM MODELING

The focus of this work is on dehumidifier materials and performance. As a result, a detailed dehumidifier model developed and validated from previous work funded by DOE was utilized, briefly described in Section 4. In order to assure that operating conditions used in dehumidifier evaluation are appropriate, it was necessary to develop a complete desiccant/TAHP hybrid system model. In addition, this system model provides a tool for evaluating overall system performance and component sizing.

6.1 Component Performance Models

This section presents the performance modeling equations used for system components other than the dehumidifier. These component models, while representative of actual performance, are considerably simpler than the dehumidifier model, because in general their performance is well understood.

Indirect Evaporative Cooler

The indirect evaporative cooler is modeled as a constant effectiveness device. The primary air stream (stream 1) does not experience any change in humidity. The effectiveness is defined as follows (Howe 1983).

$$\varepsilon_{IEC} = \left(T_{1,in} - T_{1,out}\right) / \left(T_{1,in} - T_{2,wb}\right) \qquad (6\text{-}1)$$

A secondary air stream (stream 2) is cooled evaporatively toward its wet bulb temperature, and heat is exchanged with the primary stream.

Direct Evaporative Cooler

The direct evaporative cooler model is similar to the indirect evaporative cooler model. A constant effectiveness is defined but no secondary stream is present. The effectiveness is

$$\varepsilon_{DEC} = \left(T_{in} - T_{out}\right) / \left(T_{in} - T_{wb}\right) . \qquad (6\text{-}2)$$

Since the process air is in contact with the cooling water, the humidity rises as the air is cooled. Since a plot of constant wet bulb temperature is linear on the psychrometric diagram, outlet humidity can be found by using the following equation (Crum 1986).

$$\varepsilon_{DEC} = (w_{in} - w_{out}) / (w_{in} - w^*) . \qquad (6\text{-}3)$$

Fan

Several fans are required in the systems configurations in order to overcome the component air pressure drops. Fan power is computed from

$$\text{Fan Power} = (\dot{m}\ \Delta P\ v) / \eta_{fan} . \qquad (6\text{-}4)$$

Heat generated by the fan is assumed to be transferred to the air stream with no heat loss to the surroundings. The heat transferred to the stream is simply

$$\text{Heat} = \text{Fan Power}\ (1 - \eta_{fan}) . \qquad (6\text{-}5)$$

The temperature rise of the air stream is found from

$$\text{Heat} = \dot{m}\ Cp_{air}\ (T_{in} - T_{out}) . \qquad (6\text{-}6)$$

Heat Exchangers

Three types of heat exchangers are used in the system performance predictions: air-to-air, exhaust-to-air, and water-to-air. They are modeled with equations for cross flow heat exchangers by using different fluid properties. Constant effectiveness is assumed. Two modes of calculation are programmed: given effectiveness and inlet temperatures, outlet temperatures are found or given inlet and outlet temperatures, effectiveness is found.

In either case, the capacitance rates of the two fluids are computed.

$$C_i = \dot{m}_i\ Cp_i, \text{ for } i = \text{hot, cold} \qquad (6\text{-}7)$$

The minimum capacitance rate is then identified, and the maximum heat transfer rate can be calculated.

$$Q_{max} = C_{min} \left(T_{hot,in} - T_{cold,in}\right) \tag{6-8}$$

Either effectiveness or outlet temperatures can be found from the following definition:

$$\varepsilon_{HX} = C_i \left(T_{max,in} - T_{min,in}\right) / Q_{max} \ . \tag{6-9}$$

If the effectiveness is calculated, a check is included to assure values between zero and one. In addition, for the air-to-air heat exchanger, the hot stream outlet temperature is checked against the dew point temperature to assure no condensation occurs.

The above calculations assume a constant fluid specific heat. For the temperature ranges encountered, this assumption introduces little error for air and water. The large temperature changes result in significant changes in the specific heat of the internal combustion exhaust stream, however. Once an exhaust outlet temperature is found, the exhaust specific heat is recalculated using the average of the inlet and outlet temperatures. Iteration continues until the change in capacity rate is less than 0.1%.

Another limitation in the exhaust-to-air heat exchanger routine is that the exhaust outlet temperature must be greater than 175°C (350°F). Lower exhaust temperatures result in condensation of gases which are highly corrosive (Segaser 1977).

We used an exhaust inlet temperature of 620°C (1150°F) for the heat exchanger calculations. Direct use of the exhaust gases for regeneration of the desiccant was ruled out for the following three reasons. There is not enough heat in the exhaust to regenerate the desiccant without mixing the exhaust with a supplementary air stream. The mixed regeneration gas would most probably drop below 175°C in the dehumidifier, resulting in corrosive condensation. Some of the exhaust products may reduce the moisture removing

capability of the desiccant by poisoning the sorption sites of the desiccant. And, the possibility for cross contamination of the supply air exists with direct exhaust regeneration.

Internal Combustion Engine

Parameters for the internal combustion engine were calculated using equations in Segaser (1977) as recommended by ORNL. This report contains generalized performance for current engine technology. We used performance equations for a turbo-charged, 4-cycle gas engine. The equations found in this report are programmed in the engine routine. For this work, we used a constant value of the load fraction which resulted in the values listed in Table 6-1.

The fuel consumption is calculated as follows.

consumption = fuel ratio * full load fuel rate * load/heating value (6-10)

Other waste heat is rejected through the lubrication oil and by radiation/convection from the engine surface. Recovery of the oil waste heat was not included in this study since only a small amount of energy (5 to 10% of fuel input) is available. We did not consider the performance decrease of the engine due to increased exhaust back pressure.

Building Loads

The building cooling load calculations are used to find the supply air flow rate, temperature, and humidity. For the simulations presented in this report, a cooling load of 37 kW (10 tons) was used. This value includes cooling loads from internal generation and transfer through the building perimeter. It does not include the load imposed by the fresh air requirement. A fresh air requirement of 15 liters per kJ of cooling was used in this study (0.56 m^3/s). This value is representative of many buildings but higher ventilation rates may be required for energy efficient construction or specialized applications. As discussed further in the section on systems configurations, using this fresh air requirement implies a partial recirculation mode of operation.

In addition to specifying cooling loads, the split between latent and sensible load is specified. While many studies of building loads have been performed, breakdown of loads into sensible and latent fractions cannot be generalized (Piette et al. 1985). For this report, we used a latent/total load ratio of 0.25, which is typical for studies of this type (Howe 1983).

A final assumption of the load calculations is that the enthalpy difference between the room and supply air is limited to 15 kJ/kg. This value is derived from comfort considerations (Howe 1983).

The supply temperature can be found from the following:

$$\frac{\dot{m}_{sup}\ Cp\ (T_{room} - T_{sup})}{\dot{m}_{sup}\ (h_{room} - h_{sup})} = \frac{Q_{sen}}{Q_{sen} + Q_{lat}} \qquad (6\text{-}11)$$

As mentioned earlier, AIR design room conditions are used for this study (T_{room} = 26.7°C, w_{room} = 0.011 kg/kg). Once the supply temperature is found, the supply mass flow rate is determined from the definition of sensible load.

$$Q_{sen} = \dot{m}_{sup}\ Cp\ (T_{room} - T_{sup}) \qquad (6\text{-}12)$$

A check is included in the routine to assure the supply mass flow rate is greater than the fresh air requirement. This constraint may be important for high fresh air ventilation rates. Supply air humidity is found from psychrometric relations using the specified temperature and enthalpy. The load routine contains a final check to assure that the specified supply air state is not to the left of the psychrometric saturation line. If it is, the supply humidity is set to saturation, and the latent cooling supplied by the system is greater than the specified load. This situation was not encountered in this study.

The building load routine is written so that different values of load, fresh air requirement, and latent fraction can be examined. The values discussed above were used in this report, and are representative of many small commercial buildings. In addition, the sizing is close to the capacity of the TAHP hardware being developed at ORNL. (ORNL is currently developing a 3 ton

residential TAHP with a Stirling engine and a 20-ton commercial TAHP with a gas internal combustion engine).

Vapor Compression Chiller

Two routines are used to calculate the parameters for the vapor compression chiller. The first finds the cooling load of the device from inlet and outlet air states and the air mass flow rate. For this study, the desired inlet and outlet air humidity ratios are equal (the chiller does only sensible cooling). In this case the vapor compression load is

$$Q_{VC} = \dot{m}\ Cp\ \left(T_{in} - T_{out}\right) . \qquad (6\text{-}13)$$

While not used in this study, other load calculations are included in the routine. If the outlet humidity ratio is lower than the inlet, the load is computed from enthalpy differences since dehumidification is required, and reheat energy is computed. If the outlet humidity is higher than the inlet, the load is computed as if humidities were equal and a message stating that there is potential for evaporative cooling is printed.

The second routine calculates the performance of the chiller. The coefficient of performance (COP), defined as the cooling load divided by the work input, is calculated from a curve fit developed by non-linear regression techniques from data for Trane 20-70 ton units. Non-standard operating conditions were taken into account by using data from a heat pump (Carrier Weathermaster III). The equation for COP from Howe (1983) is

$$\begin{aligned} COP = {} & 3.68 + 0.162\ FLR\ tons\ \exp(-0.183\ FLR\ tons) - 0.753\ FLR \\ & - 0.0073\ tons - 0.03998\ \left(T_{cond,in} - T^{*}_{evap,in} - 15.0\right) \end{aligned} \qquad (6\text{-}14)$$

where FLR is the fractional load ratio (load/full capacity) set to 0.90 in this study and Tons is the load in those units. The work required to run the compressor is

$$W_{comp} = Q_{evap}\ /\ COP . \qquad (6\text{-}15)$$

The heat rejected in the condenser is

$$Q_{cond} = Q_{evap} (1 + 1/COP) .$$

The temperature rise of the condenser cooling air is

$$T = Q_{cond} / (\dot{m} Cp) .$$

Component Pressure Drops

For complete analysis, the pressure loss through the various components must be accounted for. The pressure drops for standard components are in Table 6-2. These pressure drops are not varied and correspond to typical component design air velocities. The total pressure drop which must be overcome by a given fan depends on the system configuration and is discussed in Section 7.

These pressure drops and component routines were coupled with the dehumidifier model to predict the overall system performance as discussed in Section 7.

6.2 System Configurations

Many component arrangements are possible for both conventional desiccant systems (Crum 1986; Kettleborough et al. 1986; Meckler 1986) and hybrid systems (Howe 1983; Schlepp & Schultz 1984; Domingo 1986). Most hybrid systems begin with two air streams similar to conventional desiccant systems. The process air stream, which is delivered to the space to meet the load, typically is first passed through a dehumidifier where it is dried and warmed. Most hybrid system configurations pass the process air through the vapor compression chiller (evaporator) immediately before the air is delivered to the space. The main difference between the process stream of hybrid systems which have been previously examined is the arrangement of components between the dehumidifier and vapor compression evaporator. Possibilities include environmental and regenerative heat exchangers, and direct and indirect evaporative coolers. The regeneration stream, which is used to remove the moisture from the dehumidifier, is typically heated by a series of

components which might include the vapor compression condenser, a regenerative heat exchanger, waste heat recovery and auxiliary heat sources.

The first system configuration examined in this study is shown in Figure 6-1 (temperature increases due to fan heat losses are not included in the psycrometric representation for simplicity). In this layout, only the flow required to meet the fresh air requirement is passed through the dehumidifier. The remainder of the process air is passed through the vapor compression system only for sensible cooling. Essentially the two cooling loads, sensible and latent, are met by different supply air process paths which are mixed before entering the building. In the dehumidification regeneration stream, a sensible heat exchanger coupled to the supply stream is used instead of recovering heat from the vapor compression condenser. Temperatures at the exit of the first regeneration stream component would be limited to around 60°C if the condenser were used while utilizing the heat exchanger results in higher temperatures of around 70°C. This system configuration results in a smaller dehumidifier than the second system configuration since only a fraction of the air delivered to the building is dried.

Schlepp and Schultz (1984) concluded that, for systems with two main air streams, a regenerative heat exchanger on the process stream was not advantageous. They predicted improved performance over a wide range of conditions if an evaporative cooler was utilized instead. Use of both the regenerative heat exchanger and the vapor compression condenser for supplying regeneration heat is impractical because of the temperatures involved and the reduction in vapor compression COP as the condenser inlet temperature is raised. ORNL, in their preliminary evaluation of TAHP hybrid systems (Domingo 1986), also examined several system configurations. Both of these studies concluded that use of "free" environmental cooling potential (for example evaporative coolers or sensible heat exchangers) significantly improved performance.

Based on the results of Schlepp and Schultz (1984) and ORNL (Domingo 1986), this study included the configuration designated system 2. Figure 6-2 shows a schematic of this system and a representation of the component operations on a

psychrometric chart. After being dried, the process air is cooled in either an indirect evaporative cooler or an ambient heat exchanger. If enough regeneration heat is available to over-dry the process air, a direct evaporative cooler is included. The vapor compression evaporator supplies the remaining required sensible cooling to the process stream. Heat from the vapor compression condenser is recovered for regeneration of the desiccant, followed by waste heat recovery from the internal combustion engine water jacket and exhaust. Any additional heat required to bring the regeneration stream up to the regeneration temperature is provided by an auxiliary source, assumed to be a natural gas burner with an efficiency of 90% in this study.

While it is possible that other configurations may be conceived which result in improved system performance, the two very different concepts presented in this report assure that the conditions used for evaluating dehumidifier performance are appropriate.

6.3 Components Performance and Design Point

The performance of the two systems was compared by using effectiveness values for the evaporative coolers and heat exchangers which correspond to current off-the-shelf technology. Effectiveness of the direct and indirect evaporative coolers was set to 0.86 and 0.80, respectively. The air-air heat exchanger effectiveness was 0.79. Effectiveness of the water and exhaust heat recovery heat exchangers was determined by the routine since flow rates and heat flux was set by building load requirements and engine characteristics. The computed values are well within attainable values. A fan efficiency of 0.50 was used (Carrier 39E-7P). The system evaluations utilize equal flow rates on the supply and regeneration sides of the dehumidifier, since this performance has been verified by experiment and is shown in Section 5.3 to be more advantageous than unbalanced flow. A microbead silica gel dehumidifier is used in the system studies due to the superior performance shown in Section 5.1 and the performance of silica gel parallel passage wheels has been verified by our experiments. However, we expect that system performance at these conditions using a lithium chloride wheel should be very close to the values presented. The fractional load ratios of the gas engine and vapor compression machine are 0.9.

In this report, performance is evaluated at the American Refrigeration Institute (AIR) standard design point; 35°C and 0.0142 kg/kg humidity ratio for ambient, and 26.67°C and 0.0111 kg/kg humidity ratio for the room. While performance must be evaluated at numerous states and compared to load profiles for a given location for a complete evaluation of the system, comparison at these conditions gives an indication of relative merits. It has been found that yearly performance values are significantly higher than performance at the AIR design point for many U.S. cities (Warren 1985).

6.4 Influence of Design Conditions on Operating Mode

Classical desiccant dehumidification systems typically operate in a ventilation mode, a recirculation mode, or a mixture of the two. The system COP varies for a given set of building load and design conditions for these modes.

In the ventilation mode, supply air which is delivered to the building is drawn from ambient while the regeneration air stream originates with the room exhaust. The recirculation mode switches these sources of air flow. The process stream which is delivered to the building to meet the cooling load is drawn from the room while the regeneration stream originates from ambient.

The mode which results in the maximum performance of a system for a set of conditions depends mainly on the room and ambient state. The COP of a TAHP in meeting sensible cooling load is approximately one. The COP of a desiccant subsystem in meeting latent cooling load is also close to one. Therefore, for a TAHP/desiccant hybrid system, it is generally advantageous to minimize the cooling load imposed on the equipment regardless if the load is sensible or latent. This implies that the optimum performance is obtained when the process stream air originates from the lowest enthalpy source. For example, at AIR conditions, the ambient enthalpy at 35°C and 0.0142 kg/kg absolute humidity is 71.6 kJ/kg and the room enthalpy at 26.67°C and 0.0111 kg/kg humidity is 55.1 kJ/kg. Maximum performance with these design conditions is obtained when the supply air stream is drawn from the room. The fresh air requirement must be imposed on this condition. For the system studies, the

supply air is a mixture of fresh air and room air. For system two, only the minimum fresh air is mixed with room air for the supply stream. In system one the amount of air which passes through the dehumidifier in order to meet the latent load is just slightly greater than the fresh air requirement so ambient was used for the source of the dehumidification supply and the room for the source of the vapor compression supply for simplicity.

If no heat is exchanged between the supply and regeneration air, the source of the regeneration air stream is decided on the basis of obtaining the minimum process side outlet humidity. The heat transfer from the waste heat sources to the regeneration air stream is generally not limited by temperature differences. The waste heat from the internal combustion engine is available at much larger temperatures than is needed or desirable for regenerating the desiccant. For a given specified wheel design a general assumption of constant heat transfer to the regeneration stream independent of regeneration temperature results in constant enthalpy and a generally fixed F_1 transfer line. The process outlet humidity can be lowered by changing the F_2 transfer line. Therefore, optimum performance is obtained by using the lowest relative humidity source for the regeneration air. The AIR room condition is 50% relative humidity, and the AIR ambient condition is 40% relative humidity. Therefore, it is desirable to use ambient air as the regeneration source for our study.

The performance of the systems presented in this section as well as the operating points of the components are presented in Section 7.

Table 6-1. Engine Characteristics

Parameter	Definition	Units	Value
Load fraction	load/rated power	—	0.90
Full load Fuel rate	fuel consumption/work delivered (at full load)	—	2.44
Fuel ratio	full load/actual fuel rate	—	1.02
Water jacket heat	jacked waste heat/fuel input	—	0.226
Exhaust gas heat	exhaust waste heat/fuel input	—	0.274
Fuel heating value	natural gas lower heating value	MJ/m^3	33.53

Table 6-2. Standard Component Pressure Drop

Component	Pressure Drop (Pa)
	Commercial
Direct Evaporative Cooler	140
Dehumidifier	150
Vapor Compression Evaporator	60
Vapor Compression Condenser	60
Air-Air Sensible Heat Exchanger	40
Air-Exhaust Sensible Heat Exchanger	40
Air-Water Sensible Heat Exchanger	50
Air Delivery	100
Air Filter	150

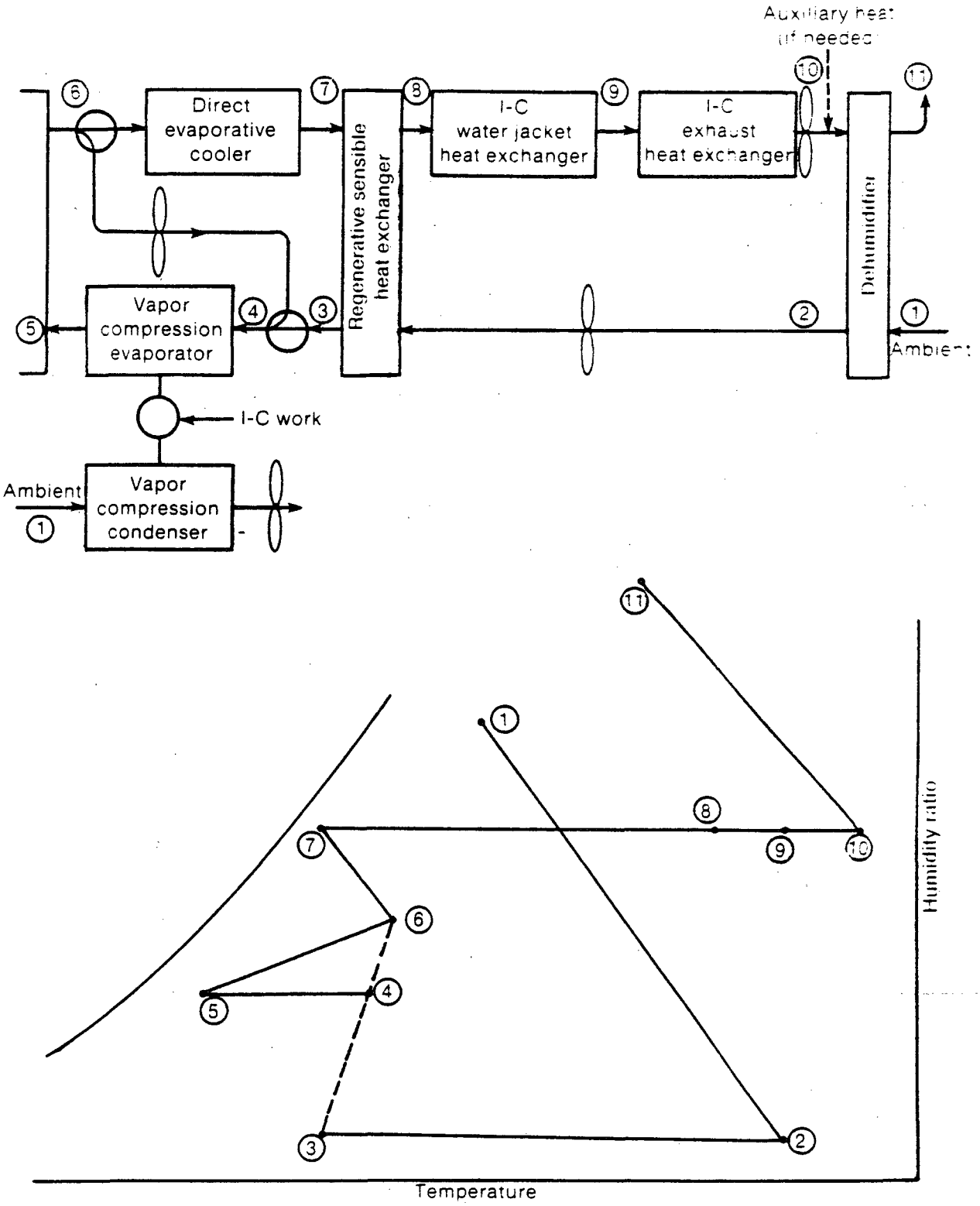

Figure 6-1. Schematic and Psycometric Chart Representation of System 1

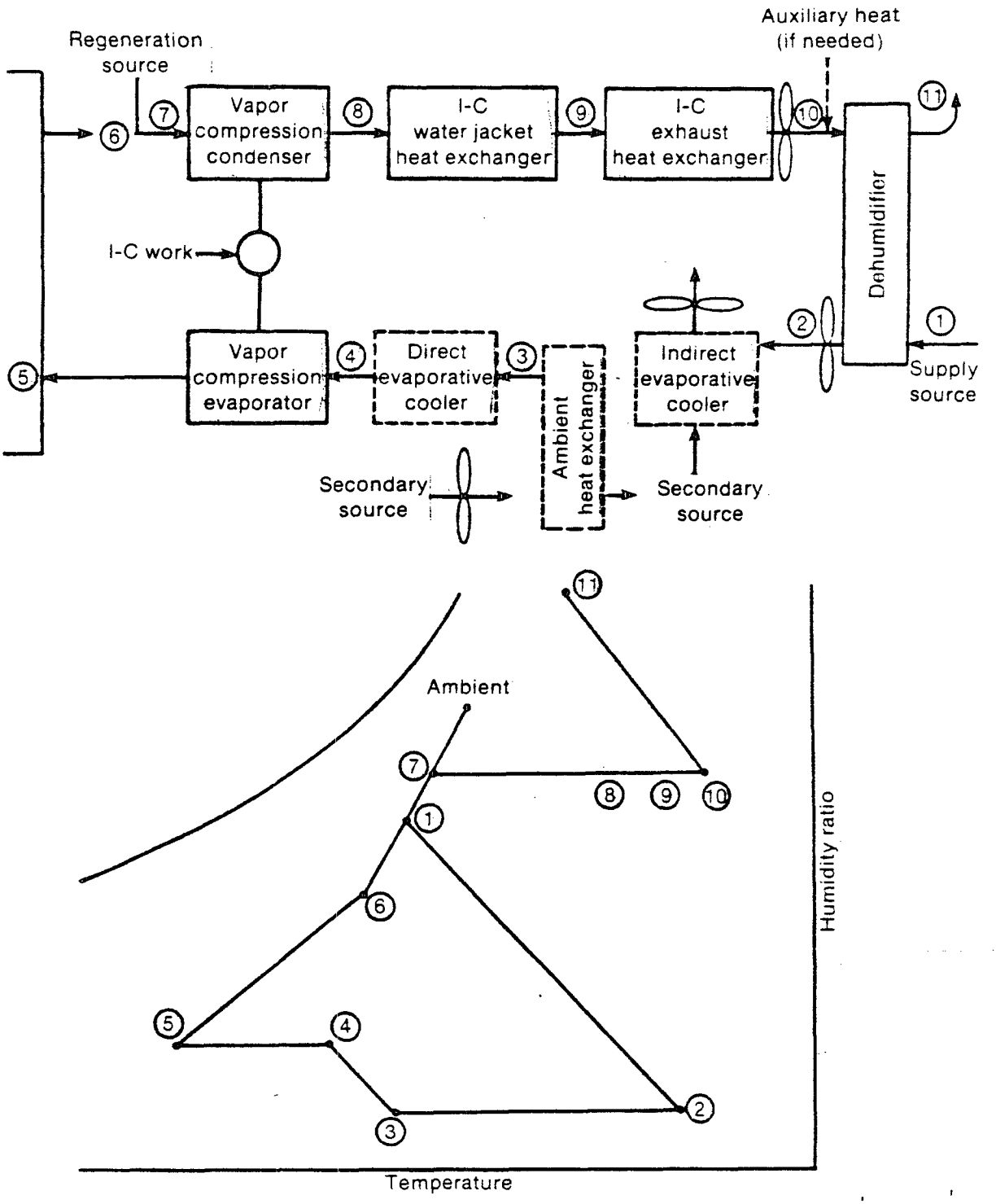

Figure 6-2. Schematic and Psycometric Chart Representation of System 2

7.0 SYSTEM STUDIES RESULTS

This chapter shows the results of the studies on system performance for the two configurations presented in Section 6 and presents possible options for further improving the results. The performance projections suggest that adding a desiccant subsystem to a TAHP cooling system, results in significant improvement in COP and latent load capacity.

Table 7-1 summarizes key design conditions used for comparison. Further discussion of the design points and other component parameters can be found in Section 6.

The results presented in the following sections correspond to the systems introduced in the previous chapter. Note that the system which is described in Section 8 on layout and costs uses a slightly different waste heat recovery scheme. The detailed analysis assumes that an exhaust-to-air heat exchanger is used to directly heat the regeneration air while the layout calls for an exhaust-water heat exchanger to post-heat the cooling water; then a water-air heat exchanger is used as the final regeneration air heater before auxiliary energy addition. While hardware is different, overall performance for the two systems are similar. The postwater heating scheme is more typical of commercial waste heat recovery systems.

7.1 System 1 Performance Results

Table 7-2 presents the design-point calculations for the system illustrated in Figure 6-1. This table summarizes performance of the system using commercial component pressure drops presented in Table 6-2 and commercial component efficiencies discussed in Section 6.3. Ambient air is used for the dehumidifier process, since the flow rate dictated by the latent load is equal to the ventilation requirement. Since heat is exchanged between the supply and regeneration air streams, room air is used for the dehumidifier regeneration to obtain optimum benefit of the direct evaporative cooler and regenerative heat exchanger, and room air is also used for the air routed through the vapor compression evaporator to minimize the load seen by the machine.

The fans are located in three places: between the dehumidifier and regenerative heat exchanger for the latent subsystem process air, between the exhaust heat-recovery heat exchanger and the dehumidifier for the regeneration air, and between the room and vapor compression evaporator for the sensible process air. These fan placements were selected to minimize the disadvantages and to maximize the benefits of the heat added to the air streams by the fans.

The regeneration temperature of 85°C was chosen to minimize auxiliary energy and to achieve high overall COP. Coincidentally, this regeneration temperature also coincides with the test conditions under which the silica-gel dehumidifier model was validated experimentally and with the temperatures typical of solar energy regenerated desiccant cooling systems.

Adding on the desiccant dehumidification subsystem (including the dehumidifier heat exchangers, evaporative cooling, and additional fans) to the vapor compression unit increases the performance of the total system in several ways. First, since the vapor compression subsystem does not handle any dehumidification load, no reheat of air is required. The reheat energy for the above load had it been met by vapor compression alone, would have been approximately 7.2 kW. Second, the temperature and humidity of the air entering the vapor compression evaporator in the hybrid system is different than if a vapor compressor was meeting the total cooling load. The COP of the vapor compression unit is dependent on the wet bulb temperature of the entering air (see Equation 6-14). If the same fresh and recirculation air flows were used in a vapor compression system alone, the entering wet-bulb temperature would have been 20.51°C and the resulting vapor compression COP (defined as cooling/compressor work) would have been 3.07. The hybrid system evaporator wet bulb for the conditions presented in Table 7-2 is 18.95°C and the vapor compression COP is 3.18. This higher COP results in a decrease in the amount of fuel required to meet a given load.

The third and most important advantage of adding the dehumidification subsystem is the added cooling capacity. The desiccant subsystem itself adds 15.5 kW of cooling capacity while utilizing the engine waste heat. The above conditions require only a small amount of supplementary gas heat (1.3 kW

compared to 30.9 kW to run the gas engine) to regenerate the desiccant. If one considers the waste heat as a free heat source, the energy input to obtain this increased capacity is only 1.3 kW in the above example. A gas COP of the desiccant subsystem computed on this basis is near 12. At other conditions, this add-on COP can be infinite as no auxiliary gas is needed; all regeneration heat is supplied by the waste heat from the engine.

The COP's presented in Table 7-2 are defined as follows. For gas, the COP is the cooling energy delivered divided by the energy content of the gas. For electric, the COP is the cooling energy delivered divided by the electric power required to run the fans. Water pumping power for the water jacket and evaporative coolers and power to rotate the dehumidifier are small and have not been included.

A gas engine-driven cooling system operating with vapor compression only and under conditions comparable to the hybrid system presented in Table 7-2, has an overall gas COP of 0.84 when reheat is considered with a 100 percent efficient burner. The use of the desiccant dehumidifier subsystem increases the gas COP by 70 percent to 1.42. Section 8 addresses the cost associated with this increase in performance.

We were interested in quantifying the effect of certain possible component improvements on the system performance. The system performance presented in Table 7-2 was based on component effectiveness and pressure drops corresponding to existing commercial equipment. Table 7-3 compares the component effectiveness and pressure drop for commercial evaporative cooler equipment and regenerative heat exchangers with "developmental" equipment that could be developed with advanced technology, and the resulting system performance improvements. The supply-to-regenerative stream heat exchanger performances for both systems are determined by limitations on temperatures and are well within current commercial technology.

The use of developmental components resulted in a slight increase in performance. These advanced components resulted in supply air leaving the regenerative heat exchanger which was 6°C cooler than with commercial components. Therefore, the mixing point of the dehumidified air and the

recirculated room air was moved to a position downstream of the vapor compression evaporator. The change in evaporator inlet conditions resulted in a higher vapor compression COP and lower gas engine fuel consumption. Less air is passed through the vapor compression machine in the developmental system resulting in lower fan power and higher electric COP.

The increase in system performance with developmental components is noticeable and may warrant investment of research effort into advancing the state of the art in the direct evaporative cooler and gas-to-gas heat exchanger components.

7.2 System 2 Performance Results

In the second system configuration, presented in Figure 6-2, all the process air passes through the dehumidifier subsystem components and the vapor compression evaporator. The system performance model contains several component design options. First, either an indirect evaporative cooler or an ambient air-to-air heat exchanger is used to cool the process air exiting the dehumidifier. The decision may be based on which component results in the maximum amount of "free" sensible cooling. The selection depends on the effectiveness of the two devices and the primary and secondary air stream conditions. By referring to equations 6-1 and 6-9 and setting the primary air stream cooling for the two devices equal to each other, the break-even point can be defined as follows:

$$\varepsilon_{IEC}(T_{1,in} - T_{2,wb}) = \varepsilon_{HX}(T_{1,in} - T_{2,in}) \ . \qquad (7\text{-}1)$$

Therefore, if

$$T_{2,wb} < T_{1,in} - \varepsilon_{HX}\,(T_{1,in} - T_{2,in}) \,/\, \varepsilon_{IEC} \ , \qquad (7\text{-}2)$$

using an indirect evaporative cooler results in more free sensible cooling. For these system studies, using $\varepsilon_{IEC} = 0.70$, $\varepsilon_{HX} = 0.79$ and AIR ambient air as the secondary air stream, this relation results in the indirect evaporative cooler being selected.

The second option is whether to include a direct evaporative cooler before the

vapor compression evaporator. If enough heat is available to regenerate the desiccant and to dry the process air to humidities lower than the required delivery humidity, additional free sensible cooling can be obtained by using a direct evaporative cooler. If a low regeneration temperature is used, very little auxiliary energy is needed and the supply outlet of the dehumidifier is still slightly over-dry. As a result a direct evaporative cooler was included in the system. The inlet conditions were set by the performance of the dehumidifier and indirect evaporative cooler. The outlet humidity was set to the room supply humidity. These conditions were used in Equation 6-30 to define the direct evaporative cooler effectiveness. Equation 6-2 then defined the outlet temperature.

For system 2 studies, the supply air fan was placed between the dehumidifier and the indirect evaporative cooler, and the regeneration air fan was placed between the waste-heat recovery system and the dehumidifier.

Room air was mixed with the minimum required fresh air, as the source of the supply air to minimize the required capacity and the ambient mixed with the remaining room air as the source of the regeneration stream. Both air process paths used a flow rate of 2.47 kg/s.

Table 7-4 presents the component operating conditions and the performance for system 2 for a regeneration temperature of 50°C. Higher regeneration temperatures resulted in increasing auxiliary regeneration energy requirements, while lower regeneration temperatures resulted in excess waste heat being available.

Note that the electric COP is not broken down into vapor compression and desiccant subsystem contributions since in this system the two subsystems have the same air flow paths.

7.3 System Selection

The system two design is quite different from the system one design. The gas COP for system two is somewhat higher but since all the process air passes through the dehumidifier and other desiccant subsystem components, the

electric COP decreased by around 40 percent. While these performance parameters are important, perhaps the largest difference between the two systems is the component size. The vapor compression/engine capacity is around 25 percent lower for system two, since the desiccant subsystem handles more of the sensible load through the evaporative coolers. The desiccant subsystem components for system two are around 4.5 times larger than those used in system one because the full supply air flow passes through them. Larger air-flow rates result in a dehumidifier diameter of greater than two meters for system two, while the dehumidifier for system one is one meter in diameter. The probable increase in cost for system two over system one is perhaps not warranted by the increase in performance. Therefore, in spite of a higher gas COP for system configuration two, system configuration one has been chosen as the better of the two systems. A rough cost estimate and a layout of the desiccant subsystem of configuration one is presented in Section 8.

The low regeneration temperature identified for system two is consistent with the findings of Schlepp and Shultz (1984). Notice that the direct evaporative cooler only cools the supply air by about 4°C. This small amount of evaporative cooling indicates that the air is only slightly over-dried by the dehumidifier. While system performance would decrease slightly, it may be advantageous from an initial cost view point to remove the direct evaporative cooler.

7.4 Other Possible Performance Improvements

This study identifies two desiccant subsystems which significantly increase the performance (both gas COP and capacity) of a TAHP cooling system. Other system configurations and operating strategies may result in even higher COP and/or lower cost.

In addition, component options may improve system performance. MacLaine-cross (1986) suggests that the temperature of the air entering the condenser be lowered by an evaporative cooler or cooling tower to increase the vapor compression COP. Crum (1986) and Wangaman and Kettleborough (1987) have suggested and evaluated several desiccant subsystem component improvements--including substituting conventional evaporative coolers with multiple-stage

evaporative coolers, cooling towers, and heat exchange/evaporative coolers.

Each of these possible improvements in component and system performance should be evaluated on a cost/benefit basis before a true "optimum" hybrid TAHP system can be defined.

Table 7-1. System Design Conditions

Building load	37 kW
Building latent fraction	0.25
Ventilation requirement	0.56 kg/s
Room and Ambient air state	ARI design point
Engine load fraction	0.90
Vapor compression load fraction	0.90
Fan efficiencies	0.50
Dehumidifier material	Microbead silica gel
Balanced dehumidifier air flow	
Nominal dehumidifier loading (air flow divided by frontal flow area)	1.49 kg/m^2

Table 7-2. System 1 Performance Results for Low Component Efficiencies

Air States	Temperature (C)	Humidity (kg/kg)
Ambient	35.00	0.0142
Room exit	26.67	0.0111
Room suppy	16.48	0.0097
Dehumidifier process in	35.00	0.0142
Dehumidifier process out	68.51	0.0050
Regenerative HX process in	69.00	0.0050
Regenerative HX process out	30.94	0.0050
Vapor compression evaporator in	28.62	0.0097
Vapor compression evaporator out	16.48	0.0097
Vapor compression condensor in	35.00	0.0142
Vapor compression condensor out	50.82	0.0142
Direct evaporative cooler in	26.67	0.0111
Direct evaporative cooler out	20.83	0.0139
Regenerative HX regeneration in	20.83	0.0139
Regenerative HX regeneration out	58.36	0.0139
Water-air HX in	58.36	0.0139
Water-air HX out	70.73	0.0139
Cooling water inlet	100.00	—
Cooling water outlet	94.86	—
Exhaust-air HX in	70.73	0.0139
Exhaust-air HX out	82.30	0.0139
Exhaust inlet	620.00	—
Exhaust outlet	175.00	—
Dehumidifier regeneration in	85.00	0.0139
Dehumidifier regeneration out	51.78	0.0231

Total Flow Path Pressure Drops	Pascals
Dehumidification supply stream	500
Dehumidification regenertion stream	670
Vapor compression supply stream	310
Vapor compression condenser stream	210

Component Effectiveness	
Direct evaporative cooler	0.86
Regenerative heat exchanger	0.79
Water-air heat exchanger	0.30
Exhaust-air heat exchanger	0.83
Vapor compression COP	3.18

Flow Rates	kg/s
Dehumidifier supply	0.56
Dehumidifier regeneration	0.56
Recirculation	1.91
Vapor compression evaporator	2.47
Vapor compression condenser	2.47
Engine cooling water	0.33
Engine exhaust	0.013

Cooling Load	kW	
Building		
sensible	27.7	Internal/environmental gains
latent	9.3	
total	37.0	
Ventilation		
sensible	4.6	Difference between ambient
latent	4.6	and room for dehumidifica-
total	9.2	tion air flow
Total loads		
sensible	32.3	
latent	13.9	
total	46.2	

Hardware Capacities	kW	
Vapor compression		
evaporator	30.7	All sensible cooling
condenser	40.3	Heat rejection
compressor	9.6	Work input
Dehumidification subsystem		
sensible	1.6	Due to DEC and HX
latent	13.9	
total	15.5	
Total hardware		
sensible	32.3	
latent	13.9	
total	46.2	

Energy Inputs	kW
Internal combustion engine (gas)	30.9
Auxiliary regeneration (gas)	1.3
Fans (electric)	
vapor compression subsystem	2.0
dehumidification subsystem	1.3
total	3.3

Performance	COP
Complete System	
Gas	1.42
Electric	13.77
Vapor Compression Subsystem	
Gas	0.99
Electric	15.35
Desiccant Subsystem	
Gas	11.92
Electric	11.92

Table 7-3. Affect of Commercial vs. Developmental Component Performance

Component	Effectiveness		Pressure Drop (Pa)	
	Commercial	Developmental	Commercial	Developmental
Direct evaporative cooler	0.86	0.97	140	45
Air-Air heat exchanger	0.79	0.90	40	50
Air-Exhaust heat exchanger	0.79	0.90	40	50

System Performance Parameter	Components	
	Commercial	Developmental
Vapor compression COP	3.18	3.24
Engine gas input (kW)	30.9	26.8
Auxiliary regenration gas (kW)	1.3	1.0
Total system electric COP	13.8	15.1
Total system gas COP	1.42	1.65

Table 7-4. System 2 Performance Results

Air States	Temperature (C)	Humidity (kg/kg)
Ambient	35.00	0.0142
Room exit	26.67	0.0111
Room supply	16.48	0.0097
Dehumidifier process in	29.33	0.0118
Dehumidifier process out	39.10	0.0079
Indirect evaporative cooler in	39.76	0.0079
Indirect evaporative cooler out	28.71	0.0079
Direct evaporative cooler in	28.71	0.0079
Direct evaporative cooler out	24.34	0.0097
Vapor compression evaporator in	24.34	0.0097
Vapor compression evaporator out	16.48	0.0097
Vapor compression condensor in	33.34	0.0135
Vapor compression condensor out	43.54	0.0135
Water-air HX in	45.31	0.0135
Water-air HX out	46.98	0.0135
Cooling water inlet	100.00	—
Coolng water outlet	94.86	—
Exhaust-air HX in	47.42	0.0139
Exhaust-air HX out	49.38	0.0139
Exhaust inlet	620.00	—
Exhaust outlet	175.00	—
Dehumidifier regeneration in	50.00	0.0136
Dehumidifier regeneration out	39.20	0.0174

Pressure Drops	Pascals
Supply air stream	740
Regeneration air stream	550
Indirect evaporative cooler secondary stream	290

Component Effectiveness	
Indirect evaporative cooler	0.70
Direct evaporative cooler	0.22
Water-air heat exchanger	0.08
Exhaust-air heat exchanger	0.80
Vapor compression COP	3.25

8.0 PHYSICAL DESCRIPTION OF A WASTE HEAT DRIVEN DESICCANT COOLING SUB-SYSTEM

8.1 System Layout and Subsystem Integration

The system layed out and costed in this section is based on the configuration of system one, discussed in Section 6, and the performance of system 1 summarized in Table 7-2.

The physical integration of a desiccant dehumidifier subsystem and thermally activated heat pump components can be accomplished with stand-alone units for the two subsystems as shown in Figure 8-1. The interfaces for the two units are :

- o Hot water delivered to the desiccant subsystem from the internal combustion engine cooling system;
- o Hot exhaust gas delivered to the engine cooling water post heater;
- o Supply air delivered from the desiccant subsystem to the vapor compression evaporator.

In the analysis presented in Sections 6 and 7, hot exhaust gas is delivered directly to the desiccant subsystem to achieve the final temperature boost in the dehumidifier regeneration airstream. An alternative (assumed in the layouts of this section) which is more practical and easily integrated into the system, utilizes an exhaust gas-to-cooling water heat-exchanger. The engine cooling water delivered to the desiccant subsystem, therefore, operates at boosted temperature. The performance of this modified system is assumed to be equivalent to the system introduced in Section 6.

Finally, since the air delivered from the desiccant dehumidifier is subcooled in the evaporator coil, an interface is established between the two subsystems supply air streams. The pressure loss through the evaporator coil is provided by each subsystem fan so that sizing of the desiccant air system need only overcome ventilation air pressure losses.

Several limitations of the design and cost presented in this section are:

- The cost of the desiccant subsystem regeneration air heater probably should be credited against the cost of the internal combustion engine cooling radiator. This credit has not been included in our cost estimate.

- We have not accounted for the effect of the increased back pressure in the exhaust system on engine performance.

- Integration of the two subsystems allows an increase in the vapor compression evaporator refrigerant pressure and temperature which results in an increase in the chiller COP, reflected in the increased overall system COP. There may also be a change in chiller capacity at higher evaporator temperature which would require a re-sizing of the coil. However, we have assumed that the chilled capacity is the same.

The schematic shown in Figure 8-2 represents rough layout of the dehumidification subsystem for system configuration number 1. It is contained within an envelope which is 1.0 by 1.0 by 1.8 meters and has the operating specifications shown in Table 8-1.

8.2 Desiccant Subsystem and Component Descriptions

The desiccant subsystem is built around four major heat and mass transfer components; each operates with low air velocity (which is necessary to achieve high component effectiveness and low air side pressure losses). These four components, which will be discussed in further detail in the following paragraphs, are:

- Desiccant dehumidifier wheel;
- Waste heat fired air heater;
- Counterflow air heat exchanger;
- Direct evaporative cooler;

The dehumidification subsystem selected in the system study operates on a pure ventilation cycle handling all of the building ventilation requirements of

around 0.56 kg/s. The desiccant subsystem cooling capacity at ARI standard design conditions is approximately 15.5 kW (4.4 tons) of which 10% is sensible and 90% is latent cooling. The subsystem utilizes a rotating silica-gel dehumidifier wheel, a rotating polymer counterflow heat exchanger, a direct evaporative cooler utilizing a wettable gauze structured packing, and a regeneration coil (platefin heat recovery exchanger). (Not included in the envelope of Figure 8-2 is an exhaust gas heat recovery exchanger which will boost the water jacket temperature).

The electrical components in the system include two blowers (driven by a single motor), a supply water pump for the evaporative cooler, a drive motor for the desiccant wheel, and an electronic controller for the system. Finally, the system requires a structural frame and housing with associated thermal insulation. Details of other minor components such as filters, dampers, actuators, and miscellaneous other mechanisms should be developed for a complete detailed design.

Table 8-2 provides a summary of the cost breakdown for the system (described as a nominal 4.4 ton capacity). The cost estimates presented in this section come from MacLaine-cross (1986), and MacLaine-cross and Parsons (1986), plus current quotes from manufacturers. These sources are recent, and all presented costs can be assumed to be 1987 dollars. The breakdown of these costs is discussed in the following paragraphs. The conclusion is that the manufacturing first cost of a desiccant cooling add-on to an internal combustion engine driven vapor compression system would be $490/ton in the sizes described in this report--using current state-of-the-art technology. This represents a realistic cost goal and there is opportunity for performance gain in achieving higher effectiveness for mass transfer systems (dehumidifier, heat exchangers, and evaporative cooler).

The desiccant cooling dehumidification subsystem described in this report is assembled using components which are, for the most part, conventional in HVAC equipment. The single exception is the desiccant bed which corresponds to the design used in recent SERI test articles. A desiccant drier bed, which may have nearly the same performance using lithium chloride solution impregnated into a porous matrix, is commercially available. In general, the performance

of the dehumidifier and the other heat exchangers can be improved by increasing their thermal effectiveness. This can be done by decreasing air velocity and increasing flow length in the components. This, however, increases the size, cost, and air pressure drop. A complete economic/performance trade-off study is required to fully resolve these issues.

If we assume that the cost estimates for the conventional equipment are within 10% (applicable to general engineering estimates) and the cost of the silicon-gel dehumidifier is within ±50%, the overall subsystem cost estimate has an uncertainty of 18% since the dehumidifier cost is only 20% of the total desiccant subsystem manufacturer first cost.

Dehumidifier

Description: The 1.00-m diameter rotary dehumidifier is made by spirally winding 100-mm wide desiccant coated tape on a 200-mm diameter cast aluminum hub over 0.5-mm thick by 3-mm wide aluminum spacers. The tape is a 10-um thick polyester with 10-um of acrylic adhesive on both sides coated with 75-um to 105-um mesh grade 3A microbead silica-gel. The design pressure drop is 150 Pa for the dehumidification air and 150 Pa for the regeneration air.

The cost breakdown below reflects an accounting for the materials and labor coast associated with assembling the dehumidifier, assuming sufficient production level so that set up and tooling costs do not appear as a significant cost element.

Item	Quantity	Price	Cost
Aluminum Sheet	1.73 kg	$1.84/kg	$ 3
Aluminum Wire, Extrusion and Casting	13.96 kg	2.84/kg	37
Adhesive Tape	95 m^2	2093/m^2	198
Silica-gel	10 kg	10.00/kg	100
Seals	–	–	2
Labor	6 hr	20/hr	120
Estimated Manufacturing Cost			$ 460

Heat Exchanger

There are three options for exchanging heat between the process and regeneration air streams. They are counterflow platefin, finned heat pipe, and rotary heat wheel. Maximum thermal effectiveness with minimum cross leakage probably is achieved with the fixed counterflow heat exchanger; however, its cost is higher than the rotary wheel. The heat pipe unit can achieve some economy through relatively inexpensive finned tube construction, but is larger than the other two alternatives. The rotary wheel has been chosen for the costing exercise since it appears to have the best potential for compactness and low cost although like the desiccant dehumidifier the wheel fabrication process may still need further development.

The 0.88 diameter rotary heat exchanger is made by spirally winding 100-mm wide by 50-μm thick polyester film on a 200-mm diameter cast aluminum hub over 0.5-mm thick by 3-mm wide aluminum spacers. The design pressure drop is 40 Pa for the dehumidified air and 40 Pa for the regeneration air.

Item	Quantity	Price	Cost
Aluminum Sheet	1.73 kg	$1.89/kg	$ 3
Aluminum Wire, Extrusion and Casting	13.23 kg	2.84/kg	37
Polyester Film	3.86 kg	7.497/kg	78
Seals	-	-	2
Labor	4 hr	20/hr	80
Estimated Manufacturing Cost			$ 200

Regeneration Heater Coil

(Engine Cooling Fluid Heat Recovery) The regeneration coil could very easily be a standard automotive radiator. We have chosen to specify a 0.4-m high × 0.9-m wide × 0.30-m deep regeneration coil which has sixteen rows of copper coils and aluminum fins with Trane pattern 8.0-3/8 T (Kays and London 1964). The design pressure drop is 100 Pa. The coil takes engine cooling water which as been heated to approximately 105°C in an exhaust gas heater and provides the final temperature boost to the regeneration air stream.

Item	Quantity	Price	Cost
Aluminum Sheet	30.6	$1.89/kg	$ 59
Copper Tubing	23.52	2.59/kg	61
Labor	1.5 hr	20/hr	30
Estimated Manufacturing Cost			$ 150

Evaporative Cooler

Evaporative coolers are commercially available in two types: direct and indirect. In system one, a direct type can be used, since the regenerative

heat exchanger is used not only to preheat regeneration air, but to pre-cool the supply air by coupling with the evaporatively cooled regeneration stream. The liquid/vapor contacting medium is typically some sort of split organic fiber fabricated into mesh or pad configurations. These tend to be very large since face velocity for high effectiveness is low (typically 1.3 m/s). Indirect evaporative coolers using structured packings are now appearing on the market. A polymer sheet is typically manufactured in a shape which promotes high mass transfer with enhanced surface wetability. A surface topography which increases packing stiffness and efficiently channels liquid flow contributes further to the potential of this medium. Possible extension of the technique to the fabrication of gauze packings make this a promising approach to compact, high effectiveness evaporative coolers.

For this application, we have specified a 1.0 m by 0.5 m by 0.3 m wet surface heat exchanger assembled from 0.2-mm thick UV resistant polystyrene sheets thermoformed with 0.2-mm thick non-woven polyester cloth on the wet surfaces. The composite sheet is embossed with 1.2-mm thick horizontal ridges every 40-mm on each surface for stiffness. The wet passages are effectively parallel plates as the inside of the dry ridges fill with water and act as horizontal wick to aid wetting. The passages have a 2.7-m spacing. The design air pressure drop is 140 Pa.

Item	Quantity	Price	Cost
Polystyrene Sheet	15.0 kg	$1.06/kg	$ 16
Aluminum Frame	10.8 kg	1.84/kg	20
Plumbing and Misc. Hardware			50
Control Valve			20
Non-woven Polyester	1.9 kg	10/kg	19
Labor	2 hr	20/hr	40
Estimated Manufacturing Cost			$ 165

Desiccant Wheel Drive Motor

1/20 hp, 600 rpm squirrel cage induction type	$22.00

Heat Exchanger Drive Motor

1/20 hp, 1200 rpm squirrel cage induction type	$22.00

Speed Reducers

A 30:1 belt drive and pulley speed ratio with exchanger and dehumidifier rotors mounted directly on shafts	$25.00

Fans

Description: The fan motor is a 1.5 hp, 1740 rpm double wound squirrel cage induction unit with a shaft extension for the small rotor.

Second winding gives 870 rpm.

The fan wheels are centrifugal rotors specifically designed to deliver appropriate flow rate and pressure head in the desiccant subsystem process and regeneration loops.

Item	Cost
375-mm diameter forward curved single inlet rotor	$ 65
225-mm diameter forward curved single inlet rotor	40
Extension shaft 2 hp motor	165
Estimated Manufacturing Cost	$270

Evaporative Cooler Water Pump

Little giant pump Model #CP6500 $7
(9/18/1985, Pat Koenig, Duvall-Koenig
Co. ((303) 733-5555)

Sheet Metal Enclosure

The housing is a 1.0-m by 1.0-m by 2.2-m box of 1.0-mm thick aluminum sheet assembled onto a 5.0 by 2.5-cm box section frame.

Item	Quantity	Price	Cost
Aluminum Frame	17.14 kg	$2.84/kg	$ 105
Aluminum Sheet	36.62 kg	1.89/kg	70
Labor	2 hr.	20/hr.	40
Estimated Manufacturing Cost			$ 213

Fresh Air Filter	$ 5
Return Air Filter	10
Four Way Damper Actuator	30
Estimated Manufacturing Cost$	$ 45

Microprocessor Control System

It is anticipated that the control of a desiccant cooling system will be relatively straightforward in the sense that actuators will simply be turned on or off in response to some combination of signals from a number of sensors located in the systems. The controlled functions will include all drive motors and pumps as well as solenoid valves controlling the flow of hot water and auxillary fuel.

The more complex aspect of control are the algorithms which relate performance to such variables as ambient humidity ratio and dry-bulb temperatures. Those

same parameters for the building space as well as exhaust gas temperatures also effect the system operating configuration. When the interaction of the vapor compression chiller and the desiccant dehumidifier are factored in the controls, it can get fairly sophisticated even if the strategy is straightforward.

The multiplicity of functions and the need to process the signals from multiple sensors to derive the control signal(s), points to a microprocessor controller as the preferred approach. Microprocessor controllers have a significant initial cost, but they allow additional control functions to be added at very low cost. They currently add about $50 to the cost of mass-produced appliances, such as microwave ovens, washing machines, and sewing machines, but this is decreasing. Microcomputers are now available that include processor, all memory, communications, and analog-to-digital converters on a single chip of silicon (Motorola 1985). It is proposed that a single microprocessor controller be used to control the system with sensors for ambient, building space, and internal combustion engine temperatures.

The microprocessor could be programmed in read only memory to perform the following functions.

- o Control auxiliary energy using ambient air state and internal combustion engine status to minimize auxiliary energy cost;
- o Control room state within comfort standards (ASHRAE 1980) but maximizing use of building temperature swing to reduce energy cost;
- o Assist in system checkout, maintenance, and fault diagnosis.

The microprocessor will ensure predicted performance is achieved and minimize maintenance costs (estimated cost $50.00).

Three-Way Valve$	$10
Miscellaneous Unspecified Components$ (sensors, wiring, etc.)	50
Estimated Manufacturing Cost	$60

Subsystem Assembly Labor

6 hours at $20 hr $120

The total subsystem cost is summarized in Table 8-2. The physical, performance and cost descriptions of a desiccant dehumidifier which can be effectively integrated with a nominal 37 kW thermally activated heat pump are shown in Tables 8-1, 8-2, and 8-3.

In summary:

- o The additional first cost of adding the desiccant dehumidifier subsystem is $490/ton of added capacity;
- o Physical interfaces between the TAHP and the dehumidifier are not critical and the unit can easily be designed as a stand-alone package with the following connections:
  - inlet and outlet connection to the internal combustion engine cooling water
  - 1000 CFM duct connection to the TAHP evaporator air handler
  - 1000 CFM inlet and exhaust duct to ambient air
  - 120 VAC electrical power connection (nominal 1.5 AMP service)
  - tap water connection (nominal 1.5 GPH - 2.5 GPH maximum);
- o The nominal 4.4 ton desiccant subsystem modular unit can be contained in a 1.0 m by 1.0 m by 1.8 m envelope.

The costs and capacities outlines in this section are for a specific size system. However, the components could probably be decreased to 1/4 of the nominal size (or 1/16 of the nominal capacity: 1/4 ton of dehumidification), to double the nominal size (or four times the capacity 17.5 tons of dehumidification) with little change in proportional costs or system feasibility. Outside of this range (0.25-17.5 ton of latent cooling) it is likely that some alternative physical configuration might be desirable. Larger systems should consider the possibility of liquid desiccants in spray

columns to achieve dehumidification due to large economics of scale for those systems. Such approaches could have the potential for lower costs per ton in the large sizes (possibly even less than 17.5 tons).

Table 8-1. Dehumidifier Subsystem Operating Specification

Cooling Capacity	15.5 kW (4.4 tons)
Air Flow Rate	2.47 kg/s (~1000 CFM)
Electrical Power	1.3 kW @120 VAC
Water Consumption	0.1 liter/min (1.56 PH) for evap. cooler
Waste Heat Recovery	13.5 kW
Auxilliary Gas Consumption	1.3 kW
Gas COP	11.92
Thermal COP	1.05
Dehumidifier wheel diameter	1.0 m
Dehumidifier Rotational speed	20 rph

Table 8-2. Desiccant Cooling Subsystem Cost (Nominal 4.4 Ton Capacity)

Component	Estimated Cost
Desiccant Dehumidifier	$460
Counterflow Heat Exchanger	200
Regeneration Heater	150
Direct Evaporative Cooler	165
Dehumidifier, HX Drive Motors and Speed Reducers and Speed Reducers	70
Fans (2) & Fan Drive Motor	270
Evaporative Cooler Pump	7
Sheet Metal Enclosure	215
Air Filters & Dampers	45
Electronic Controller	50
Miscellaneous Actuators & Mechanical Hardware	60
Assembly Labor	120
Subtotal for desiccant subsystem packaged unit	$1812
Exhaust Heat Recovery Unit (Mounted on Internal Combustion Engine)	350
Estimated Manufacturing Cost	$2162
$/TON of cooling (additional cost/additional capacity)	$491

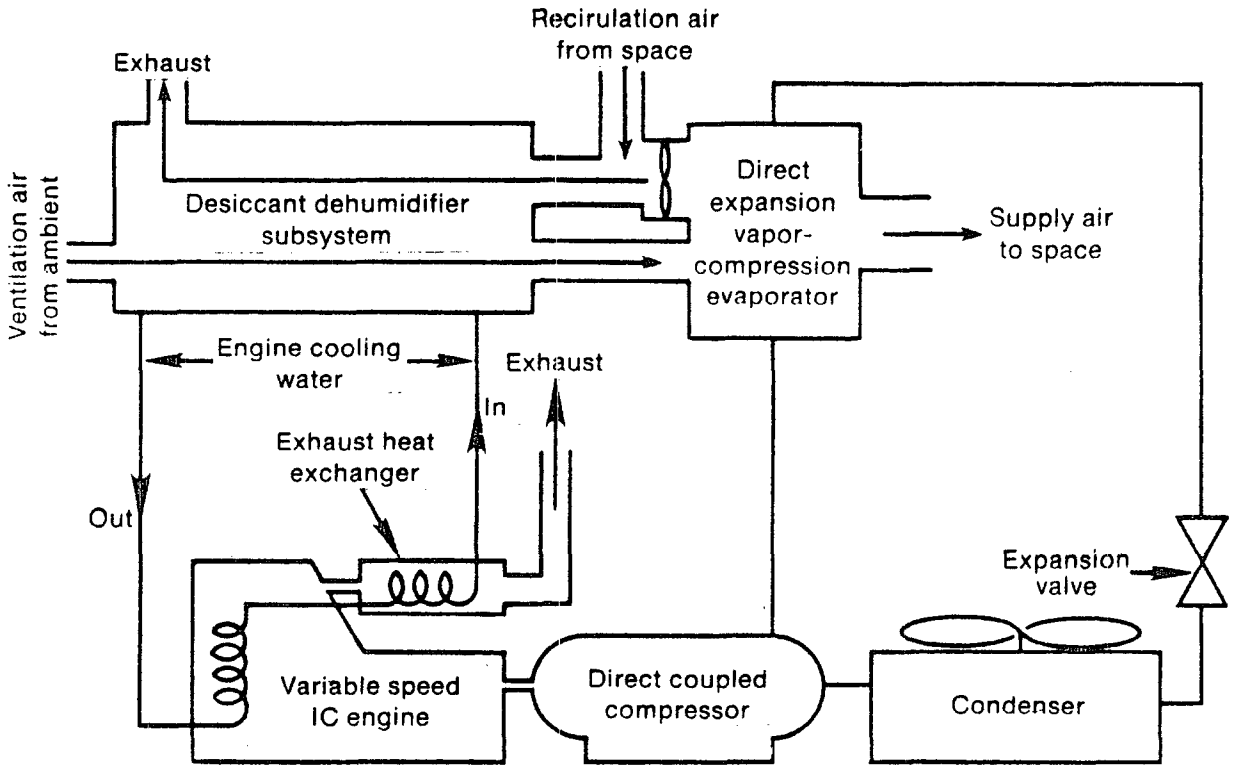

Figure 8-1. Integrated System Schematic Showing Subsystem Interferences

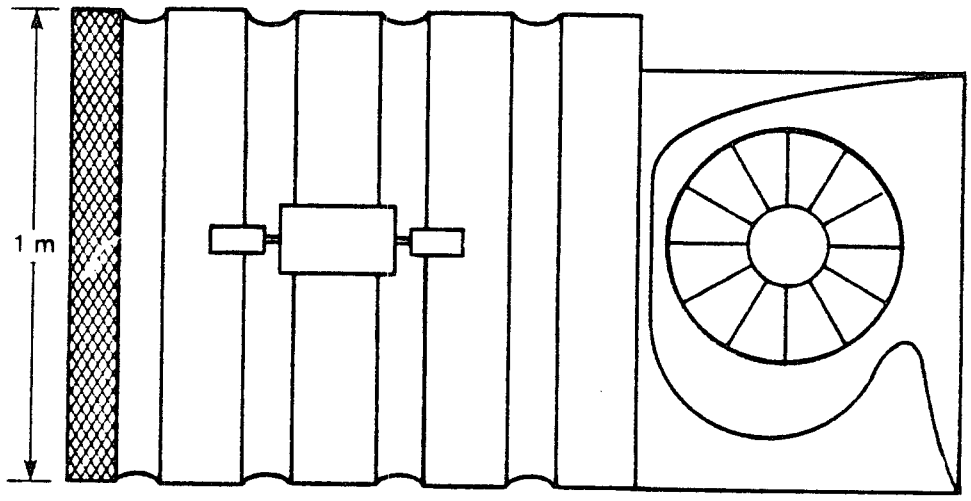

Side view

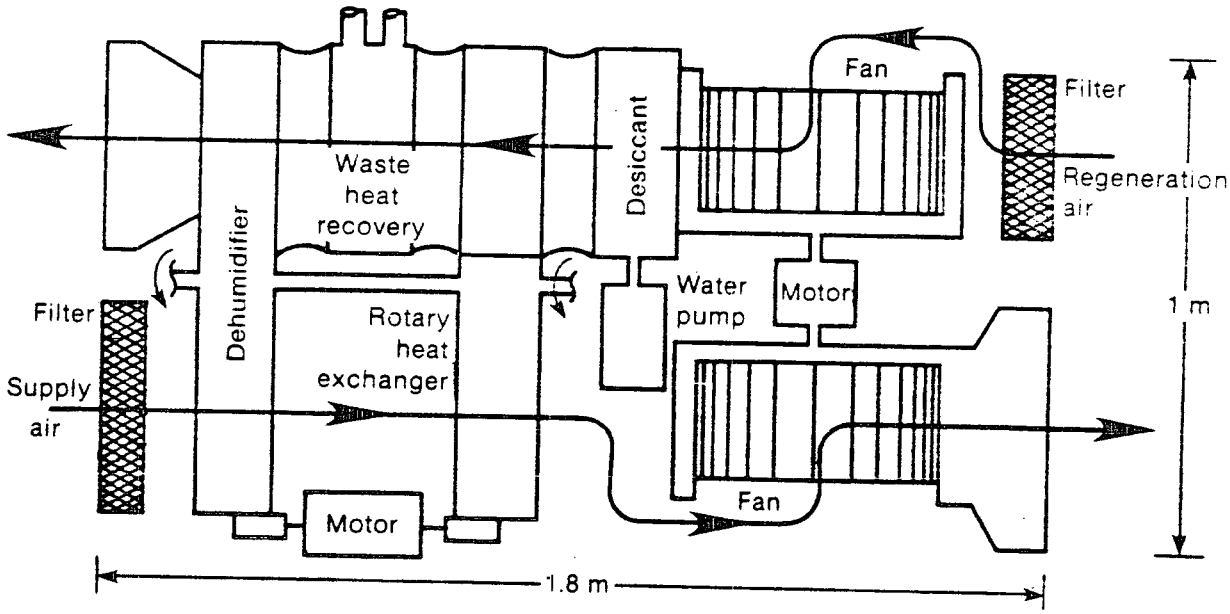

Plan view

Figure 8-2. Plan View Desiccant Dehumidifier/THHP Hybrid Schematic

9.0 CONCLUSIONS AND RECOMMENDATIONS

9.1 Conclusions

For this study we investigated desiccant materials and geometries for desiccant dehumidifiers and studied the performance of various dehumidifiers. We also studied performance and cost of thermally activated heat pump/desiccant hybrid systems that utilize the waste heat from internal combustion engines for desiccant regeneration. The following are the major conclusions of this
study.

For desiccant materials and dehumidifier performance:

- Among the desiccant materials we studied, three desiccant materials; molecular sieve, lithium chloride, and silica-gel, were identified as promising. Because of high heat and mass transfer/pressure drop ratio of parallel-plate geometry, we selected this as the preferred geometry for dehumidifiers. Detailed designs illustrated how these materials can be integrated into an advanced parallel-plate rotary dehumidifier similar to prototype articles tested by SERI.
- We compared the performance of the three materials by integrating detailed material property relations with a verified dehumidifier phenomenological model. Use of silica gel resulted in the highest moisture removal effectiveness. Predictions using lithium chloride resulted in only 5% less moisture removal. Molecular sieve dehumidifier performance predictions indicated 35% less moisture removal than silica gel thus, this material is not as suitable for regeneration temperatures of less than 100°C.
- Optimum dehumidifer regeneration temperatures were found to be lower than initially expected. While engine waste heat is available at 100°C from cooling water, and about 600°C from the exhaust system, analysis indicates that dehumidifier regeneration air temperatures of 50°C to 85°C are preferred. The dehumidifier performance results which support this conclusion are:

- For balanced flow where supply and regeneration airflow rates are equal, higher regeneration temperature dictates large amounts of auxilliary heat input.
- Unbalanced flow was examined for both constant regeneration temperature and constant regeneration heat input. In both cases, lowest process outlet humidity was achieved with nearly balanced flow, resulting in the preferred regeneration temperatures mentioned above.

For system performance and cost:

- We identified two promising TAHP/desiccant hybrid systems configurations. System 1 features nearly independent handling of latent and sensible cooling loads by vapor compression and desiccant subsystems in parallel. System 2 has the desiccant subsystem and TAHP components in series along the process and regeneration air paths.
- We modeled the two system configurations by developing and integrating component performance models. Components include a gas internal combustion engine and a vapor compression machine for the TAHP subsystem and heat exchangers, a dehumidifier and evaporative coolers for the desiccant subsystem.
- The performance of a thermally activated heat pump (TAHP) system can be greatly improved by adding a desiccant cooling subsystem. Specifically, at ARI standard design conditions:
  - the gas coefficient of performance (COP) is increased by 70% to 100%.
  - the total cooling capacity is increased by approximately 50% to 100%.
- The second configuration has about 25% higher gas COP at standard ARI conditions than the first configuration. For equal total cooling load the second system results in a 25% decrease in required TAHP capacity but the desiccant subsystem components are over 4 times larger than the first configuration. This is because all building supply air is processed by both subsystems.
- The hybrid system which separately handles latent and cooling load (system 1) can be designed as a stand-alone add-on package with simple, standard system interfaces. For a unit which adds about 4 1/2 tons of

cooling capacity to a 9 ton TAHP, components can be integrated in a 1 m by 1 m by 1.8 m package.

- We estimate the first manufacturing cost of the add-on desiccant subsystem package is $2150 or about $490/ton of additional cooling capacity. Current TAHP system first costs are about $1500/ton which includes manufacturer, distributer and retail profit but not installation. Maclaine-cross and Parsons (1986) indicate a cost factor of approximately 2 should be applied to the $490/ton figure to find a retail cost. Therefore, it is likely that the addition of a desiccant subsystem may decrease the retail first cost per unit of cooling delivered while reducing fuel consumption by 70%.
- This study supports the addition of a desiccant subsystem to a TAHP since first costs per unit of cooling do not increase and energy consumption is significantly reduced.

9.2 Recommendations

The results of this project demonstrate the significant potential of hybrid TAHP/desiccant systems, but some additional work is necessary to characterize fully the optimum configuration and to validate the conclusions listed above. We believe the following additional points should be examined.

- Verify component model performance predictions and integrate component cost relations in order to allow optimization on a life-cycle cost or cost of service basis.
- Research priorities should be established by performing sensitivity studies and comparing the effects of component improvements on overall system cost and performance.
- Extend the systems model to allow evaluation of seasonal performance and perform evaluations with climatic data for several typical cities.
- Performance predictions of the parallel plate lithium chloride dehumidifier described in this report should be verified by experiment.
- Detailed models of alternative dehumidifier geometries such as switched beds and liquid spray columns should be adapted, developed and verified. These

models could then be used to perform detailed comparisons of dehumidifier performance and allow hybrid and desiccant cooling system sizes outside the range examined in this project to be evaluated.

- Experimental research should include complete cooling system performance validation to verify system model predictions.

10.0 REFERENCES

Aldrich, 1987, Catalog Handbook of Fine Chemicals, Milwaukee, WI, 1986-1987.

Anzelius, A., Angew Z., 1962, Math Mech., 6, 291-4

Banks, P. J., 1972, "Coupled Equilibrium Heat and Single Adsorbate Transfer in Fluid Flow through a Porous Medium - I Characteristic Potentials and Specific Capacity Ratios," Chem. Engng. Sci., Vol. 27, pp. 1143-1155.

Banks, P.J., Feb. 1985, "Prediction of Heat and Mass Regenerator Performance Using Nonlinear Analogy Method: Part 1 — Basis," and "Prediction of Heat and Mass Regenerator Performance Using Nonlinear Analogy Method: Part 2 — Comparison of Methods," Heat Transfer, Vol. 107, pp. 222-238.

Banks, P. J. and Close, D. J., 1972, "Coupled Equilibrium and Single Adsorbate Transfer in Fluid Flow through a Porous Medium-II. Predictions for Silica-gel Air-Drier using Characteristic Charts," Chem. Eng. Sci., Vol. 27, pp. 1157-1169.

Banks, P. J., Close, D. J., and Maclain-cross, I. L., Sept. 1970, "Coupled Heat and Mass Transfer in Fluid Flow through Porous Media- An Analogy with Heat Transfer," Proc. 4th Int. Heat Transfer Conf., Versailles.

Barrer R. M., Fender, B. E. F., 1961, "The Diffusion and Sorption of Water in Zeolites - I. Sorption, "J. Phys. Chem. Solids, Vol. 21, Nos. 1/2, pp. 1-11.

Bharathan, D., J. R. Parsons, I. L. Maclaine-cross, 1986a, Experimental Study of an Advanced Silica Gel Dehumidifier, SERI/TR-252-2983, Golden, CO: Solar Energy Research Institute.

Bharathan, D., J. R. Parsons, I. L. Maclaine-cross, 1986b, "Experimental Results on Advanced Rotary Desiccant Dehumidifiers," Proceedings of the Third Annual Symposium on Improving Building Energy Efficiency in Hot and Humid Climates, November 18-19, 1986, Arlington, TX.

Biswas, P., Kim, S., and Mills, A. F., "A Compact Low-Pressure Drop Desiccant Bed for Solar Air Conditioning Applications: Analysis and Design," Journal of Solar Energy Engineering, May, 1984, Vol. 106, pp. 153-158.

Bowlen, K. L., 1986, "A Desiccant/Refrigeration Hybrid System for Air Conditioning Buildings," DOE/SERI Desiccant Cooling and Dehumidification Opportunities for Buildings Workshop, June 1986, Chattanooga, Tennessee.

Bullock, C. E., J. L. Threlkeld, 1966, "Dehumidification of Moist Air by Adiabatic Adsorption," Trans. Am. Soc. Heat Refrig. Air-Condit. Eng. 72, pp. 301-313.

Cargocaire Engineering Corporation, 1982, The Dehumidification Handbook, Amesbury, MA. Also Cargocaire Bulletin HC 324, 1979.

Carrier, Form 39e-7P, Controlled Speed Fan Drive 39E,ER, Product Literature.

Carter, J. W., D. J. Barrett, 1973, "Comparative Study for Fixed Bed Adsorption of Water Vapour by Activated Alumina, Silica Gel, and Molecular Sieve Adsorbents," Trans. Instn. Chem. Engrs. Vol 51, p. 75.

Collier, R. K., 2-3 October 1985, "GRI Desiccant Cooling Workshop," Chicago IL.

Collier, R. K., T. C. Cale, Z. Lavan, 1986, Advanced Desiccant Materials Assessment, GRI-8610181, Chicago, IL: Gas Research Institute.

Crum, Daniel R., 1986, "Open Cycle Desiccant Air Conditioning Systems," MS Thesis, University of Wisconsin, Madison, WI.

Domingo, N., (1986), "Thermally Actuated Heat Pumps with Desiccant Cooling," presentation materials sent to Charles Kutscher, Solar Energy Research Institute, Golden, CO.

Edwards, D. K., V. E. Denny, A. F. Mills, 1979, Transfer Processes, Hemisphere/McGraw-Hill Book Company, Inc., New York.

Encyclopedia of Chemical Technology, 1979, Volume 8, Third Edition, New York, John Wiley & Sons.

Foote Minerals Company, 1956, Chemical and Physical Properties of Litkium Compounds.

Fuji-Davison Chemical Ltd., MicroBead Silica Gel Technical Bulletin #81110575, Nagoya, Japan.

Gifford, E. W., 1957, "Dehumidification by Liquid Sorbents," Heating, Piping Air Conditioning, J. Sect. 29 (Apr.), pp. 156-159.

Griffiths, W., U. S. Patent No. 4,164,125.

Hawlicka, E., 1984, "Self-diffusion in water-alcohol mixtures. Part II. Water-methanol solutions of lithium chloride and sodium chloride," Ber. Bunsen-Ges. Phys., Vol. 88(10), pp. 1002-6.

Henry, P. S. H., (1939), "Diffusion in Adsorbing Media," Proc. Roy. Soc., Ser. A, VOl. 171, pp. 215-241.

Hilsenrath, J., et al., (1960), "Tables of Thermodynamic and Transport Properties of Air, Argon, Carbon Dioxide, Carbon Monoxide, Hydrogen, Nitrogen, Oxygen, and Steam," Oxford, England: Pergamon Press.

Hougen, O. A., Dodge, F. W., 1947, The Drying of Gases, Edwards Brothers, Inc., Ann Arbor, MI.

Hougen, O. A., Watson, K. M., 1953, Chemical Process Principles, Part III, Kinetics and Catalysis, pp. 1080-1105, New York: John Wiley.

Howe, R. R., 1983, "Model and Performance Characteristics of a Commercially-Sized Hybrid Air Conditioning System which Utilizes a Rotary Desiccant Dehumidifier," MS thesis, University of Wisconsin, Madison, WI.

Howe, R. R., Beckman, W. A., and Mitchell, J. W., "Commercial Applications for Solar Hybrid Desiccant Systems," Proceedings of the 1983 Annual Meeting of ASES, (1983).

Johnson, E. F., M. C. Molstad, 1951, "Thermodynamic Properties of Aqueous Lithium Chloride Solutions," J. Phys. Chem., Ithaca; 55; pp. 257-281.

Jurinak, J. J., 1982, "Open Cycle Desiccant Cooling--Component Models and Systems Simulations," Ph.D. Dissertation, Madison, WI: University of Wisconsin, Solar Energy Laboratory.

Jurinak, J. J., and P. J. Banks, Nov. 1982, "A Numerical Evaluation of Two Analogy Solutions for a Rotary Silica Gel Dehumidifier," Heat Transfer in Porous Media, edited by J. V. Beck and L. S. Yao, ASME Pub. HTD — Vol. 22.

Jury, S. H., H. R. Edwards, Oct. 1979, "The Silica Gel Water Vapor Sorption Therm," Can. J. Chem. Engr., Vol. 49, pp. 663-666.

Kays, W. M., and London, A. L. (1964), Compact Heat Exchangers, 2nd edition, New York: McGraw-Hill.

Kettleborough, M. R., M. R. Ullah, D. G. Waugaman, 1986, "Desiccant Cooling Systems - A. Review," Proceedings of the Third Annual Symposium on Improving Energy Efficiency in Hot and Humid Climates. November 18-19, 1986, Arlington, TX.

Kim, S., P. Biswas, A. F. Mills, 1984, "A Compact Low-Pressure Drop Desiccant Bed for Solar Air Conditioning Application: 2. Bench Scale Tests," J. Solar Energy Eng., Vol. 107, pp. 153-158.

Lambertson, T. J., (1958), "Performance Factors of a Periodic-Flow Heat Exchanger," Trans. ASME, pp. 586-592.

Lange, E., F. Durr, 1926, "Losungs- und Verdunnungswarmen von Salzen von grosser Verdunnung bis zur Sattigung. II. Lithiumchlorid," Z. phys. Chem., Vol. 121. pp. 361-384.

Lightfoot, E. N., R. J. Sanchez-Palma, D. O. Edwards, 1962, "Chromatography and Allied Fixed-Bed Separations Processes," in Schcen, H. M., New Chemical Engineering Separation Techniques, pp. 99-182: John Wiley.

Lof, G. O., Cler, G., and Brisbune, T., 1987, "Performance of a Solar Desiccant Cooling System," ASME/JSME Solar Engineering Conference Proceedings, Honolulu, Hawaii, March 1987, pp. 828-834.

Maclain-cross, I. L., and Parsons, J., 1986, "A Five-Ton Advanced Solid-Desiccant Solar Cooling System with Heating and Service Hot Water," SERI/SP-252-2832, Solar Energy Research Institute, Golden, Colorado.

Maclaine-cross, I. L., (1974), "A Theory of Combined Heat and Mass Transfer in Regenerators," Ph.D. Dissertation, Australia: Monash University, Department of Mechanical Engineering.

Maclaine-cross, I. L., Aug. 1978, "Comparison of the Analogy Theory of Combined Heat and Mass Transfer in Regenerators with a Finite Difference Solution," New South Wales, Australia: Department of Mining and Mineral Sciences, Unviersity of New South Wales.

Maclaine-cross, I. L., (1973), "Combined Heat and Mass Transfer in Regenerators with Multiple Film Transfer Coefficients," Paper presented at the First Australian Conference on Heat and Mass Transfer, Melbourne, Australia.

Maclaine-cross, I. L., (1980), "Effect of Interstitial FLuid Heat Capacity on Regenerator Performance," Heat Transfer, Vol. 102, pp. 572-573.

MacLaine-Cross, I. L., (1986), "Brief Notes and Sample Cost Calculations on Gas Engine Desiccant Hybrid Cooling for Australian Conditions," University of New South Wales, School of Mechanical and Industrial Engineering.

Maclaine-cross, I. L., and Banks, P. J., (1972), "Coupled Heat and Mass Transfer in Regenerators — Prediction Using an Analogy with Heat Transfer," Int. J. Heat Mass Tansfer, Vol. 15, pp. 1225-1242.

Mason, E. A., and Monchick, L., (1965), "Survey of the Equation of State and Transport Properties of Moist Gases," Humidity and Moisture, edited by A. Wexler, New York: Reinhold, Vol. 3, pp. 257-272.

McCormick, P., S. Brown, S. Theker, June 1983, Performance of a Glazed Open Flow Liquid Desiccant Solar Collector for Both Summer Cooling and Winter Heating, Final Report, LMSC-HREC TR D867353, Huntsville, AL: Lockheed Missiles and Space Company, Inc., Huntsville Engineering and Research Center.

Meckler, G., July 1982, "It's Not the Heat, It's the Humidity," The Energy Daily, Vol. 10, No. 123.

Meckler, G., 1987, "Solar Dehumidification System Applications," ASME/JSME Solar Engineering Conference Proceedings, Honolulu, Hawaii, March, 1987, pp. 855-865.

Meckler, G., 1986, "Energy-Integrated Desiccant HVAC System Applications," DOE/SERI Desiccant Cooling Workshop Proceedings, Chatanooga, Tennessee, June, 1986.

Mikhail, R. S., and Shebl, F. A., 1970, "Adsorption in Relation to Pore Structure of Silicas: II. Water Vapor Adsorption on Wide-Pore and Microporous Silica Gels," Journal Collid and Interface Sci., Vol 34, pp. 6-75.

Nienberg, J. W., 1977, "Modeling of Desiccant Performance for Solar-Desiccant-Evaporative Cooling Systems," Masters Thesis, Los Angeles: University of California.

Onischak M., Gidaspow, D., 1969, "Reaction of Water with Anhydrous Lithium Chloride in a Parallel Plate Flow Reactor," The Canadian Journal of Chemical Engineering, Vol. 47, pp. 98-99.

Peng, C. S., J. R. Howell, 1981, "Optimization of Liquid Desiccant Systems for Solar/Geothermal Dehumidification and Cooling," J. of Energy, Vol. 5, No. 6, pp. 401-408.

Pesaran, A. A., 1983, "Moisture Transport in Silica Gel Particle Beds," Ph.D. Dissertation, Los Angelels, CA: University of California.

Pesaran, A. A., I. L. Maclaine-cross, E. Van den Bulck, April 1986, Measurements on Promising Desiccant Dehumidifier Materials and Geometries, SERI/TR-252-2898, Golden, CO: Solar Energy Research Institute.

Piette, M. A., Wall, L. W., and Gardiner, B. L., 1985, "Measured Energy Performance of Energy-Efficient New Commercial Buildings: Results from the BECA-CN Data Compilations," LBL-19413, Lawrence Berkeley Laboratory, Berkeley, CA.

Pla-Barby, F. E., G. C. Vliet, R. L. Panton, 1978, "Performance of Rotary Bed Silica Gel Solid Desiccant Dryers," ASME 78-h-36, presented at the ASME Annual Meeting.

Carrier Product Literature, "Carrier Weathermaster III Heat Pump System," form 38HQ-1P, Carrier Corporation, Syracuse, NY.

Trane Product Literature, "Trane Rooftop Air Conditioners, 20 to 75 Tons," Form DS PKG-4, The Trane Company, La Crosse, WI (July 1981).

Robison, H., H. Harris, 1982, "Year-Round Operational Test Results of a Chemical Heat Pump Powered by Waste Heat, Off-Peak Electricity, or Solar Energy," Energex '82: Conf. Proc. Solar Energy Society of Canada, Regina, Saskatchewan

Robison, H., June 1982, "Open-Cycle Chemical Heat Pump and Energy Storage Systems," Columbia: University of South Carolina, Coastal Carolina College, Energy Lab.

Rousseau, J., 1981 (Mar.). "Development of a Solar Desiccant Dehumidifier: Phase II Technical Progress Report." AiResearch Manufacturing Company Report No. 81-17773. Prepared for the U. S. Department of Energy.

Ruthven, D. M., 1984, Principles of Adsorption and Adsorption Processes, New York: John Wiley & Sons, Inc.

Schlepp, Dennis R., Barlow R., September 1984, "Performance of the SERI Parallel-Passage Dehumidifier," SERI/TR-252-1951, Golden, CO: Solar Energy Research Institute.

Schlepp, Dennis R., and Schultz, Kenneth, (1984), "Analysis of Advanced Solar Hybrid Desiccant Cooling Systems for Buildings," SERI/TR-252-2527, Solar Energy Research Institute, Golden, CO.

Schlünder, E. U., 1963, "Einfaches Verfahren zur Messung von Dampfdrucken Uber wassrigen Salzlösungen," Chemie-Ingr-Tech., 35, pp. 482-487.

Schultz, K. J., 1985, SERI Desiccant Cooling Test Facility: Status Report, SERI/TR-252-2718, Golden, CO: Solar Energy Research Institute.

Segaser, Charles L., 1977, "Internal Combustion Piston Engines," Integrated Community Energy Systems — Technology Evaluations, Oak Ridge National Laboratory, ANL/CES ITE 77-1.

Sladek, K. J., E. R. Gilliland, R. F. Baddour, 1974, "Diffusion on Surfaces II: Correlation of Diffusivities of Physically and Chemically Adsorbed Species," Ind. Eng. Chem. Fundam., Vol. 13, No. 2, pp. 100-105.

Smith, C. W., M. Dole, 1956, "Specific Heat of Synthetic High Polymers VII Polyethylene Terephthalate," J. Polymer Science, Vol. 20, pp. 37-56.

Thakker, M. T., C. W. Chi, R. E. Peck, D. T. Wasan, October 1968, "Vapor Pressure Measurements of Hygroscopic Salts," Journal of Chemical Engineering Data, Vol. 13, No. 4, pp. 553-558.

Touloukian, Y. S., E. H. Buyco, 1970, "Specific Heat-Nonmetalic Solids," Thermophysical Properties of Matter, Vol. 5, New York: IFI PLENUM.

Uemura, T., 1967, "Studies on the Lithium Chloride-Water Absorption Refrigerating Machine," Technology Rep. Fac. Engng. Kansai Univ., 9, pp. 71-88.

Van Den Bulck, E., Klein, and Mitchell, J. W., (1985), "Second Law Analysis of Solid Desiccant Rotary Dehumidifiers," Paper presented at the National Heat Transfer Conference, AIChE, Denver, CO, Nov.

W. R. Grace Co., 1966, Fluid Processing Handbook, Baltimore, MD.

W. R. Grace Co., Davison Molecular Sieves Technical Bulletin #5696, and Davison 4A Molecular Sieves, Technical Bulletin #1C96-B; Baltimore, MD.

W. R. Grace Co., Davison Silica Gel, Bulletin No. 1C-15-378, Baltimore, MD.

Warren, Mashuri L., 1985, "Performance Comparison of Absorption and Desiccant Solar Cooling Systems," Lawrence Berkeley Laboratory, Berkeley, CA.

Waugaman, D. G., and Kettleborough, C. F., 1987, "Combining Direct and Indirect-Evaporative Cooling with a Rotating Desiccant Wheel in Residential Applications," ASME/JSME Solar Energy Conference Proceedings, Honolulu, Hawaii, March, 1987, pp. 848-854.

Worek, W. M., Lavan, Z., Aug. 1981, "Peformance of a Cross-Cooled Desiccant Dehumidifier Prototype." Illinois Institute of Technology Report No. DES-81-1. Prepared for the U. S. Department of Energy.

Wurm, J., et al, 1979 (Nov.), "SOLAR-MEC^R Development Program: Semi-annual Progress Report," Institute of Gas Technology Report No. COO-4495-23. Prepared for the U. S. Department of Energy.

Wylie, R. G., June 1969, "The Psychrometer Problem — A Precise Analysis," PIR Report No. 65, Australia: Commonwealth Scientific and Industrial Research Organization.

Wylie, R. G., and Lalas, T. 1981, "The WMO Psychrometer," Technical Paper No. 3, Australia: Commonwealth Scientific and Industrial Research Organization, Division of Appied Physics.

APPENDIX A

Evaluation of F_i Transfer Properties

The evaluation of F_i transfer properties for desiccant/air/water system follows the procedures described by Banks (1972), and Banks and Close (1972). A brief outline of the procedure is provided here.

The basic heat and moisture transfer equations are written as

$$\frac{\partial w}{\partial \theta} + \nu \frac{\partial w}{\partial x} + \mu \frac{\partial w}{\partial \theta} = 0 \qquad \text{(A-1)}$$

$$\frac{\partial h}{\partial \theta} + \nu \frac{\partial h}{\partial x} + \mu \frac{\partial H}{\partial \theta} = 0 \qquad \text{(A-2)}$$

Here w and W are the ratios of mass of moisture to that of dry air, and matrix, respectively, w represents the absolute humidity, and W, the matrix moisture content. h and H represent the specific enthalpies of the dry air and matrix, respectively, x represents a distance in the direction of fluid flow, and θ , time.

When h, H, and W can be represented as functions of temperature, t, and w alone, Eqs. (A-1) and (A-2) can be written as

$$\frac{\partial t}{\partial \theta} + \alpha_i \frac{\partial w}{\partial \theta} + A_i \mu \left(\frac{\partial t}{\partial x} + \alpha_i \frac{\partial w}{\partial x}\right) = 0 \ , \ i = 1,2 \qquad \text{(A-3)}$$

where

$$2\alpha_i = \left(\lambda\ \alpha_h + \sigma\nu + \alpha_w\right) - (-1)^i \left[\left(\lambda\alpha_h + \alpha\nu + \alpha_w\right)^2 - 4\alpha_w\lambda\alpha_h\right]^{1/2} \ , \ i = 1,2$$

and

$$A_i = \left(1 + \mu\gamma_i\right)^{-1} \ , \ i = 1,2 \qquad \text{(A-5)}$$

For air-water systems at ambient pressures,

$$\frac{\gamma_i}{\sigma} = \left(\frac{\alpha_i - \alpha_w}{\sigma\nu}\right) \text{ , } i,j = 1,2 \text{ and } i \neq j \text{ .} \qquad \text{(A-6)}$$

The quantities α_i and γ_i have been expressed in terms of convenient parameters derived from partial differentials of the properties of the fluid mixture and matrix with respect to each other. Thus;

$$\sigma_h = -\left(\frac{\partial t}{\partial w}\right)_h \text{ and } \alpha_w = -\left(\frac{\partial t}{\partial w}\right)_W \qquad \text{(A-7), (A-8)}$$

are the slopes of lines of constant h and W respectively on a t-w plot;

$$\lambda = 1 - \frac{(\partial H/\partial W)_t}{(\partial h/\partial w)_t} \qquad \text{(A-9)}$$

is the ratio of the heat of sorption and the enthalpy of the sorbate in the fluid mixture;

$$\alpha = \frac{(\partial H/\partial t)_w}{(\partial h/\partial t)_w} \qquad \text{(A-10)}$$

is the ratio of the specific heats of the porous medium and the fluid mixture, and

$$\nu = -\left(\frac{\partial t}{\partial W}\right)_w$$

is a sorption parameter, which contributes to the parameter

$$\beta = \frac{\alpha w}{\nu} = \left(\frac{\partial W}{\partial w}\right)_t \qquad \text{(A-12)}$$

which is termed the sorbability of the porous medium for the sorbate.
For mixture of perfect gases,

$$\left(\frac{\partial W}{\partial t}\right)_w = -r\left(\frac{\partial W}{\partial r}\right)_t \left(\frac{\partial \ln p}{\partial t}\right)_w \qquad \text{(A-13)}$$

where p is the partial pressure of the water vapor in the gas mixture, and r its relative humidity, p/p_s.

For water vapor in air, at near atmospheric pressures

$$\frac{p}{p_t} = \frac{w}{0.622 + w} \tag{A-14}$$

Defining the parameter Ψ as

$$\Psi = \frac{(\partial h/\partial w)_t}{hs} \tag{A-15}$$

an expression for the sorption parameter ν is

$$\nu = (\zeta\lambda\Psi S)^{-1} \tag{A-16}$$

where

$$S = \frac{\partial \ln p_S}{\partial t} \tag{A-17}$$

depends on the variation of the saturation vapor pressure of the sorbate with temperature, and

$$\zeta = r\left(\frac{\partial W}{\partial r}\right)_t \tag{A-18}$$

depends on the sorption isotherm slope.

From partial differentation and equation (A-14), one derives

$$\beta = \left(\frac{\partial W}{\partial w}\right)_t = \zeta\Omega w^{-1} \tag{A-19}$$

where

$$\Omega = 1 - \frac{p}{p_t} \tag{A-20}$$

The above set of equations provide means to evaluate α_i and γ_i as defined in equations (A-4) and (A-6), provided the vapor pressure isotherm relationship

is available. Conventionally adopted convention of $\gamma_2 > \gamma_1$ is used in all evaluations.

Evaluation of the Intersection Points

Given the process and regeneration inlet conditions, t_{pi}, w_{pi}, and t_{ri}, w_{ri}, respectively, initial values of the αs and λs at these points are evaluated as described earlier. The intersection point is projected as the intersection of a line with the slope of $\alpha_i \{= \frac{\partial t}{\partial w} F_1\}$, originating from the process inlet condition and of a line with a slope of α_2 originating from the regeneration inlet condition. An incremental step is taken towards the intersection, updated values of are evaluated. Estimate of the intersection point is revised and the procedure is continued until the final intersection is achieved.

During this procedure, continual updating process means values of $\bar{\gamma}_2$ along the F_1 lines and $\bar{\gamma}_1$ along the F_2 line are also evaluated by integrating the local values of γ_1 and γ_2 .

Evaluation of F_1 and F_2 Transfer Efficiencies

The specific capacity ratios γ_1 and γ_2 for the F_1 and F_2 exchange, vary widely over the nominal process and regeneration conditions. At nominal process and regeneration temperatures of 30 and 80°C, respectively, and an air humidity ratio 0.015, γ_1 of silica gel varies from 0.81 down to 0.39; the variation of γ_2 is larger with values from 41 down to 4.6 for silica gel. These variations impact in overall reduction in the transfer efficiency from the case with constant capacity.

The theoretical efficiency for each wave is calculated using the numerical finite-difference method developed by Lambertson (1958). The finite-difference method was modified to account for capacity variations of four characterizing parameters, $(NTU)_o$, C_{min}/C_{max} C_r/C_{min}, and (ha)'. The capacity variation was introduced using a parameter $\Delta C/C$ representing the overall variation in C_r, normalized by its mean value. An iterative scheme was employed to calculate outlet states based on inlet states for every element.

Further details of the calculation procedure may be found in Bharathan et al. (1986a).

The process effectiveness for F_1 and F_2 transfer are defined as

$$\eta_{2p} = \frac{(h_{po} - h_{pi})(w_{ri} - w_{pint}) - (w_{po} - w_{pi})(h_{ri} - h_{pint})}{(h_{pint} - h_{pi})(w_{ri} - w_{pint}) - (w_{pint} - w_{pi})(h_{ri} - h_{pint})} \quad \text{(A-21)}$$

and

$$\eta_{1p} = \frac{w_{po} - w_{pi}}{w_{ri} - w_{pint}} - \eta_{2p} = \frac{(w_{pint} - w_{pi})}{(w_{ri} - w_{pint})} \quad \text{(A-22)}$$

The corresponding dimensionless wheel rotational speeds for the process stream are calculated as

$$C_i = \frac{m_{dd}\ \bar{\gamma}_i\ X_{eff}}{\dot{m}_p\ \tau} \quad \text{(A-23)}$$

where m_{dd} is the dry desiccant mass per period, (kg) X_{eff} represents the fraction of active desiccant, $\dot{m}_p$ is the process air mass flow rate (kg/s) and τ is the residence time per period (s).

For both process and regeneration streams, mean Reynolds number, Prandtl number and Graetz number are evaluated at their corresponding mean temperatures between inlet and outlet conditions. For each stream, mean Nusselt number is evaluated for the assumed matrix geometry. Their corresponding NTU are evaluated as: NTU = Nu/Gr. Passage uniformity affects the value of Nusselt number. For our study, we used a value of 8.235 which assumes uniform passages, similar to those achieved in the SERI microbead silica-gel test article.

For each stream, the effective Lewis number is evaluated as follows:

- The effective Lewis number can be expressed in terms of an efficiency of the desiccant particle substrate matrix e_s as

$$Le = \frac{Sc}{Pr}\left\{1 + \frac{Sh}{6.0}\left(\frac{d_p}{D_h}\right)\left(\frac{1}{e_s P^f}\right)\left(\frac{\mu_m}{\rho_d D_W}\right)\left(\frac{dw}{dW}\right)_t\right\} \quad \text{(A-24)}$$

where $\left(\frac{Sc}{Pr}\right)$ represents the Schmidt over Prandtl number ratio for air.

Sh = the Sherwood number

dp = the mean desiccant particle size (m)

ρ_d = the dry desiccant density (kg/m^2)

pf = the desiccant particle packing factor on the substrate

D_W = the diffusivity of moisture in the desiccant (m^2/s)

$\left(\frac{dw}{dW}\right)_t$ = the isothermal rate of change of moisture in desiccant with respect to moisture content of air, evaluated at t_m.

The geometry factor, e_s, can be viewed as the ratio of actual available surface area for exchange to the area if the particles were distributed as uniform spheres of diameter d_p, closely packed in a single layer. Note that the higher the e_s, the lower the solid-side resistance.

For F_1 and F_2 transfer, the dimensionless transfer coefficients are evaluated for both streams as:

$$\Lambda_i = \frac{(NTU)\left\{Le - \frac{\alpha_i}{\alpha_{3-i}}\right\}}{Le\left\{1 - \frac{\alpha_i}{\alpha_{3-i}}\right\}} \quad i = 1,2 \qquad \text{(A-25)}$$

For calculation of a theoretical effectiveness, the four E parameters, for the process stream are calculated as:

$$E_1 = \frac{\Lambda_p}{1 + E_4} \qquad \text{(A-26)}$$

$$E_2 = \frac{C_r}{C_p} \qquad \text{(A-27)}$$

$$E_3 = C_p \qquad \text{(A-28)}$$

$$E_4 = \frac{\Lambda_p C_r}{\Lambda_r C_p} \qquad \text{(A-29)}$$

for each of the F_1 and F_2 waves.

The preceeding four parameters are equivalent to the four parameters for sensible heat exchange defined by Lamberston (1958). Once these are defined, the effectiveness of exchange can be readily calculated by integrating the exchange process element by element. For varied capacity of the wheel, an iterative scheme is required.

Once efficiencies are evaluated, Eqs. A-21 and A-22 are used to evaluate process and regeneration outlet air states.

The computer code which implements these equations is available on floppy disk from ORNL.

SUGGESTED EXTERNAL DISTRIBUTION LIST

William M. Anderson
Anderson Consulting
7605 E. Windlawn Way
Parker, CO 80134

Bill Belding, PhD
Chemical Research, Kaiser Chemicals
Division of Kaiser Aluminum and
Chemical Corporation
Pleasanton, CA 94566

Carl Bergt
Trane Systems Engineering Co.
6200 Troup Highway
Tyler, TX 75711

Kennard L. Bowlen
Cargocaire Engineering Corp.
79 Monroe St.
Amesbury, MA 01913

Fang Chen
Oak Ridge National Laboratory
Building Equipment Research Program
P.O. Box Y
Oak Ridge, TN 37831

Glen Chinery
Tennessee Valley Authority
217 Power Board Bldg
Chattanooga, TN 37401

James Coellner, Director R&E
American Solar King Corp.
700 Loop 340 South
Waco, TX 76710

Barry Cohen
Thermal Products Division
ThermoElectron Corporation
45 First Avenue
Waltham, MA 02154

Kirk Collier, Ph.D.
Everscope, Inc.
4886 W. Port Au Prince
Glendale, AZ 85306

Noberto Domingo
Oak Ridge National Laboratory
Building Equipment Research Program
P.O. Box Y
Oak Ridge, TN 37831

Michael Epstein
Fauske & Associates, Inc.
162070 West 83rd Street
Burr Ridge, IL 60521

Phillip Fairchild
Oak Ridge National Laboratory
Building Equipment Research Program
P.O. Box Y
Oak Ridge, TN 37831

Phillip Fairey
Florida Solar Energy Center
300 State Road, 401
Cape Canaveral, FL 32920

A. Hunter Fanney, Ph.D.
Bldg. 226, Room B310
National Bureau of Standards
Washington, DC 20234

Ronald Fiskum
U.S. Department of Energy
Route CE-132, Room GF-217
1000 Independence Ave., S.W.
Washington, DC 20585

Stephen D. Fitch
Bry-Air
P. O. Box 795
Sunbury, OH 43074

Paul Gandhidasan, Ph.D.
Dept. of Mechanical Engineering
Texas A&M University
College Station, TX 77843

John Goldsmith
U.S. Department of Energy
Route CE-311, Room 5H065
1000 Independence Ave., S.W.
Washington, DC 20585

William C. Griffiths
Midland Ross Corporation
P. O. Box 791
New Brunswick, NJ 08903

R. Harkins
ASES
2030 17th St.
Boulder, CO 80302
Richard B. Hayter, Ph.D.
Engineering Extension
Ward Hall, Kansas State University
Manhattan, KS 66506

Jim Hill, Ph.D.
National Bureau of Standards
Technology B-148
Washington, DC 20585

Anthony Hines, Ph.D.
College of Engineering
Oklahoma State University
Stillwater, OK 74078

Ralph Johnson
NAHB Research Foundation, Inc.
3720 T St., N.W.
Washington, DC 20007

Robert Jones
Los Alamos National Laboratory
P.O. Box 1663
Mail Stop H577
Los Alamos, NM 87545

Theodore Kapus
U.S. Department of Energy
Route CE-132, Room GF-217
1000 Independence Ave., S.W.
Washington, DC 20585

Michael A. Kuliasha
Oak Ridge National Laboratory
Building Equipment Research Program
P.O. Box Y
Oak Ridge, TN 37831

Zalman Lavan, Ph.D.
Illinois Institute of Technology
Department of Mechanical Engineering
Illinois Institute of Technology
Center
Chicago, IL 60616

George O. G. Lof, Ph.D.
Colorado State University
Solar Energy Applications Laboratory
Fort Collins, CO 80523

Ian Maclaine-cross, Ph.D.
University of New South Wales
School of Mechanical and Industrial
Engineering
P.O. Box 1
Kensington, NSW 2033 Australia

John Millhone
U.S. Department of Energy
Route CE-132, Room GH-068
1000 Independence Ave., S.W.
Washington, DC 20585

Anthony F. Mills
Bollter Hall
School of Engineering and Applied
Science
University of California
Los Angeles, CA 90024

John Mitchell, Ph.D.
University of Wisconsin-Madison
Engineering Research Building
1500 Johnson Drive
Madison, WI 53706

Frederick Morse, Ph.D.
U.S. Department of Energy
Route CE-31, Room 5H-095
1000 Independence Ave., S.W.
Washington, DC 20585

Stanley A. Mumma
104 Engineering "A" Building
University Park, PA 16802

Janet Neville
U.S. Department of Energy
San Francisco Operations Office
1333 Broadway
Oakland, CA 94612

Davor Novosel
Gas Research Institute
8600 West Bryn Mawr Avenue
Chicago, IL 60631

Yves O. Parent
Res. Eng.
Industrial Chemicals Research
Davison Chemical Division
W. R. Grace & Co.
Washington Research Center
7379 Route 32
Columbia, MD 21044

David Pellish
Solar Buildings Technology Division
Office of Solar Heat Technology
U.S. Department of Energy
Forrestal Building, Room 5H-041
1000 Independence Ave., S.W.
Washington, DC 20585

Dr. John L. Peterson
University of Tesas at Austin
Balcomes Research Center
10100 Burnet Road
Austin, TX 78758

D. M. Ruthven, Ph.D.
University of New Brunswick
P. O. Box 4400
Fredericton, N.B.
Canada E58 5A3

John Ryan
U.S. Department of Energy
Route CE-132, Room GF-217
1000 Independence Ave., S.W.
Washington, DC 20585

William Seaton
ASHRAE
1791 Tullie Circle, NE
Atlanta, GA 30329

Robert Turner
Department of Mechanical Engineering
University of Nevada-Reno
Reno, Nevada 89557

M. Wahlig, Ph.D.
Lawrence Berkeley Laboratories
University of California
1 Cyclotron
Berkeley, CA 94720

Alex Willman
ACEC Resource and Management
Foundation
1015 15th Street, N.W.
Washington, DC 20005

Byard Wood, Ph.D.
Department of Mechanical & Aerospace
Engineering
Arizona State University
Tempe, AZ 85287